Radiology: Cardiothoracic Imaging

REVIEW

Role of CT in the Pre- and Postoperative Assessment of Conotruncal Anomalies

Parveen Kumar, MD, DCBCCT, EDiR, DICR • *Mona Bhatia, MD, FRCR*

From the Department of Radiodiagnosis and Imaging, Fortis Escort Heart Institute, Okhla Road, New Delhi 110025, India. Received March 27, 2021; revision requested May 5; revision received April 25, 2022; accepted May 19. **Address correspondence to** P.K. (email: *drparveenbatra@gmail.com*).

Authors declared no funding for this work.

Conflicts of interest are listed at the end of this article.

Radiology: Cardiothoracic Imaging 2022; 4(3):e210089 • https://doi.org/10.1148/ryct.210089 • Content codes: CA CH PD CT VA

Conotruncal anomalies, also referred to as outflow tract anomalies, are congenital heart defects that result from abnormal septation of the great vessels' outflow tracts. The major conotruncal anomalies include tetralogy of Fallot, double-outlet right ventricle, transposition of the great arteries, truncus arteriosus, and interrupted aortic arch. Other defects, which are often components of the major anomalies, include pulmonary atresia with ventricular septal defect, pulmonary valve agenesis, aortopulmonary window, and double-outlet left ventricle. CT has emerged as a robust diagnostic tool in preoperative and postoperative assessment of various congenital heart diseases, including conotruncal anomalies. The data provided with multidetector CT imaging are useful for treatment planning and follow-up monitoring after surgery or intervention. Unlike echocardiography and MRI, CT is not limited by a small acoustic window, metallic devices, and need for sedation or anesthesia. Major advances in CT equipment, including dual-source scanners, wide-detector scanners, high-efficiency detectors, higher x-ray tube power, automatic tube current modulation, and advanced three-dimensional postprocessing, provide a low-risk, high-quality alternative to diagnostic cardiac catheterization and MRI. This review explores the various conotruncal anomalies and elucidates the role of CT imaging in their pre- and postoperative assessment.

Conotruncal anomalies refer to a group of congenital heart defects that involve outflow tracts of the heart and great vessels. This class of defects includes tetralogy of Fallot (TOF), double-outlet right ventricle (DORV), transposition of the great arteries (TGA), truncus arteriosus (TA), and interrupted aortic arch (IAA) (1). The list also includes pulmonary atresia with ventricular septal defect (VSD), pulmonary valve agenesis, aortopulmonary window, and double-outlet left ventricle. Patients with conotruncal anomalies can be evaluated with transthoracic echocardiography, CT angiography (CTA), cardiac MRI, and cardiac catheterization. Transthoracic echocardiography is the most commonly available imaging tool, but it is limited by small field of view, dependence on operator skill, and inability to visualize the RV apex, distal pulmonary arteries (PAs), pulmonary veins, aortic arch, and ascending aorta (2). Cardiac MRI provides a comprehensive assessment of conotruncal anatomy, flow velocities, and ventricular function and is free of ionizing radiations. An important advantage of cardiac MRI over CT is its ability to help assess blood flow, ejection fraction, and shunt quantification, making it vital during follow-up of patients with TOF for assessment of pulmonary insufficiency. There are also specific scenarios where cardiac MRI may suffer from artifacts and CTA is more appropriate (ie, stents, occluder devices, pacemakers, defibrillators, and unstable patients) (3). Catheter angiography can be used to measure blood pressure and blood oxygen saturation and to estimate cardiac output and pulmonary vascular resistance. It is, however, an invasive procedure and requires separate punctures (arterial and venous) to individually visualize the right and the left side of the heart structure. The potential risks of catheter-related complications, radiation exposure, and contrast agent nephropathy and the difficulty in differentiating overlapping structures make it less suitable as a primary diagnostic modality (4). CT, which can be used to assess cardiac structures and functions, is an alternative method to assess the preoperative anatomy and postoperative complications of conotruncal anomalies. Current CT scanners with the latest technologies, including fast gantry rotation, high-pitch scanning, wider detector systems, automated tube voltage selection, tube current modulation, and three-dimensional printing, have revolutionized the role of CT imaging (5–7). Radiation exposure is a major concern in pediatric patients, as they are more sensitive to radiation and have longer life expectancy than adults. While radiation exposure is similar to that of catheter angiography, the radiation dose is much lower. Einstein et al (8) analyzed multiple studies and concluded that the mean effective dose using prospective gating, ranging from 0.5 to 1.8 mSv, is much lower than in conventional catheter angiography, which varies from 2.3 to 22.7 mSv. Additionally, the improvements in the CT equipment have allowed for higher quality images at lower doses. All modern CT scanners enable acquisition with less than 1 mSv of radiation exposure. Furthermore, the model-based iterative reconstruction algorithm reduces noise, thus enabling scanning with lower radiation exposure while maintaining image quality (9). Although there is a risk of contrast agent–induced nephropathy, the risk is less compared with catheter angiography. Potential reasons for this include the following: The volume of contrast agent used for CTA is usually lower than that for catheter angiography; patients who undergo CTA are usually less hemodynamically unstable than ones undergoing catheter angiography; and intra-arterial contrast agent injection in catheter angiography may

Abbreviations

ASO = arterial switch operation, BT = Blalock-Taussig, CTA = CT angiography, DORV = double-outlet right ventricle, D-TGA = D-loop TGA, ECG = electrocardiography, IAA = interrupted aortic arch, L-TGA = L-loop TGA, LVOT = left ventricular outflow tract, MAPCA = major aortopulmonary collateral artery, PA = pulmonary artery, PDA = patent ductus arteriosus, PS = pulmonary stenosis, PVR = pulmonary valve replacement, REV = réparation à l'etage ventriculaire, RV = right ventricle, RVOT = right ventricular outflow tract, TA = truncus arteriosus, TGA = transposition of the great arteries, TOF = tetralogy of Fallot, VSD = ventricular septal defect

Summary

CT is a useful, noninvasive imaging modality for the pre- and postoperative assessment of conotruncal anomalies.

Essentials

- The major conotruncal anomalies include tetralogy of Fallot, double-outlet right ventricle, transposition of the great arteries, truncus arteriosus, and interrupted aortic arch.
- CT is a useful, noninvasive imaging modality to help assess the preoperative anatomy and postoperative complications of conotruncal anomalies.
- Current generations of CT scanners made with the latest technologies, such as fast gantry rotation, high-pitch scanning, wider detector systems, automated tube voltage selection, tube current modulation, and three-dimensional printing, have revolutionized the role of CT in pre- and postoperative evaluation of congenital heart diseases.

Keywords

CT, CT Angiography, Stents, Pediatrics

incidentally cause atheroembolism, which is not expected to occur with intravenous contrast agent injection in CTA (10,11).

Furthermore, three-dimensional printed cardiovascular models using CT imaging techniques reproduce an accurate replica of the patient's anatomy, allowing surgical simulation and maneuvers to be performed as real operations. These advances have made CT an excellent imaging modality in pre- and postoperative evaluation of various congenital heart diseases, including conotruncal anomalies (12). In this article, we describe and illustrate the applications of CT imaging for evaluating major conotruncal anomalies, including TOF, DORV, TGA, TA, and IAA. The embryologic development, anatomy, surgical repair, and pre- and postoperative appearances are also described.

Embryologic Development

The outflow tract of the embryonic univentricular heart is called the conotruncus. The conotruncus comprises two myocardial subsegments, the conus and truncus. The conus is the myocardial segment between the atrioventricular and semilunar valves that develops into the right ventricular outflow tract (RVOT) and left ventricular outflow tract (LVOT). The truncus is the fibrous segment between the semilunar valves and aortic sac that develops into the great arteries (13). During embryonic development, proliferation of neural crest cells in the conus forms the aortopulmonary septum, which separates the aorta and pulmonary trunk. Similarly, the proliferation of neural crest cells in the truncus leads to the formation of cushions, which run throughout the conus in a spiral manner. These cushions form the primordium, which is necessary for the development of the arterial roots. Fusion across the central portion of the major cushions leaves two distinct valvar primordia, which subsequently develop semilunar valves. The distal margins of the cushions produce the valvar leaflets and their semilunar hinges. The proximal cushions fuse both the leaflets and their hinges with each other and the crest of the muscular ventricular septum (14). Developmental abnormalities of the conus arteriosus (infundibulum) and the truncus may result in stenosis or atresia (ie, TOF), abnormal ventriculoarterial alignments (ie, DORV), abnormal ventriculoarterial connections (ie, TGA), outlet septation defects (ie, TA), or outlet hypoplasia (IAA).

Protocol

Patient Preparation

The main challenges in pediatric cardiac CT are high heart rates, breath holding, and patient immobilization. Patient preparation is a prerequisite for successful scan acquisition. Detailed preprocedural patient assessment including age, body size indexes, cooperativity, oxygen saturation, renal function, and venous accessibility should be done by a qualified physician. Patient positioning at the isocenter of the CT gantry should be ensured to avoid image quality degradation and inappropriate high or low radiation exposure. An additional vacuum device or patient pad may be required for smaller children, as they are commonly positioned below the isocenter even at the highest CT table position. It is preferable to use radiolucent carbon electrocardiographic (ECG) leads for ECG-synchronized CT; if used, radiopaque leads should be placed outside the scan range (eg, on the arms and upper abdomen) to avoid artifacts. Both arms should be placed above the head for optimization of image quality and reduction of radiation dose. Patient immobilization is also very important. It not only reduces motion artifacts but also helps to reduce the amount of sedation needed. An inflatable cushion device can be helpful for immobilization; however, if not available, a blanket with bands may be used as an alternative. Infants younger than 6 months can be swaddled and scanned without sedation. Oral 25% dextrose solution and a pacifier may help to calm infants who are upset or uncooperative. However, to clearly visualize the coronary anatomy of the infant, administration of general anesthesia may be preferred to the feed-and-swaddle method. Patients aged 6 months to 3 years often require sedation to lie still in the scanner. Immobilization devices or video distraction are available for patients in this age group. Patients who are 4 to 6 years old can often cooperate without sedation. The presence of a parent in the room may be helpful. Similarly, most patients aged 7 years or older cooperate with scanning instructions. General anesthesia should be administered for young patients who cannot hold their breath for extended periods of time, particularly when data acquisition is done over several heartbeats (ie, detailed imaging of coronary arteries at higher heart rate and ventricular function measurement) (15).

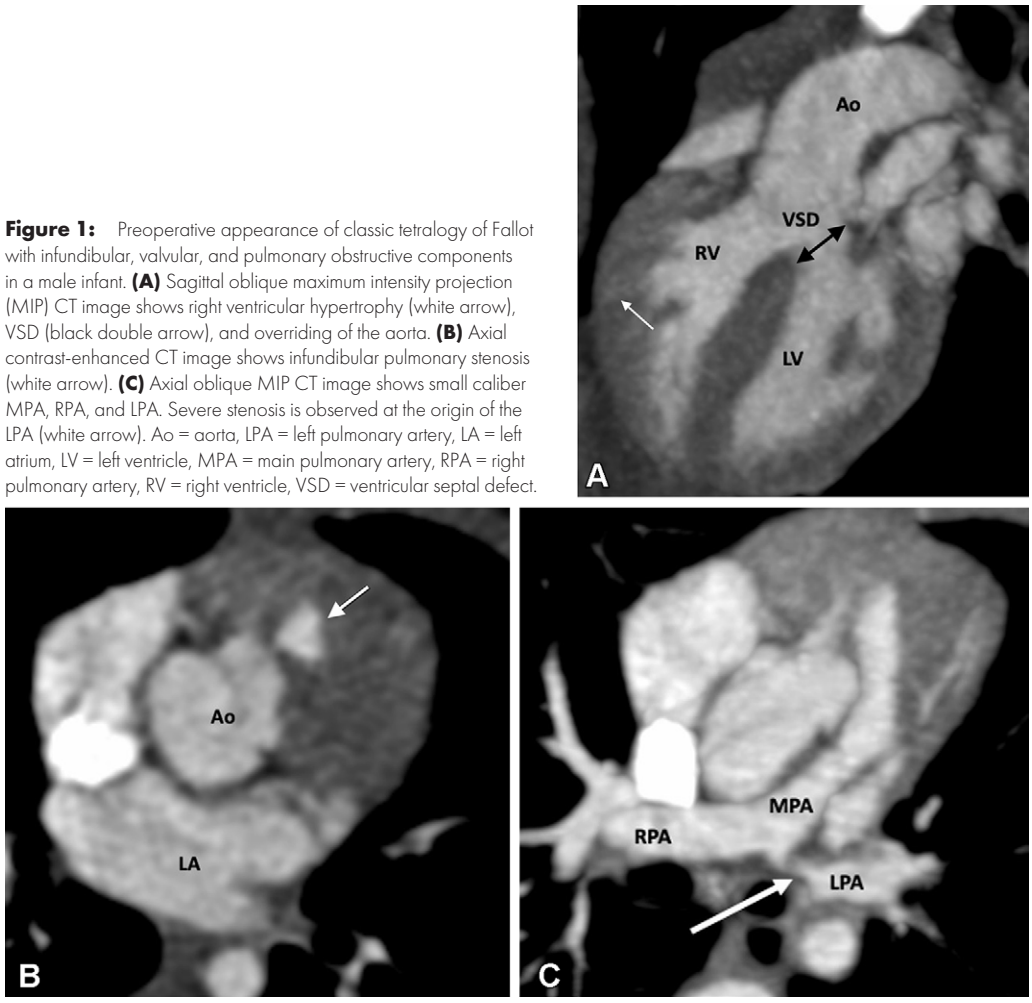

Figure 1: Preoperative appearance of classic tetralogy of Fallot with infundibular, valvular, and pulmonary obstructive components in a male infant. **(A)** Sagittal oblique maximum intensity projection (MIP) CT image shows right ventricular hypertrophy (white arrow), VSD (black double arrow), and overriding of the aorta. **(B)** Axial contrast-enhanced CT image shows infundibular pulmonary stenosis (white arrow). **(C)** Axial oblique MIP CT image shows small caliber MPA, RPA, and LPA. Severe stenosis is observed at the origin of the LPA (white arrow). Ao = aorta, LPA = left pulmonary artery, LA = left atrium, LV = left ventricle, MPA = main pulmonary artery, RPA = right pulmonary artery, RV = right ventricle, VSD = ventricular septal defect.

Image Acquisition

Sixty-four–section multidetector CT is the minimum requirement for obtaining optimum quality diagnostic images. Newer-generation technologies, such as the dual-source and wide-detector scanners, have improved temporal resolution, leading to reduced scan duration and fewer motion artifacts. The dual-energy scanner allows high-pitch scanning without missing data, with pitch values up to 3.4. Similarly, a 320- or 640-section 16-cm detector used with newborns and young children provides increased z-axis coverage, resulting in faster image acquisition in less than 0.3 second (16). Additionally, by reducing or eliminating overlapping helical imaging, both these techniques reduce radiation exposure by 60%–80% compared with 64-section CT. Furthermore, the reduced scan time obviates breath holding and sedation in neonates and infants (17,18).

Nonionic contrast agents are used because of their safe nature. The antecubital vein is the most preferred intravenous access site. The volume of intravenous contrast agent is calculated from body weight (1–2 mL per kilogram of body weight). The combined volume of contrast agent and saline flush kept at 2–3 mL per kilogram of body weight is generally well tolerated. The manual bolus tracking is the preferred method to trigger the scan. The monitoring sequence is planned at mid-heart level to allow simultaneous visualization of cardiac chambers and descending thoracic aorta, and the region of interest is indicated outside the body. The scan is initiated manually when the contrast agent is seen in all four chambers. The commonly used contrast agent injection technique is triphasic protocol, which includes two contrast agent injection methods. The first method is to inject half of the contrast agent volume at the usual arterial rate for patient size and the remainder at a slower rate, followed by a saline flush. In the second method, the injection rate is kept constant, and 100% contrast agent is injected in the first phase, followed by a contrast agent and saline mix (eg, 30:70 to 50:50 mix) in the second phase. Either method results in biventricular opacification (18,19).

There are two acquisition modes: non–ECG gated and ECG gated. ECG-gated acquisition modes can be prospective or retrospective. The main difference between prospective and retrospective modes is the timing of data acquisition with respect to cardiac cycle. In the prospective mode, the x-ray tube is turned on in a predefined phase of the cardiac cycle (ie, end systole [30%–40%] or end diastole [70%–80%]); while in the retrospective mode, tube current is on throughout the cardiac cycle (0%–100%). As image acquisition is performed within a

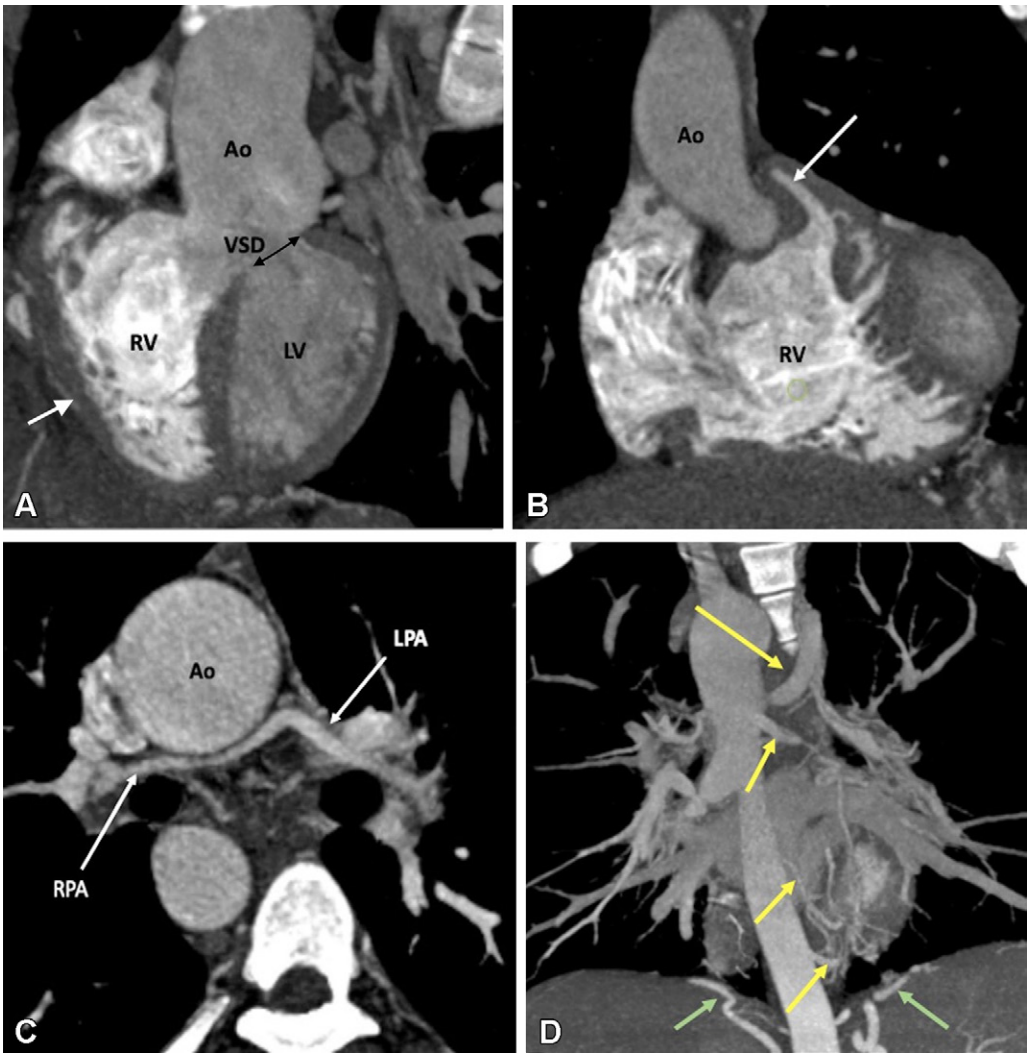

Figure 2: Preoperative appearance of tetralogy of Fallot with pulmonary atresia in a male infant. **(A)** Sagittal oblique maximum intensity projection (MIP) CT image shows right ventricular hypertrophy (white arrow), VSD (black double arrow), and overriding of the aorta. MPA is not visualized. **(B)** Coronal oblique MIP CT image shows pulmonary atresia (white arrow). **(C)** Axial oblique MIP CT image shows severe hypoplasia of the branch pulmonary arteries. MPA is absent. Thin but confluent branch pulmonary arteries produce the typical "seagull wing" appearance. White arrows indicate RPA and LPA. **(D)** Coronal oblique MIP CT image shows multiple MAPCAs arising from the descending thoracic aorta (yellow arrows) and upper abdominal aorta (green arrows). Ao = aorta, LPA = left pulmonary artery, LV = left ventricle, MAPCA = major aortopulmonary collateral artery, MPA = main pulmonary artery, RPA = right pulmonary artery, RV = right ventricle, VSD = ventricular septal defect.

limited time frame in the prospective mode, limited data sets are available for reconstruction; whereas, in the retrospective mode, acquisition is performed throughout the cardiac cycle, providing a large volume of data sets and hence, more flexibility for reconstructions. The main advantage of the prospective ECG-gated protocol is lower radiation dose, as x-ray exposure occurs during the selected cardiac phase only. Limitations of prospective gating include the requirement of low and regular heart rate and the lack of functional evaluation of left ventricle or cardiac valves.

The imaging sequence used is highly dependent on the clinical indication. In general, ECG-gated scans are required for evaluation of structures prone to cardiac motion artifact (intracardiac anatomy, coronary arteries, and the aortic root) and functional assessment. All other patients can be scanned with a nongated sequence, although image quality is often inferior to that obtained with ECG-gated sequences. However, higher-pitch or volumetric scan modes can provide higher quality images without ECG triggering because of rapid image acquisition. If available, these sequences can be used with all patients who do not require thin-section coronary artery evaluation (20).

Although low heart rate is a prerequisite for prospective ECG-triggered scanning, there are few studies demonstrating the role of a dual-energy prospectively triggered scan to generate diagnostic coronary imaging in pediatric patients with higher heart rates. Duan et al (21) evaluated the role of dual-source coronary CTA with 19 infants and children (age range, 3 months to 5 years; mean heart rate, 112 beats per minute [range, 83–141 beats per minute]) with coronary artery aneurysms due to Kawasaki disease using prospective ECG-triggering with

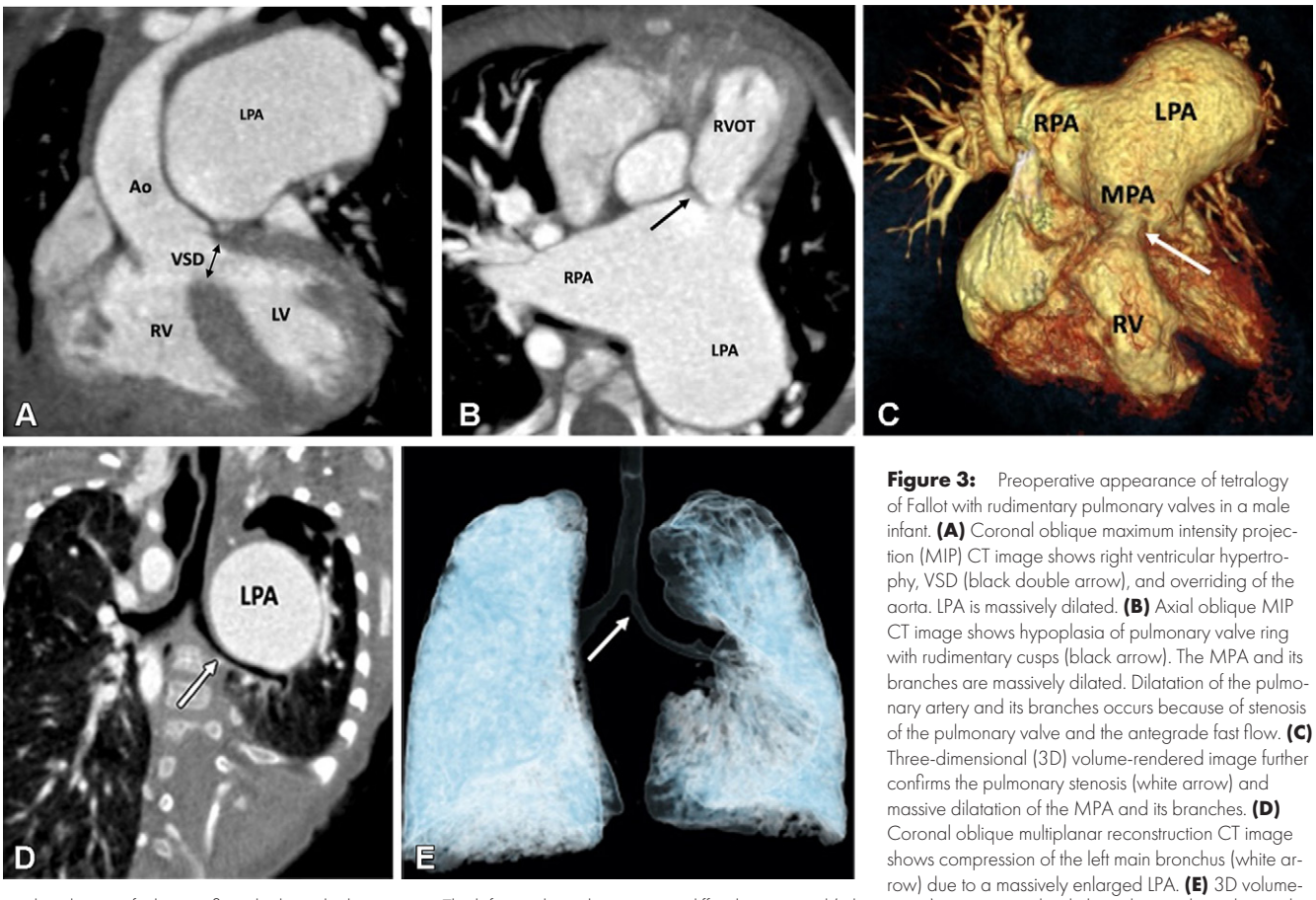

Figure 3: Preoperative appearance of tetralogy of Fallot with rudimentary pulmonary valves in a male infant. **(A)** Coronal oblique maximum intensity projection (MIP) CT image shows right ventricular hypertrophy, VSD (black double arrow), and overriding of the aorta. LPA is massively dilated. **(B)** Axial oblique MIP CT image shows hypoplasia of pulmonary valve ring with rudimentary cusps (black arrow). The MPA and its branches are massively dilated. Dilatation of the pulmonary artery and its branches occurs because of stenosis of the pulmonary valve and the antegrade fast flow. **(C)** Three-dimensional (3D) volume-rendered image further confirms the pulmonary stenosis (white arrow) and massive dilatation of the MPA and its branches. **(D)** Coronal oblique multiplanar reconstruction CT image shows compression of the left main bronchus (white arrow) due to a massively enlarged LPA. **(E)** 3D volume-rendered image further confirms the bronchial narrowing. The left main bronchus appears diffusely narrowed (white arrow) as compared with the right main bronchus, with focal stenosis in the osteoproximal part. Ao = aorta, LPA = left pulmonary artery, LV = left ventricle, MPA = main pulmonary artery, RPA = right pulmonary artery, RV = right ventricle, RVOT = right ventricular outflow tract, VSD = ventricular septal defect.

free breathing. The results showed excellent image quality and low radiation exposure. Similarly, Paul et al (22) showed that prospective ECG-gated dual-source CTA at end systole usually provides adequate thoracic and coronary artery image quality in neonates, infants, and young children with congenital heart defects, independent of heart rate.

The main disadvantage of the retrospective ECG-gated mode is the high radiation exposure in adults, which can be as high as 28 mSv per cardiac scan (23). This is, however, of less concern in infants, as the entire heart can be scanned using retrospective gating, with radiation exposure up to 2.17–3.14 mSv (24).

Furthermore, advancements in technology, such as high-pitch helical scanning, ECG-controlled tube current modulation, wider detector coverage, and iterative reconstruction techniques, have dramatically lowered radiation exposure (25–27). High-pitch dual-energy scanners use a pitch value of 3.4 to produce a table feed of 450 mm/sec with no overlapping data acquisition by filling the gaps in the data of the spiral acquisition of the first measurement system with the data from the second measurement system. The whole heart is completely scanned within one heart cycle (28). The tube current modulation technique optimizes the tube current with ECG. The x-ray tube is turned only in the predefined time points of prospective ECG triggering, allowing substantial reduction in radiation exposure (29). Furthermore, a 320- or 640-section 16-cm detector used with newborns and young children provides increased z-axis coverage, enabling volumetric imaging of the entire heart within one cardiac cycle, free of stair-step artifacts. It has not only improved the diagnostic performance of coronary CTA but has also lowered the radiation dose and volume of contrast material required (30). Recently, iterative reconstruction has emerged as a new method of image reconstruction. This technique enables reconstructing low-noise images from intrinsically noisy data, preserving the diagnostic image quality equivalent to current clinical standards (31). It is important to understand that iterative reconstruction does not reduce the radiation dose directly. Using iterative reconstruction, the radiologist can tolerate acquiring a noisier image data set, as the iterative reconstruction postprocessing reduces image noise. Therefore, radiation dose can be decreased by adjusting kilovolts and milliamperes or increasing pitch.

Patients with congenital heart defects may develop RV or LV failure and arrhythmia, necessitating the placement of electrophysiologic devices (32,33). These implanted metallic devices degrade MRI quality because of metal-induced susceptibility artifacts. Cardiac CT is a reasonable alternate modality for functional assessment in these patients. Studies have shown excellent correlation between cardiac CT and MRI for evaluating ventricular systolic function. CT has also been shown to be an

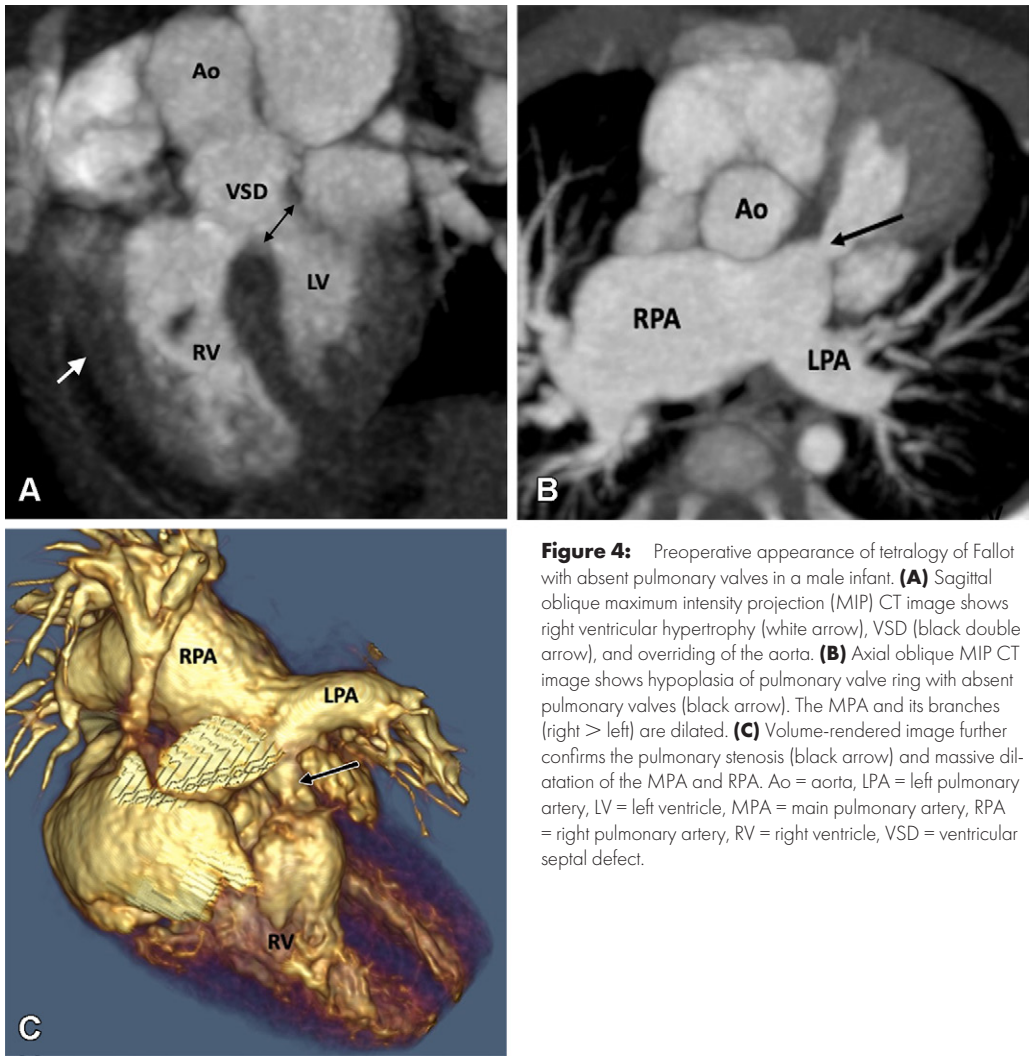

Figure 4: Preoperative appearance of tetralogy of Fallot with absent pulmonary valves in a male infant. **(A)** Sagittal oblique maximum intensity projection (MIP) CT image shows right ventricular hypertrophy (white arrow), VSD (black double arrow), and overriding of the aorta. **(B)** Axial oblique MIP CT image shows hypoplasia of pulmonary valve ring with absent pulmonary valves (black arrow). The MPA and its branches (right > left) are dilated. **(C)** Volume-rendered image further confirms the pulmonary stenosis (black arrow) and massive dilatation of the MPA and RPA. Ao = aorta, LPA = left pulmonary artery, LV = left ventricle, MPA = main pulmonary artery, RPA = right pulmonary artery, RV = right ventricle, VSD = ventricular septal defect.

excellent method for evaluating the function of prosthetic valves implanted in patients with congenital heart defects (34,35).

A meta-analysis of 27 studies (different study groups including coronary artery diseases, ischemic heart diseases, mitral regurgitation, heart transplantation, and ST-segment elevated myocardial infarction) using at least 64-section CT (15 studies comparing CT and transthoracic echocardiography and 12 studies comparing CT to MRI) showed no significant difference in LV ejection fraction between CT and cardiac MRI or between CT and transthoracic echocardiography (36). Studies have also demonstrated good correlation between cardiac CT and MRI-derived measurements of LV size, volume, and function at ejection fractions ranging from severely reduced to hyperdynamic function (30%–72%) and in patients with severe valvular disease or orthotopic heart transplant. There are no data on the effect of age and heart size on this agreement (37–39).

Postprocessing

Various image reformatting techniques, including maximum intensity projection, minimum intensity projection, linear or curved multiplanar reformation, shaded surface display, and volume rendering, are useful for processing depending upon the purpose. Maximum intensity projection is useful in evaluating the coronary arteries, shunts, and other cardiovascular structures. Minimum intensity projection is used to evaluate airway and lung parenchyma. Curved multiplanar reformation is used to evaluate curved structures such as the pulmonary and coronary arteries.

Characteristics of TOF

TOF is the most common cyanotic congenital disorder. It occurs in three of every 10 000 live births and accounts for 7%–10% of all congenital cardiac malformations (40). Embryologically, it is a cause-and-effect situation. The primary lesion in TOF is RVOT or pulmonary stenosis, which occurs because of anterior displacement of the septum. Because of RVOT or pulmonary valvular stenosis, the RV myocardium works harder, leading to RV hypertrophy. The increased RV pressure is reduced by a VSD, which acts as a pop-off valve. Furthermore, given the more-anterior positioning of the septum and large aortic diameter, the aorta overrides the VSD (41). The classic tetrad of TOF, as described by

Table 1: Checklist for Preoperative Assessment of TOF

RVOT
Obstruction (degree and level)
Pulmonary valves
Absent or hypoplastic and absent
Size of valvular ring
Pulmonary arteries
Present or absent
Confluent or discontinuous
Sizes: proximal and distal
Presence and degree of stenosis
Nakata index = ($\pi \times 2$)/diameter of pulmonary artery calculated in coronal plane at hilum just proximal to origin of first branch; normal measurements are around 330 $mm^2/m^2 \pm 30$
Source of pulmonary flow
PDA (unilateral or bilateral, size at both ends, insertional stenosis)
MAPCAs (origin, no., size, area of lung supplied, stenosis, course, and proximity to structures like veins and airways)
VSD
No., size, and site
Cardiac chambers
Enlargement or wall thickening
Systemic and pulmonary venous connections
Aorta
Aortic root
Arch (right or left sided)
Configuration of branch vessels
Coronary artery anatomy
Normal or anomalous origin
Any vessel coursing anterior to RVOT
Concomitant anomalies
Cardiac (ASD)
Aortic (right-sided aortic arch, aberrant subclavian artery, arch hypoplasia, and coarctation of aorta)
Anomalous systemic venous drainage (persistent left superior vena cava, retroaortic left brachiocephalic vein)
Anomalous pulmonary venous drainage (partial and total anomalous pulmonary venous return)
Tracheobronchial tree (atresia, pig bronchus), any vascular compression (site and level of compression)

Note.—ASD = atrial septal defect, MAPCA = major aortopulmonary collateral arteries, PDA = patent ductus arteriosus, RVOT = right ventricular outflow tract, TOF = tetralogy of Fallot, VSD = ventricular septal defect.

Table 2: Checklist for Postoperative Assessment of TOF

Status of RVOT
Residual or recurrent obstruction (degree and level)
Aneurysm (length, diameter, mass effect over nearby coronary artery or airway)
Pulmonary arteries
Residual or recurrent stenosis (site, severity)
VSD
Residual VSD (no., size, and site)
Cardiac chambers
Enlargement or wall thickening
Systemic and pulmonary venous connections
Evaluation of endovascular stents
Location, patency, and integrity
Stent related complications (pseudoaneurysms)
Aorta
Aortic root (dilatation, if any)

Note.—RVOT = right ventricle outflow tract, TOF = tetralogy of Fallot, VSD = ventricular septal defect.

Etienne-Louis Arthur Fallot, includes RVOT obstruction, RV hypertrophy, VSD, and overriding of the aorta. Mostly, the VSD is large, unrestrictive, and involves subaortic membranous septum. The extent of aortic overriding is variable. RVOT obstruction is an integral component of TOF. It is usually pronounced in the proximal region; however, it may occur at the pulmonary annulus, main PA, and/or its branches (Fig 1). The proximal PAs may be atretic, hypoplastic, or stenotic. Pulmonary valve involvement can vary from hypoplasia, thickened fused leaflets, and pulmonary stenosis to complete atresia (Figs 2, 3).

Pulmonary blood flow is dependent on the patent ductus arteriosus (PDA) when there is severe PA stenosis or atresia. Major aortopulmonary collateral arteries (MAPCAs) are another source of pulmonary blood flow that bring systemic blood flow to the PAs when RVOT is compromised. MAPCAs usually originate from the descending thoracic aorta and occasionally from the aortic arch or abdominal aorta. In rare cases, they may originate from other systemic arteries such as the carotid, subclavian, or coronary arteries. MAPCAs serve to supplement pulmonary blood supply along with smaller-sized PAs; however, in some patients, including those with TOF with pulmonary atresia, MAPCAs may be the sole blood supply to pulmonary circulation. MAPCAs gain access to the lungs through the hilum and connect with native PAs in the mediastinum, at lobar or subsegmental level. The structure of MAPCAs is highly complex, and they may undergo stenosis and complete occlusion during the course of disease (42). It is important to recognize MAPCAs early in patients with TOF, as these patients often require early surgical unifocalization of the MAPCAs, a Blalock-Taussig (BT) shunt, or RV-PA conduit.

TOF with absent pulmonary valve is a rare subtype of TOF that includes all the findings of TOF and an underdeveloped or total absence of pulmonary valve tissue. The pulmonary valve annulus is usually narrowed, and lack of pulmonary valve tissue generates severe pulmonary regurgitation. The to-and-fro blood flow across the RVOT produces substantial dilatation of the RV and the main and branch PAs. Patients will frequently present postnatally with respiratory distress secondary to severely dilated branch PAs, which may lead to extrinsic tracheal compression (Fig 4).

Multiple anomalies are associated with TOF. These could be related to the aortic arch (right sided, left sided, double aortic

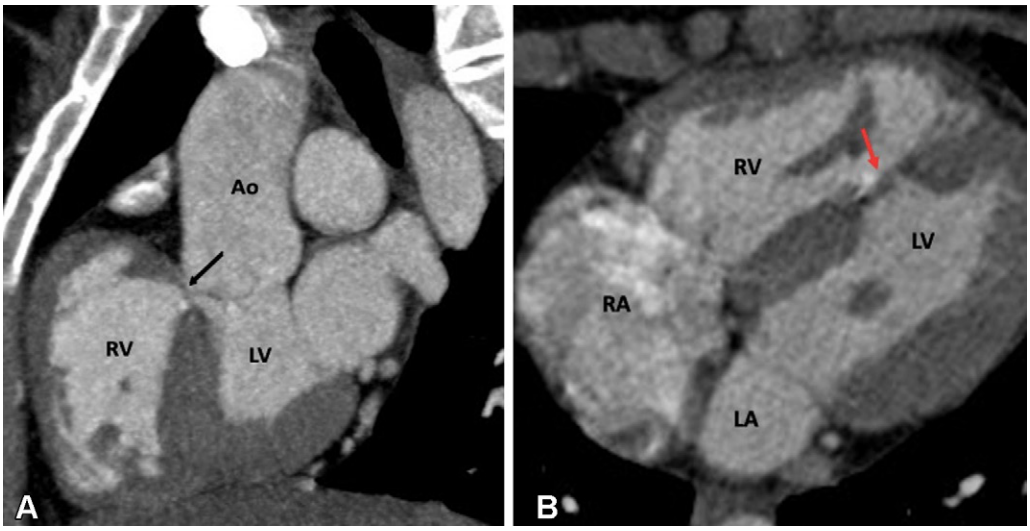

Figure 5: Postoperative appearance of tetralogy of Fallot after total correction in a 12-year-old boy. **(A)** Sagittal oblique and **(B)** axial maximum intensity projection CT images show perimembranous (black arrow in **A**) and mid muscular (red arrow in **B**) VSD patches. Ao = aorta, LA = left atrium, LV = left ventricle, RA = right atrium, RV = right ventricle, VSD = ventricular septal defect.

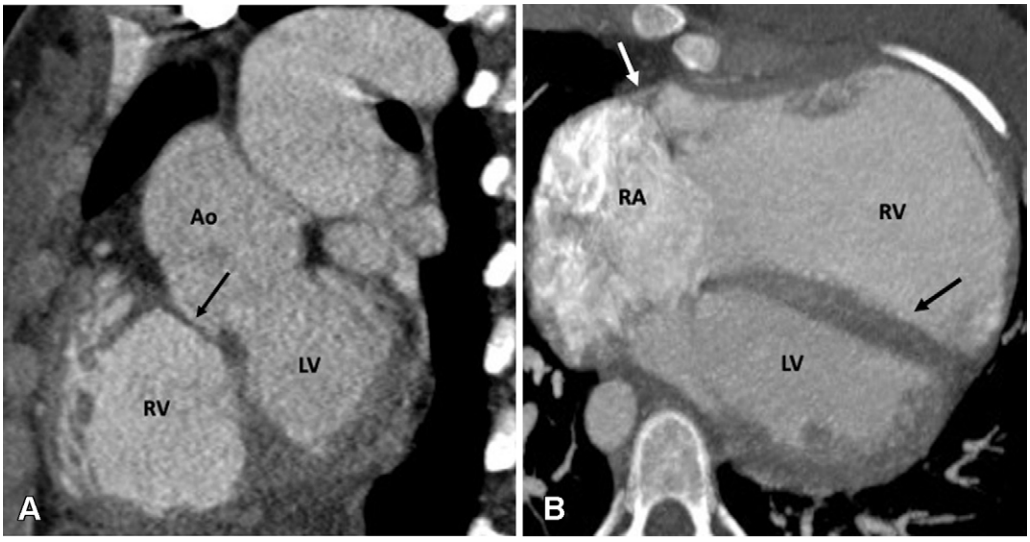

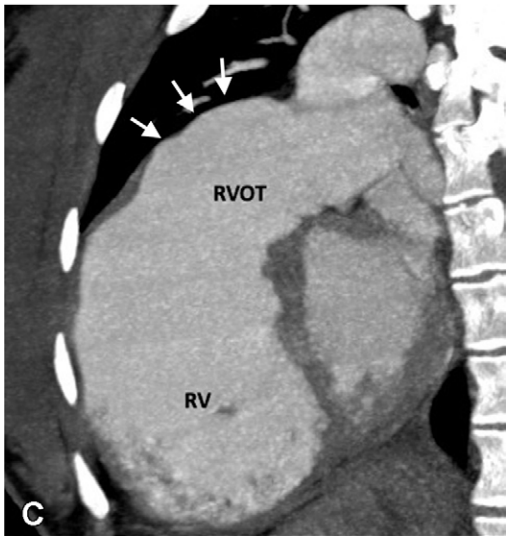

Figure 6: Postoperative appearance of tetralogy of Fallot after transannular patch repair in a 15-year-old boy. **(A)** Sagittal oblique maximum intensity projection (MIP) CT image shows a VSD patch (black arrow). **(B)** Axial oblique MIP CT image shows grossly dilated RA and RV. The severe degree of RV dilatation leads to abnormal orientation of the intraventricular septum (directed posteriorly) (black arrow) and narrowing of right atrioventricular groove (white arrow). **(C)** Sagittal oblique MIP CT image shows dilated RV and RVOT. The large caliber of the RVOT is due to the transannular patch (arrows), which is noncontractile, unlike the rest of the RV myocardium. Ao = aorta, LV = left ventricle, RA = right atrium, RV = right ventricle, RVOT = right ventricular outflow tract, VSD = ventricular septal defect.

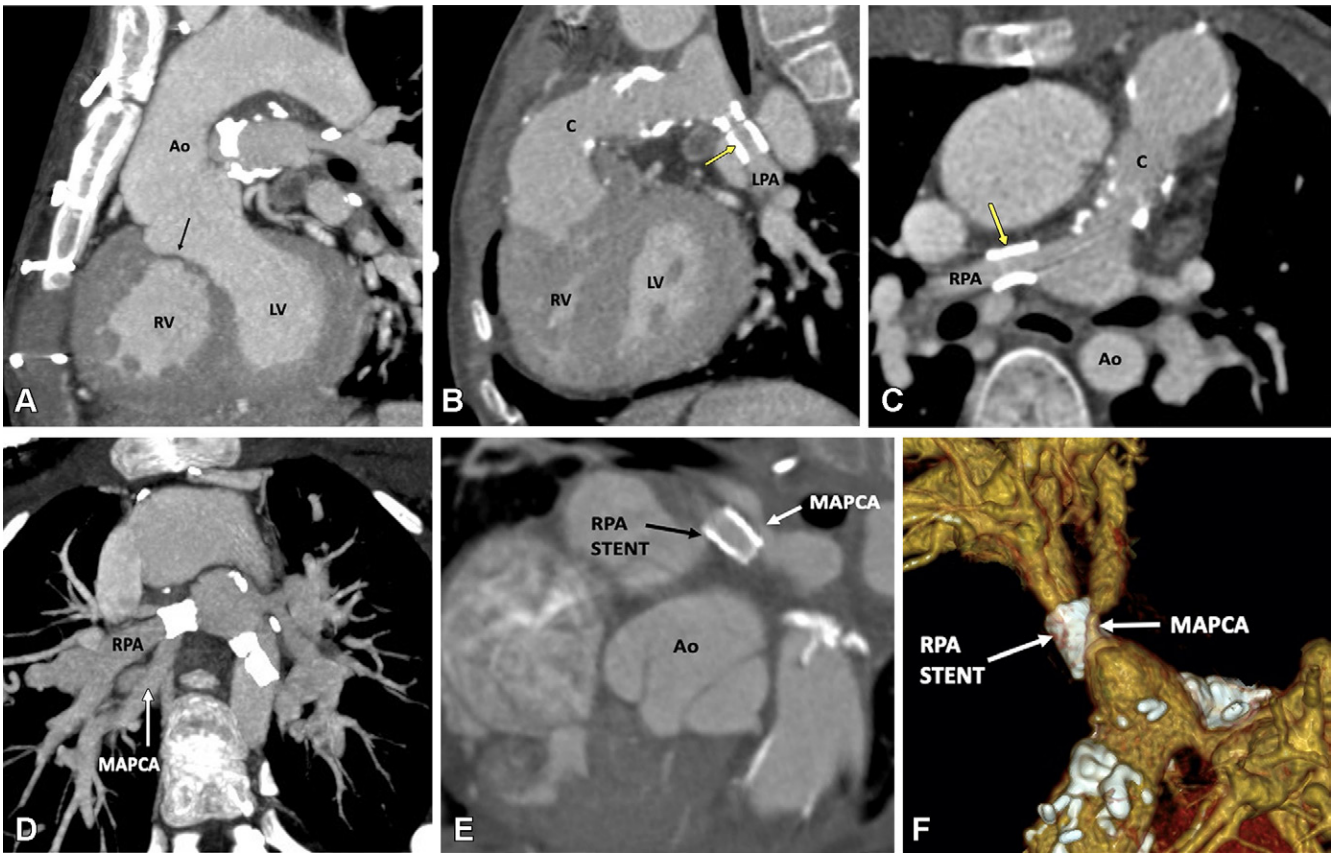

Figure 7: Postoperative appearance of tetralogy of Fallot with pulmonary atresia after RV-PA conduit (pulmonary homograft) repair, unifocalization of the MAPCAs, and angioplasty of the bilateral pulmonary arteries in a 14-year-old boy. **(A)** Sagittal oblique maximum intensity projection (MIP) CT image shows a VSD patch (black arrow). **(B)** Sagittal oblique and **(C)** axial oblique MIP CT images show RV-PA conduit with multifocal degenerative calcifications in conduit wall. Patent stents are observed in the LPA and RPA (yellow arrow). Stent placement was performed to relieve recurrent branch PA stenosis. **(D)** Axial oblique MIP CT image shows a stent in the osteoproximal RPA. Another good-sized vessel is observed arising from the RPA which has a unifocalized MAPCA attached to it (white arrow). **(E)** Sagittal oblique multiplanar reconstruction and **(F)** volume-rendered images show the origin of the unifocalized MAPCA (white arrow) just proximal to the RPA stent (black arrow in **E**, white arrow in **F**). Severe stenosis is noted in the osteoproximal segment of the unifocalized MAPCA. Ao = aorta, C = conduit, LPA = left PA, LV = left ventricle, MAPCA = major aortopulmonary collateral arteries, PA = pulmonary artery, RPA = right PA, RV = right ventricle, VSD = ventricular septal defect.

arch, and hypoplastic arch), systemic venous system (left-sided superior vena cava), pulmonary venous system (anomalous pulmonary venous drainage), and coronary arteries (anomalous origin of right coronary artery from PA, anomalous origin of left coronary artery from PA, coronary artery venous fistula, and left anterior descending artery dual course) (43).

Surgical Approach

The goal of surgery is to close the VSD and relieve RVOT obstruction. This can be done either as an early single-step reconstruction or staged reconstruction depending upon patient anatomy. Single-step reconstruction is usually performed during the 1st year of life. The prerequisites for single-step repair include large-caliber PAs, mild pulmonary stenosis, and good oxygen saturation. Reconstruction can be performed either by the transatrial-transpulmonary or transventricular approach. In the transatrial approach, VSD repair and subpulmonic resection are performed through right atrial incision, and pulmonary valvotomy, if needed, is done through pulmonary arteriotomy. This approach is helpful in preserving RV anatomy and function, as no incision is made on the RV wall (44). In the transventricular approach, the VSD is repaired by making an incision in the free wall of the infundibulum, which can be extended distal to the annulus. Thickened and stenotic leaflets are resected, and a transannular patch is placed to augment the RVOT. The transannular patch is made of autologous pericardial, dacron, or Gore-Tex fabric (expanded polytetrafluoroethylene membrane; W.L. Gore & Associates). It is sewn along the margin of the defect, increasing the diameter of the RVOT. The patch can be extended to the PA branches if they are narrow in caliber. Early surgical repair reduces hypoxia time and risk of cyanotic spells and sudden death. The prognosis of patients who have undergone surgical correction is excellent, with an early mortality rate of less than 2% (45).

Staged repair is required in patients with severely hypoplastic PAs and pulmonary atresia with extensive collaterization. The objectives of the staged approach are to restore the antegrade pulmonary flow, minimize the high-pressure collateral flow, and eventually close the intracardiac shunt. Staged correction includes palliative procedures during the neonatal period, followed by complete correction in later life. Palliative procedures are designed to increase the pulmonary arterial flow and include

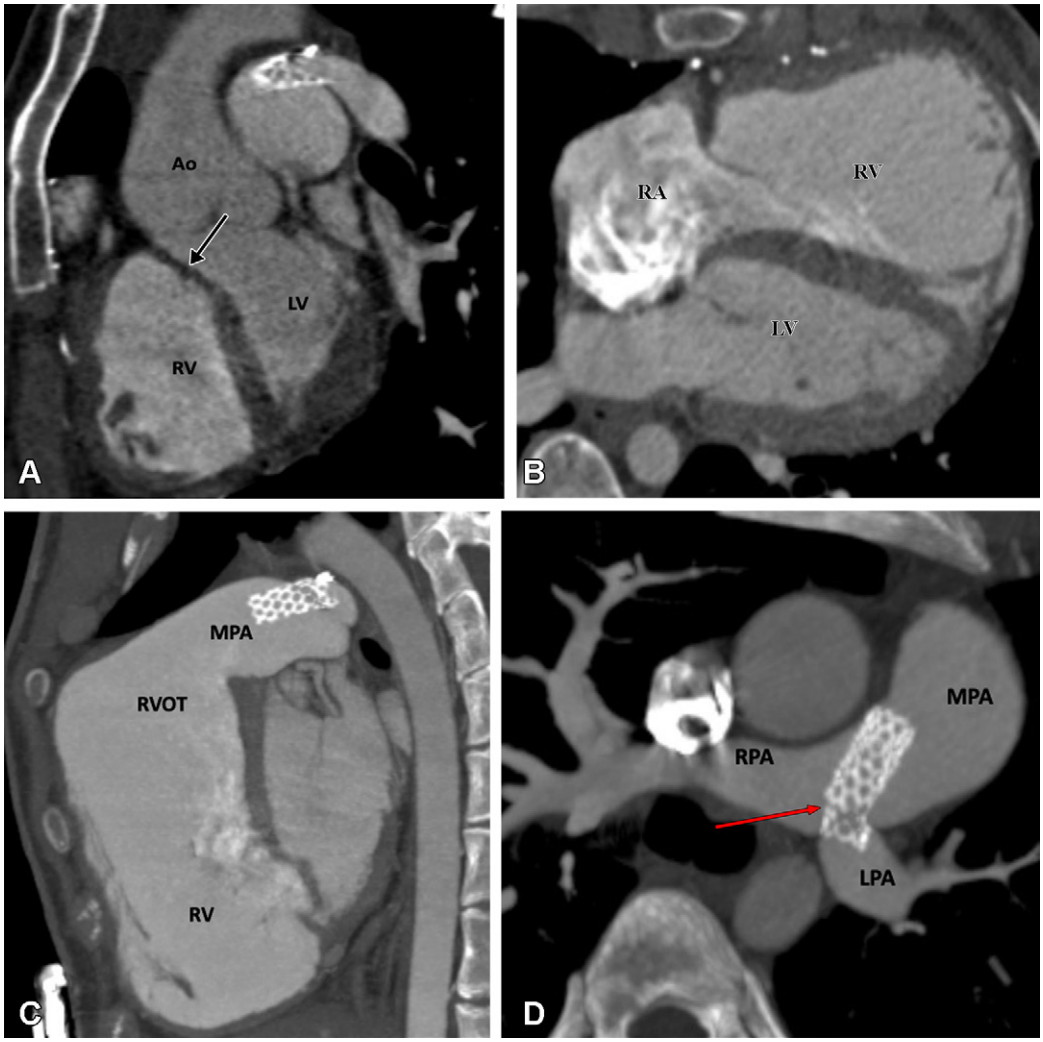

Figure 8: Postoperative appearance of tetralogy of Fallot after total correction and LPA stent placement in a 17-year-old girl. **(A)** Sagittal oblique maximum intensity projection (MIP) CT image shows a VSD patch (black arrow). **(B)** Axial oblique MIP CT image shows grossly dilated RA and RV. **(C)** Sagittal oblique MIP CT image shows dilated RV and RVOT. A patent stent is seen in the MPA extending into the LPA. Stent placement was performed to relieve recurrent LPA ostial stenosis. **(D)** Axial oblique MIP CT image shows a patent stent in the distal MPA extending into the LPA. There is proximal migration of the stent with fracture in stent scaffold integrity (red arrow), suggesting stent fracture. Ao = aorta, LPA = left pulmonary artery, LV = left ventricle, MPA = main pulmonary artery, RA = right atrium, RPA = right pulmonary artery, RV = right ventricle, RVOT = right ventricular outflow tract, VSD = ventricular septal defect.

balloon pulmonary valvuloplasty, RVOT stent placement, and the creation of a BT shunt. The original BT shunt involves scarification of the subclavian artery with distal ligation and end-to-side anastomosis of the proximal part with ipsilateral PA. Nowadays, a modified BT shunt is made using a synthetic graft, usually Gore-Tex, to connect the subclavian artery with the ipsilateral PA. It is important to understand that the BT shunt is an arterial shunt made between a systemic artery (subclavian) and PA. This is in contrast to the bidirectional Glenn shunt, a venous pressure shunt, in which the distal end of the superior vena cava (a systemic vein) is ligated, and the proximal part is anastomosed with the right PA to improve lung perfusion. The Glenn procedure, performed in the functional single ventricle of patients with tricuspid atresia, serves to redirect systemic venous blood to the pulmonary circulation, bypassing the right side of the heart. The Sano shunt is another palliative repair that involves placement of an extracardiac conduit between the RV and main PA stump. This technique prevents the reduction of diastolic blood flow into the coronary arteries (coronary steal phenomenon), an outcome that is associated with the BT shunt (46).

All these palliative repairs require complete correction in later life. If there is pulmonary atresia, an extracardiac conduit is placed from the anterior RV wall to the PAs, which can be augmented using a patch. The conduits may be synthetic or biologic and are usually valved. If the MAPCAs are large, the patient may develop signs of heart failure secondary to high-pressure arterial flow in the unprotected pulmonary vascular bed. For these patients, coil embolization of MAPCAs must be performed to prevent the delivery of systemic blood flow to the lungs. However, if the MAPCAs are supplying a substantial volume of bronchopulmonary segments, it is essential to preserve them. This is done by using a procedure called unifocalization, in which MAPCAs are

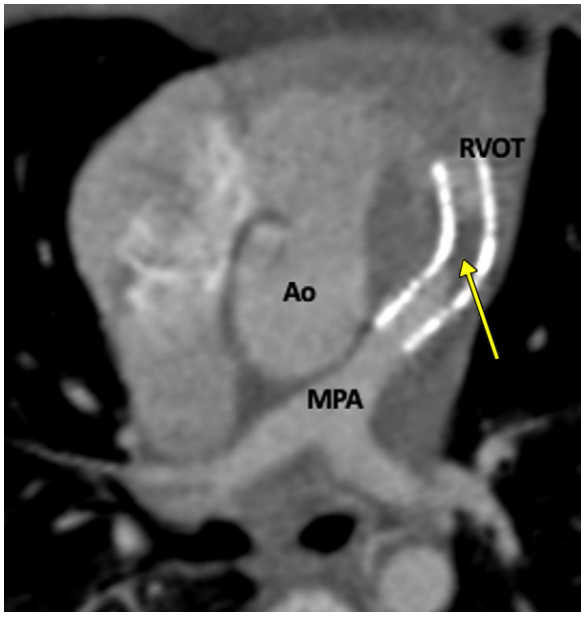

Figure 9: Postprocedural appearance of tetralogy of Fallot after RVOT stent palliation in a 1-year-old boy. Axial oblique contrast-enhanced CT image shows a stent in the RVOT extending into the MPA. A thrombus is observed in the stent (yellow arrow). Ao = aorta, MPA = main pulmonary artery, RVOT = right ventricular outflow tract.

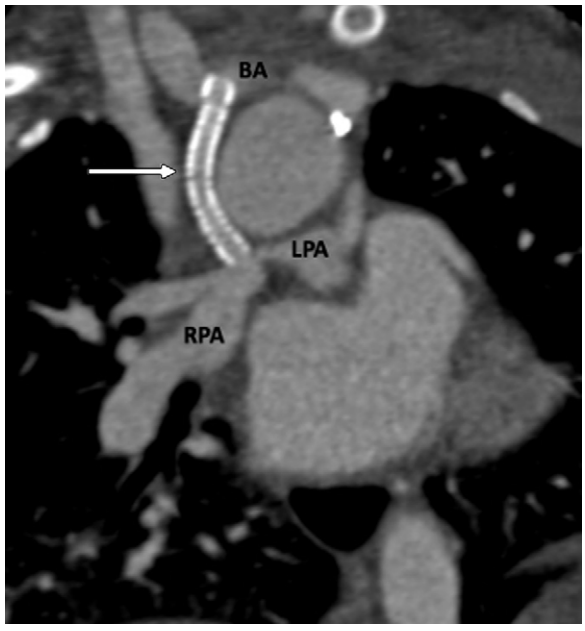

Figure 10: Postprocedural appearance of tetralogy of Fallot after modified BT shunt at birth followed by stent placement in a 2-month-old male infant. Coronal oblique contrast-enhanced CT image shows a patent stent (white arrow) in the right modified BT shunt, made between the right brachiocephalic artery and right pulmonary artery at birth. The shunt underwent stenosis, which was relieved by stent placement. The stent scaffold appears intact, and there is uniform contrast agent opacification of the stent without any stenosis or thrombosis. BA = brachiocephalic artery, BT = Blalock-Taussig, LPA = left pulmonary artery, RPA = right pulmonary artery.

Figure 11: Postprocedural appearance of tetralogy of Fallot after modified BT shunt at birth followed by stent placement in a 3-month-old female infant. Coronal oblique contrast-enhanced CT image shows a stent (white arrow) in the modified BT shunt, which was made between the RSA and RPA at birth. The stent was placed to relieve stenosis of the BT shunt. The stent appears thrombosed and shows severe stenosis at the subclavian end. BT = Blalock-Taussig, RPA = right pulmonary artery, RSA = right subclavian artery.

detached from the aorta and connected to the PAs (47). Historically, several surgical approaches for unifocalization have been proposed, but the single-stage approach is the preferred method. During single-stage unifocalization, MAPCAs are identified in the posterior mediastinum between the carina and roof of the left atrium. Unifocalization involves the dissection of MAPCAs from the aorta and a tissue-to-tissue anastomosis with the PA, with the anastomotic orifice made as long and large as possible. In patients who lack a central PA, the central PA should be reconstructed from MAPCA tissue and additional materials (48).

The most common postoperative complication of RVOT resection is free pulmonary regurgitation, which eventually leads to RV dilatation, dysfunction, and subsequent tricuspid regurgitation in advanced stages. Common postoperative complications of an RV-PA conduit include conduit stenosis and regurgitation of the conduit valve. Degeneration of a valved conduit is expected to occur in most conduits within 10 years of the surgical procedure (49). Multiple RV-PA conduit revisions are required in patients who survived to adulthood, with many replacements during adolescence. Studies have shown that 56% of conduit replacements occurred in patients aged 9 to 18 years, with many patients requiring second, third, or even fourth conduit replacements. Conduit failure is related to somatic outgrowth in young patients and progressive conduit calcification resulting in stenosis and/or regurgitation (50). Large follow-up studies of patients with bioprosthetic conduits have shown freedom from conduit replacement in 68%–95% of patients at 5 years and in 0%–59% at 10 years (51–53).

Other known postoperative complications include VSD patch leak, residual RVOT obstruction, residual or recurrent branch PA stenosis, aortic root dilatation, and residual aortopulmonary collaterals (54). Approximately 50% of patients who survive TOF

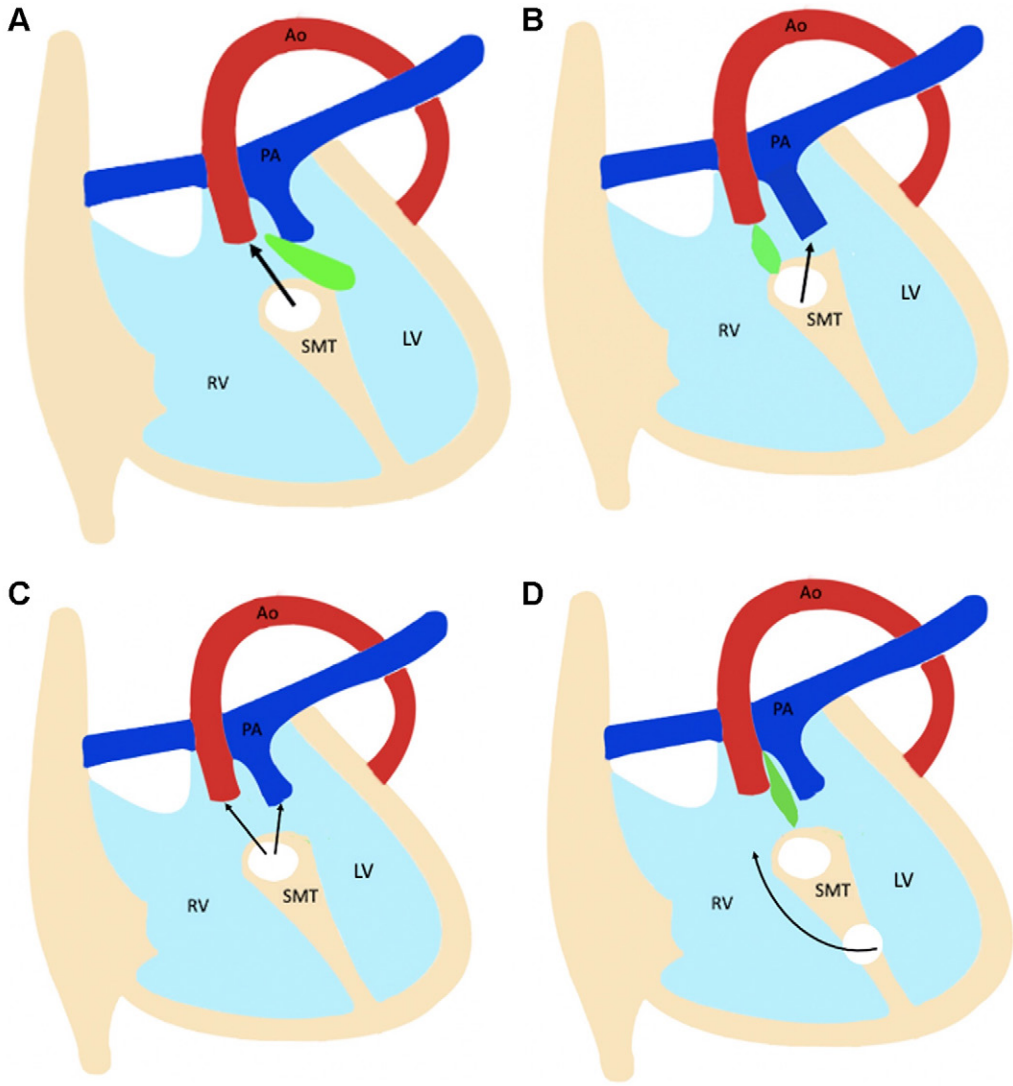

Figure 12: Diagram shows four types of ventricular septal defect (VSD). The relationship between the outlet septum (green) and septomarginal trabecula (SMT) defines the location of the VSD. **(A)** The outlet septum attaches to the anterior limb of the septal band, resulting in a subaortic VSD. **(B)** The outlet septum attaches to the posterior limb of the septal band, resulting in a subpulmonic VSD. **(C)** In the doubly committed VSD, the outlet septum is absent. **(D)** A remote VSD is not related to the outlet septum, and the distance between the VSD and semilunar valve is greater than the size of the aortic valve. Ao = aorta, LV = left ventricle, PA = pulmonary artery, RV = right ventricle.

repair undergo reoperation within 30 years, with pulmonary valve replacement (PVR) being the most common reoperation (55). Surgical PVR and percutaneous PV intervention are techniques with specific advantages and disadvantages. The open surgical procedure allows for concurrent surgical reshaping of the RVOT and PA. Residual VSDs and aortic root dilatation can also be addressed at the time of surgery. Percutaneous PVR has proven to be a safe and effective nonsurgical therapeutic alternative generally performed under general anesthesia through femoral, jugular, or subclavian vein access (56). Previous studies that analyzed pre-PVR markers of post-PVR normalization of ventricular size and/or function propose PVR in symptomatic and asymptomatic patients with moderate or severe pulmonary regurgitation and at least one (for moderate) or two (for severe) of the following quantitative criteria: end-diastolic volume greater than 150 mL/m^2 or z score greater than 4; RV end-systolic volume greater than 80 mL/m^2; RV ejection fraction less than 55%; large RVOT aneurysm; QRS greater than 160 msec; and sustained tachyarrhythmia related to right side of the heart volume load or the presence of other hemodynamically significant lesions (57,58).

Role of CT Imaging in TOF

CTA is helpful in both pre- and postoperative assessment of TOF. The main role of preoperative imaging is to delineate the status of the RVOT, PV, and main and branch PAs, including size and continuity, and any extra RV source of pulmonary blood flow (PDA or MAPCAs). It is important to identify the lung segments supplied by each MAPCA. This can help sur-

Table 3: Checklist for Preoperative Assessment of DORV

Status of great vessels
Degree of ventriculoarterial discordance (>150% or 200%)
VSD
No., size, and site
Relationship to great vessels (subaortic, subpulmonary, doubly committed, remote)
Relationship to tricuspid annulus
Conus
Location (subpulmonic only, bilateral)
Conus length
Aortomitral continuity
Present or absent
Great vessel relationship
Side by side or dextroposed or levoposed
Cardiac chambers
Enlargement or wall thickening
Systemic and pulmonary venous connections
Status of outflow tracts
LVOT (any obstruction, usually seen in subpulmonic VSD; subaortic stenosis; any hypertrophied muscle band)
RVOT (any obstruction, usually seen in subaortic VSD; any hypertrophied muscle band)
Pulmonary valve and pulmonary arteries
Pulmonary hypoplasia, atresia
Main or branch pulmonary artery stenosis
DORV variant
TOF type, VSD type, TGA type, or univentricular heart type
Coronary artery anatomy
Normal or anomalous origin
Any vessel coursing anterior to RVOT
Concomitant anomalies
Cardiac (ASD)
Aortic (right-sided aortic arch, aberrant subclavian artery, arch hypoplasia, and coarctation of aorta)
Anomalous systemic venous drainage (persistent left superior vena cava, retroaortic left brachiocephalic vein)
Anomalous pulmonary venous drainage (partial and total anomalous pulmonary venous return)
Tracheobronchial tree (atresia, pig bronchus), any vascular compression (site and level of compression)

Note.—ASD = atrial septal defect, DORV = double-outlet right ventricle, LVOT = left ventricular outflow tract, RVOT = right ventricular outflow tract, TGA = transposition of great arteries, TOF = tetralogy of Follet, VSD = ventricular septal defect.

geons decide if they need to unifocalize each vessel or if contribution of MAPCAs to pulmonary blood flow is minor and can be ignored. The degree of pulmonary hypoplasia can be established by Nakata index. While typically used in conventional angiography, it can be transposed to CTA. The diameter of the PA is calculated in a coronal plane at the hilum, just proximal to the origin of the first branch, using the following equation: $(\pi \times 2)$/diameter/body surface area. Normal measurements are around 330 $mm^2/m^2 \pm 30$. Generally, patients with a Nakata index greater than 100 mm^2/m^2 undergo complete correction with better survival (59).

Evaluation of the coronary arteries is another essential step in preoperative assessment of TOF. TOF is known to be associated with various coronary anomalies, with a reported prevalence of 2%–23%. A meta-analysis showed that 6% of patients with TOF have an anomalous coronary artery, with 72% crossing anterior to RVOT and the majority of the remaining (28%) crossing behind the aorta. The common anomalous patterns included duplicated left anterior descending artery (one left anterior descending artery coming from the right coronary artery and another from the left main artery), large conus artery, anomalous origin of the right or left coronary arteries from the PA, and coronary arteriovenous fistulas. It is important to define the coronary anatomy before surgery, as it can change the surgical approach. For example, if the anomalous right coronary artery or a prominent conal branch of the right coronary artery is seen coursing anterior to the infundibulum, then an RV-PA conduit should be performed instead of an infundibulectomy with transannular patch to avoid any ischemic myocardial damage due to vascular injury (60). A thorough report should describe all the relevant findings described above. The checklist followed at our institution is given in Table 1.

Most patients who undergo single-stage cardiac repair do not have postoperative complications and remain asymptomatic for 10–30 years. Studies have shown a survival rate of 96% following complete repair (61). Common postoperative complications include pulmonary regurgitation, RVOT dilatation, RVOT aneurysm and pseudoaneurysm, recurrent VSD, residual or recurrent RVOT stenosis, and residual or recurrent PA stenosis (Table 2). Imaging is also indicated for evaluation of stents and the RV-PA conduit (62). There is no reference value of normal RVOT diameter at CT; however, a diameter greater than 27 mm at end diastole is considered RVOT dilatation at echocardiography (63). RVOT aneurysm represents dyskinesia of the RVOT during systole and is therefore used as a synonym of RVOT dyskinesia only. It is described as an outward movement of the RVOT during the systolic phase of the ventricular wall or its reconstructed outflow tract (64). While an aneurysm (dyskinesia) represents diffuse dilatation of the RVOT, pseudoaneurysm appears as a narrow neck outpouching that arises from the site of RVOT reconstruction or anastomosis.

Pulmonary regurgitation is the most common late-onset complication of TOF repair. Chronic RV dilatation also acts as an arrhythmogenic substrate, especially in patients with prolonged QRS complex at rest (65). Timely PVR prevents irreversible RV wall changes and can reduce the incidence of ventricular arrhythmias. RV dilatation is the major determining criterion for PVR (Fig 5). Although cardiac MRI is the reference standard for volume quantification, CT can also measure it accurately. Retrospective ECG-gated cardiac CT allows comprehensive analysis of biventricular volume and function and qualitative assessment of wall motion abnormalities, with excellent correlation with cardiac MRI, and is especially useful if MRI is contraindicated (66,67). Raman et al (68) have demonstrated that

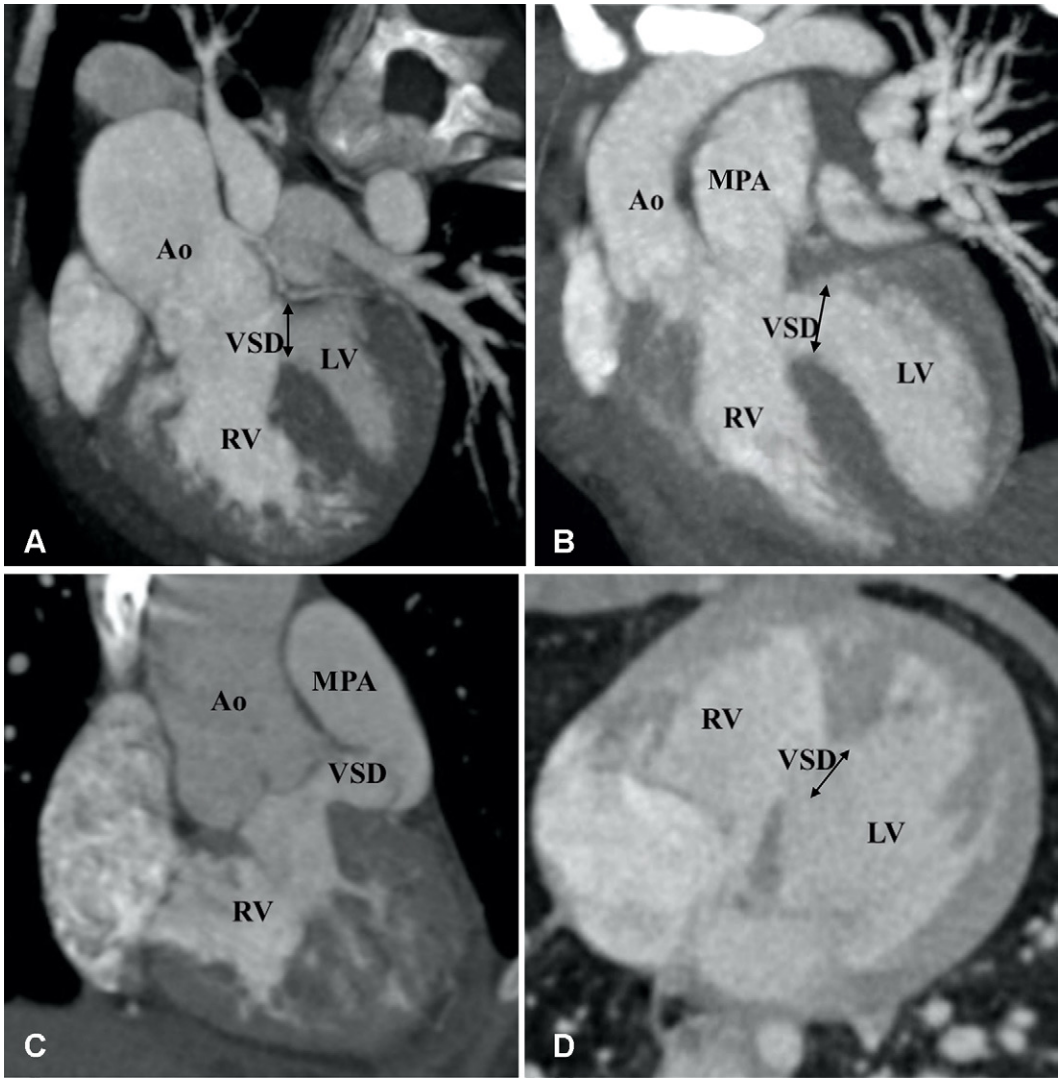

Figure 13: Types of ventricular septal defects (VSDs). **(A)** Subaortic VSD (double arrow) in a 1-year-old boy with double-outlet right ventricle (DORV). Reformatted coronal maximum intensity projection (MIP) CT image shows greater than 50% aortic overriding. The pulmonary valve and MPA were severely stenotic (not shown). **(B)** Subpulmonic VSD (double arrow) in a 2-year-old boy with DORV. Reformatted coronal MIP CT image shows the origin of both great vessels from the RV. **(C)** Doubly committed VSD in a 2-year-old girl with DORV. Reformatted coronal MIP CT image shows the origin of both great vessels from the RV. VSD is closely related to both the semilunar valves (doubly committed). **(D)** Remote VSD (double arrow) in an infant with DORV. Axial MIP CT image shows remote intramuscular VSD. Ao = aorta, LV = left ventricle, MPA = main pulmonary artery, RV = right ventricle.

multidetector CT shows comparable results to cardiac MRI in helping assess RV size and function. Xu et al (69) investigated the accuracy and feasibility of CT in quantification of ventricular volume on the basis of semiautomatic three-dimensional threshold-based segmentation in porcine hearts and children with TOF. Twenty-three children diagnosed with TOF were retrospectively included. Ventricular volumetric parameters were assessed with cardiac CT before and 6 months after surgery. The authors concluded that CT is able to help accurately assess both right and left ventricular volumetric parameters on the basis of semiautomatic three-dimensional threshold-based segmentation in children with TOF (69). Like cardiac MRI, the semiautomated software outlines the endocardial borders in the end-systolic and end-diastolic phases, and the cardiac chamber volumes, including ejection fraction, are calculated automatically. Retrospective ECG-gated scans also allow analysis of wall motion abnormalities, which are commonly seen with altered RV mechanics.

RVOT aneurysm is an independent predictor of systolic dysfunction and RV dilatation, besides providing substrate for ventricular arrhythmias (70). Extreme myectomy and transannular patching are the contributing factors to its formation. CTA allows precise depiction of the size and length of the aneurysm (Fig 6). Bulging of the RVOT, mainly during systole, is a characteristic feature of RVOT aneurysm (71). Recurrent VSD is another concern following TOF repair and may require patients to undergo further interventions depending on the shunt fraction. CT is a reliable method for assessing the size and location of recurrent VSD. The overall reported incidence of residual or recurrent PA stenosis is 10%–15% (65). Stenosis may involve the main or branch PAs. Branch PA stenosis usually develops at the site of prior BT shunt insertion secondary to scarring. CT can

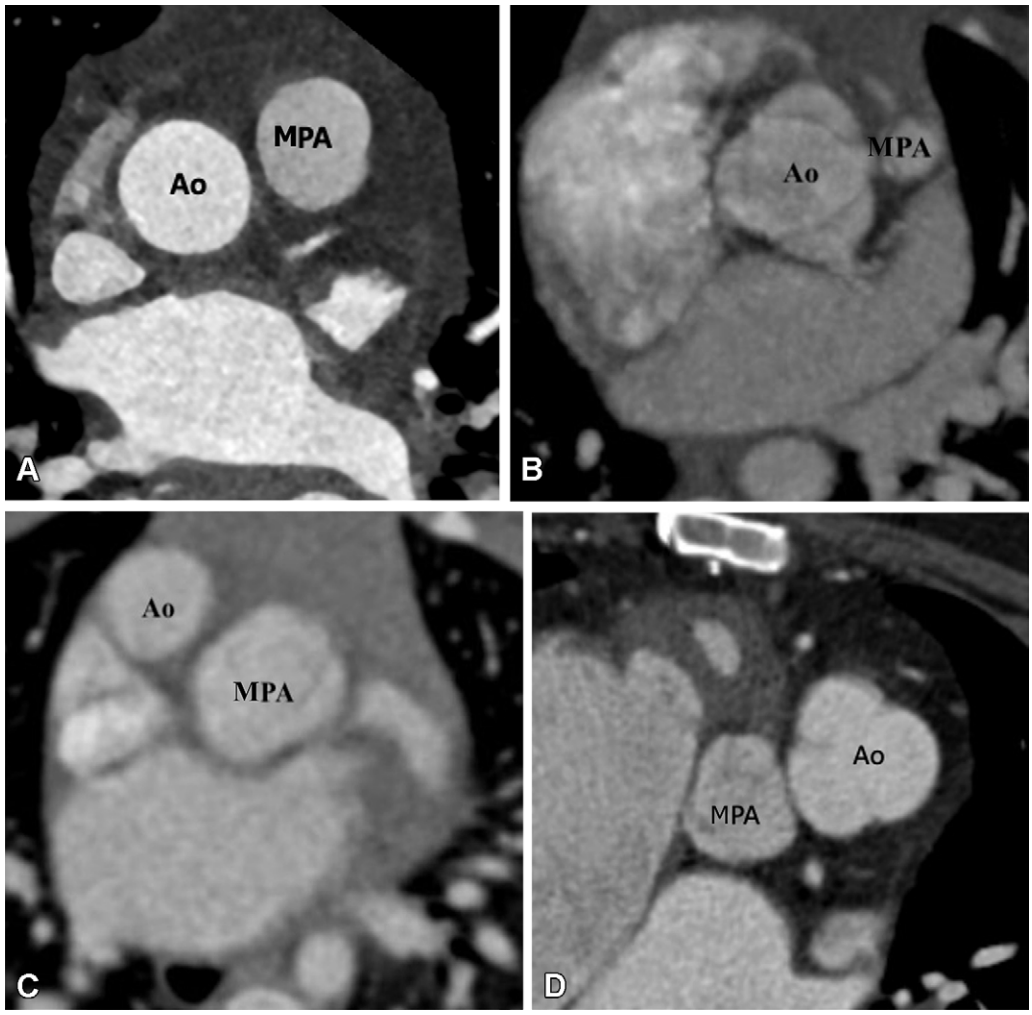

Figure 14: Great vessels relationship. **(A)** Normal great vessels relationship in a 25-year-old healthy man. Axial contrast-enhanced CT image shows the ascending aorta is in a position posterior and to the right of the pulmonary artery. **(B)** Normal relationship in a 2-year-old boy with TOF-type DORV. Axial maximum intensity projection (MIP) CT image shows the ascending aorta in a position posterior and to the right of the pulmonary artery. Pulmonary stenosis is observed, which is a common feature of TOF-type DORV. **(C)** Dextrotransposition in a 1.5-year-old girl with TGA-type DORV. Axial MIP CT image shows the ascending aorta in a position anterior and to the right of the MPA. **(D)** Levotransposition in a 2-year-old girl with TGA-type DORV. Axial MIP CT image shows the ascending aorta in a position anterior and to the left of the pulmonary artery. Ao = aorta, DORV = double-outlet right ventricle, MPA = main pulmonary artery, TGA = transposition of the great arteries, TOF = tetralogy of Fallot.

clearly delineate stenosis of the main or branch PAs and provide information about site, severity, length, and associated findings (angulation or distortion).

The evaluation of endovascular stents, stented bioprosthetic valves, and implanted devices (pacemaker, intracardiac defibrillators, and occluder devices) are other important indications for CT imaging. Endovascular stents are frequently deployed to treat branch pulmonary stenosis (Figs 7, 8). RVOT stent implantation is done as a palliative procedure in neonates or young infants to relieve RVOT obstruction (Fig 9) (72). CT can help identify any abnormal stent position, stent thrombosis, stent fracture, and pseudoaneurysm formation (Figs 10, 11). Furthermore, complications, such as endocarditis and thrombosis, related to stented bioprosthetic valves used in PVR are well visualized at CT. Implanted devices produce a lot of artifacts at cardiac MRI (73). Although there is a growing body of evidence that cardiac MRI can be performed in patients with implanted devices, there are many restrictions, including high production of imaging artifacts; therefore, CT is the primary imaging modality for evaluation of implanted devices (74).

Some patients with corrected TOF require multiple PVRs due to disease progression and ventricular dysfunction. Common indications of PVR include presence of exercise intolerance, syncope due to arrhythmias, signs of heart failure, and pulmonary regurgitation fraction greater than or equal to 25%. The proposed indications for PVR in asymptomatic patients with this pulmonary regurgitation fraction include the following: RV-indexed end-systolic volume greater than 80 mL/m^2; RV-indexed end-diastolic volume greater than 150 mL/m^2; LV ejection fraction less than 55%; RV ejection fraction less than 47%; moderate tricuspid regurgitation; RVOT obstruction; large RVOT aneurysm; severe branch PA stenosis; sustained

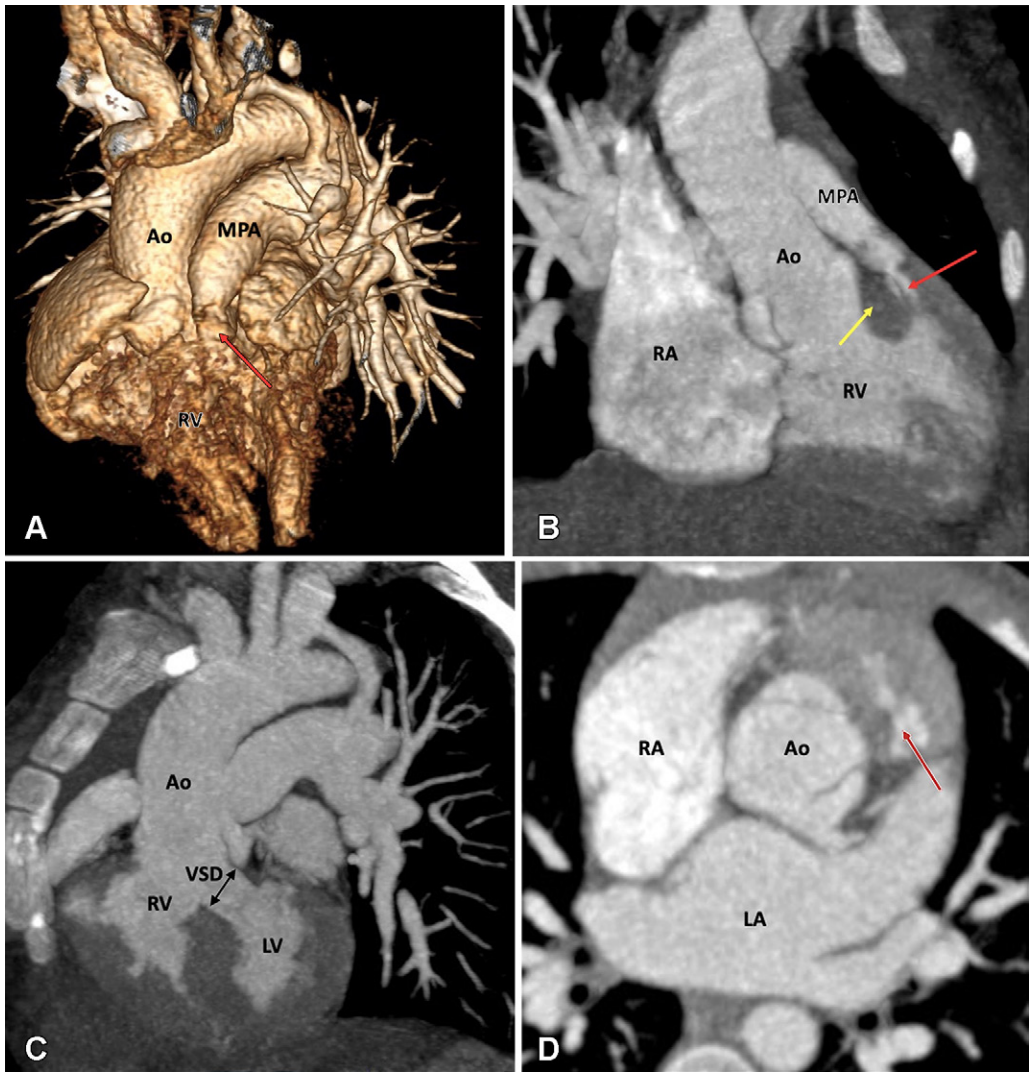

Figure 15: Preoperative appearance of TOF-type DORV in a 2-month-old male infant. **(A)** Volume-rendered image and **(B)** coronal oblique maximum intensity projection (MIP) CT image show the great arteries arising from the RV. Severe pulmonary stenosis is seen (red arrow). Note the subpulmonic conus (yellow arrow in **B**). **(C)** Sagittal MIP CT image shows the subaortic VSD (black double arrow). **(D)** Axial reformatted MIP CT image shows the normal relationship of the great vessels; the aorta is situated posterior and rightward to the pulmonary trunk. There is hypertrophy of the pulmonic infundibulum, causing severe RVOT stenosis (red arrow). Ao = aorta, DORV = double-outlet right ventricle, LA = left atrium, LV = left ventricle, MPA = main pulmonary artery, RA = right atrium, RV = right ventricle, RVOT = right ventricular outflow tract, TOF = tetralogy of Fallot, VSD = ventricular septal defect.

tachyarrhythmia; QRS duration at ECG longer than 160 msec; and residual VSD with relative pulmonary-to-systemic flow ratio (ie, Qp:Qs ratio) greater than or equal to 1.5 (75). CT imaging also provides detailed anatomic assessment before subcutaneous PVR. Multiplanar reformats allow for precise measurement of the cross-sectional area of the RVOT and valvular annulus, which is essential for proper selection of the prosthetic valve. There is a chance of coronary artery compression during valve replacement. CT-derived three-dimensional and multiplanar reformatted images provide excellent visualization of the coronary artery relationship with RVOT and pulmonary valve. This is helpful in identifying patients with a high risk of coronary compression, who subsequently need careful monitoring during balloon testing (58).

Characteristics of DORV

DORV requires both great vessels (200% rule) or the entirety of one vessel and 50% or more of the other vessel (150%) to arise from the morphologic RV. Due to extreme heterogeneity in the structure of DORV, there have been debates about its definition. In 1950, when DORV was first introduced in the literature, it was defined as a condition in which both great vessels arise completely from the RV. Since 1981, a "50% rule" has been widely accepted, according to which an overriding arterial trunk is considered to be arising from the RV when more than half of the circumference of its valve belongs to the RV. DORV is an extremely heterogeneous group of lesions showing variable morphologic features and relations at each level of cardiac segments.

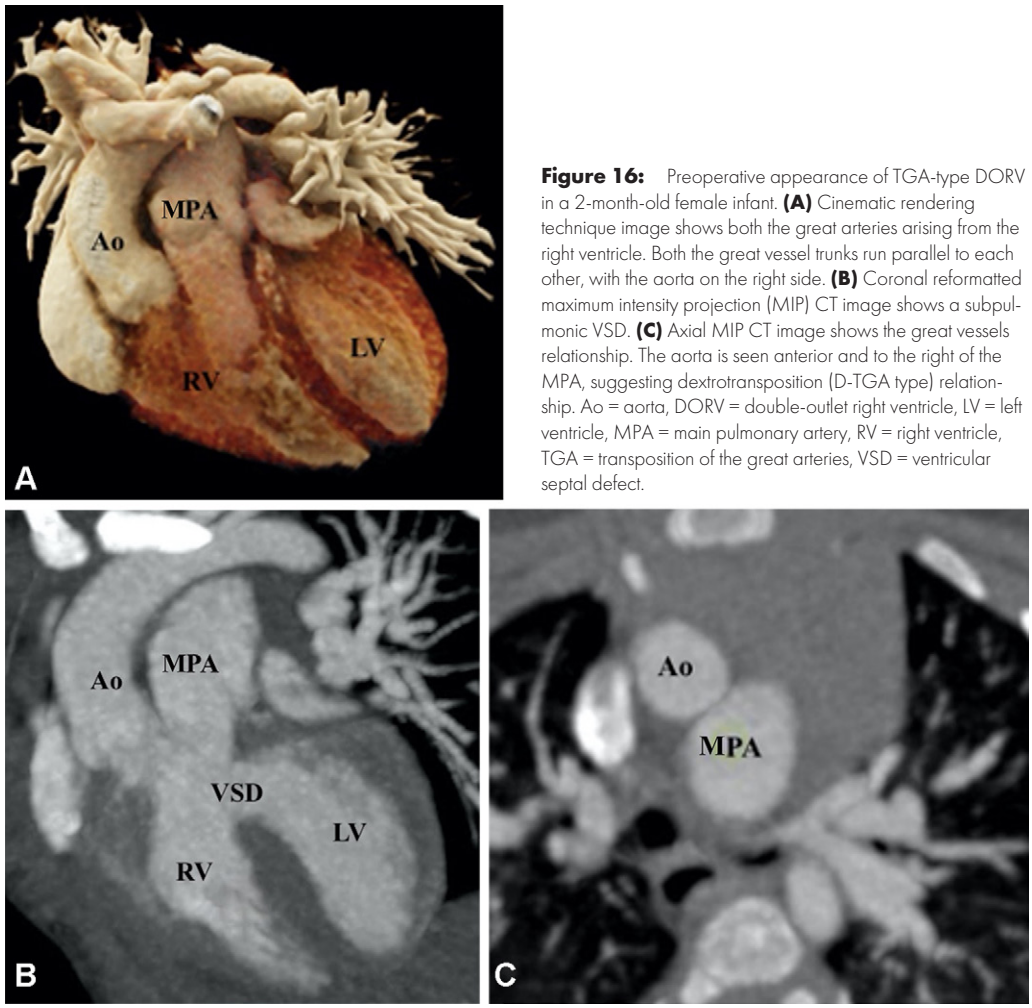

Figure 16: Preoperative appearance of TGA-type DORV in a 2-month-old female infant. **(A)** Cinematic rendering technique image shows both the great arteries arising from the right ventricle. Both the great vessel trunks run parallel to each other, with the aorta on the right side. **(B)** Coronal reformatted maximum intensity projection (MIP) CT image shows a subpulmonic VSD. **(C)** Axial MIP CT image shows the great vessels relationship. The aorta is seen anterior and to the right of the MPA, suggesting dextrotransposition (D-TGA type) relationship. Ao = aorta, DORV = double-outlet right ventricle, LV = left ventricle, MPA = main pulmonary artery, RV = right ventricle, TGA = transposition of the great arteries, VSD = ventricular septal defect.

There are several modifiers responsible for the large spectrum of heterogeneity of hearts with DORV, including VSD (type, location, and size), orientation of the outlet septum relative to the VSD margin, presence of muscular infundibulum (subaortic, subpulmonic, and bilateral), great vessel relationship, and presence or absence of outflow tract stenosis (76). Since both great vessels arise from the RV, the only pathway for the LV to empty itself is the VSD. Therefore, VSD is an essential component of DORV. The location of VSD is variable, producing different types of phenotypes. The variable relationships between VSD and the great vessels can be easily understood by embryologic development. The recent embryologic theory postulates that DORV results due to misalignment and arrest of the interventricular septum. The various relationships between the outlet septum and septomarginal trabeculation lead to different types of VSDs and DORV phenotypes. The outlet septum is a fibrous structure separating the two outflow tracts and forms the cranial margins of interventricular communication. The septomarginal trabeculation is a strap-like mass of myocardium that supports the septal surface and has both cranial and caudal limbs. Attachment of the outlet septum to the cranial limb of the septomarginal trabeculation positions the interventricular communication just beneath the aortic valve, producing subaortic VSD. Similarly, if the outlet septum attaches to the caudal limb of septomarginal trabeculation, interventricular communication is positioned beneath the pulmonary valve, producing subpulmonic VSD. If the outlet septum shows neither cranial nor caudal attachment, the interventricular defect will become doubly committed (beneath both the aortic and pulmonary valve). Last, remote or uncommitted VSD is diagnosed when the distance between VSD and the semilunar valve is greater than the size of the aortic valve (Fig 12) (77).

The great vessel relationship is another important modifier in DORV. Subaortic VSD is associated with a normal spiral pattern of the great vessels, with the aorta lying posteriorly and to the right of the pulmonary trunk. In subpulmonic VSD, the aorta can be seen either side-by-side and rightward to the pulmonary trunk, anterior and rightward to the PA (ie, D-malposition), or, very rarely, leftward and anterior to the PA (ie, L-malposition). Although the different types of vessel relationships can predict VSD position, these are only generalizations and not strict rules. Another common feature of DORV is pulmonary stenosis (PS), observed in approximately 75% of cases. In combination, the variable relationships of the VSD to the great vessels and presence or absence of PS produce four different anatomic-physiologic variants of DORV, which are described briefly below in order of decreasing frequency (78,79).

The TOF-type variant of DORV shows subaortic VSD and variable degrees of PS. The great vessels display normal

relationships, with the aorta lying posteriorly and rightward to the PA. The pathophysiology of this variant is determined by the degree of PS, which increases with age. The TGA-type variant shows subpulmonic VSD and transposition of the great vessels. The trunks of the great vessels run parallel to each other, with the aorta positioned anterior to the right of the pulmonary trunk. This configuration is also known as Taussig-Bing anomaly. The VSD-type variant shows subaortic VSD without PS. The great vessels display normal relationships. Finally, the univentricular variant is characterized by DORV with univentricular atrioventricular connections, atrioventricular valve atresia, and severe hypoplasia of one of the ventricular sinuses. This DORV classification provides comprehensive details about the relational anatomy and groups patients with DORV according to the type of surgical repair.

Surgical Approach

DORV repair depends upon VSD orientation, status of the conus, biventricular volumes, outflow obstruction, and the relationship of the great vessels. As mentioned, VSD can be subaortic (50% of cases), subpulmonic (30% of cases), uncommitted or remote, and doubly committed to the semilunar valves. TOF-type DORV with subaortic VSD and PS is treated like TOF, except VSD patch closure is replaced by the tunnel technique, routing the LV to the aorta. Biventricular repair of DORV requires adequate volumes of both ventricles after surgery. Intraventricular tunneling compromises RV volume, as a portion of the RV is incorporated into the LVOT. Therefore, it is important to assess RV cavity size and estimate the volume of the remaining RV after the intended surgery. Common postoperative complications are residual VSD and residual or recurrent PA stenosis. If there is pulmonary atresia and corrective repair is not possible, the Rastelli procedure is the optimal method for surgical treatment. In this procedure, VSD is repaired by the tunnel technique, and an extracardiac conduit is placed between the RV and main PA. Common postoperative complications of the Rastelli procedure could be related to the conduit (stenosis, calcification, and aneurysm), tunnel (stenosis and leakage), and branch PAs (stenosis). VSD-type DORV is treated by intraventricular tunnel repair, which connects the LV to the aorta. Postoperative complications include residual VSD and subaortic obstruction (tunnel or non–tunnel related). TGA-type DORV with subpulmonic VSD (Taussig-Bing anomaly) is treated by tunnelling VSD to the PA with either atrial or arterial switch. The complications of these procedures are related to the tunnel (stenosis, leakage, and obstruction), baffle (stenosis, leakage, and obstruction), PA (central or branch PA stenosis), outflow tracts (LVOT, RVOT obstruction), and/or coronary arteries (anomalous course, ostial compressions, and atherosclerotic disease). DORV with noncommitted VSD is difficult to treat due to the remote location of VSD. Options include baffling of the LV to the aorta or rerouting of VSD to the PA with an arterial switch operation. If neither aortic nor pulmonary routing of VSD is possible and there is concomitant PS, a systemic-to-PA shunt (BT shunt) is made in the neonatal period, followed by a bidirectional cavopulmonary anastomosis (Glenn shunt) at the age of 6 months and completion of cavopulmonary connection at 1 to 2 years old (80). Postoperative complications could be related to the tunnel (stenosis, leakage, and obstruction), BT shunt (thrombosis, stenosis), and Fontan circuit (conduit stenosis, calcification, thrombosis) (81).

Table 4: Checklist for Postoperative Assessment of DORV

After tunnel repair (TOF- and VSD-type DORV)
Status of tunnel (stenosis, leakage, and obstruction)
Pulmonary artery (central or branch pulmonary artery stenosis)
Outflow tracts (LVOT, RVOT obstruction)
Residual VSD (No., size, and site)
Cardiac chambers (enlargement or wall thickening)
After Rastelli procedure (TOF-type DORV with pulmonary atresia)
Status of tunnel (stenosis, leakage, and obstruction)
Status of conduit (stenosis, calcification, and aneurysm)
Outflow tracts (LVOT obstruction)
Residual VSD (No., size, and site)
Cardiac chambers (enlargement or wall thickening)
After tunnel repair with atrial or arterial switch (TGA-type DORV)
Status of tunnel (stenosis, leakage, and obstruction)
Status of baffle (stenosis, leakage, and obstruction)
Pulmonary artery (central or branch pulmonary artery stenosis)
Outflow tracts (LVOT, RVOT obstruction)
Semilunar valve (aortic or pulmonary stenosis, aortic root dilatation)
Coronary arteries (anomalous course, ostial compressions, and atherosclerotic disease)
Cardiac chambers (enlargement or wall thickening)
After Fontan repair (univentricular heart–type DORV)
Conduit related (thrombosis, stenosis, and calcification)
Vascular (pulmonary AVM, aortopulmonary collateral vessels, and systemic-to-pulmonary venovenous shunts)
Liver disease (chronic hepatic congestion, cardiac cirrhosis, regenerative hepatic nodule, and hepatocellular carcinoma)
Lymphovascular (chronic pleural effusion, pericardial effusion, chylothorax, protein losing enteropathy, and plastic bronchitis)

Note.—AVM = arteriovenous malformation, DORV = double-outlet right ventricle, LVOT = left ventricular outflow tract, RVOT = right ventricular outflow tract, TGA = transposition of great arteries, TOF = tetralogy of Fallot, VSD = ventricular septal defect.

Role of CT Imaging in DORV

Preoperative imaging should be focused on the assessment of VSD and great vessel relationship, conus categorization, and identification of associated anomalies (Table 3). As discussed, VSD could be subpulmonic, subaortic, remote, or doubly committed (Fig 13). There is a diverse spectrum of great vessel relationships in DORV. The aorta can have a normal relationship with the PA (posterior and to the right of the PA), or it

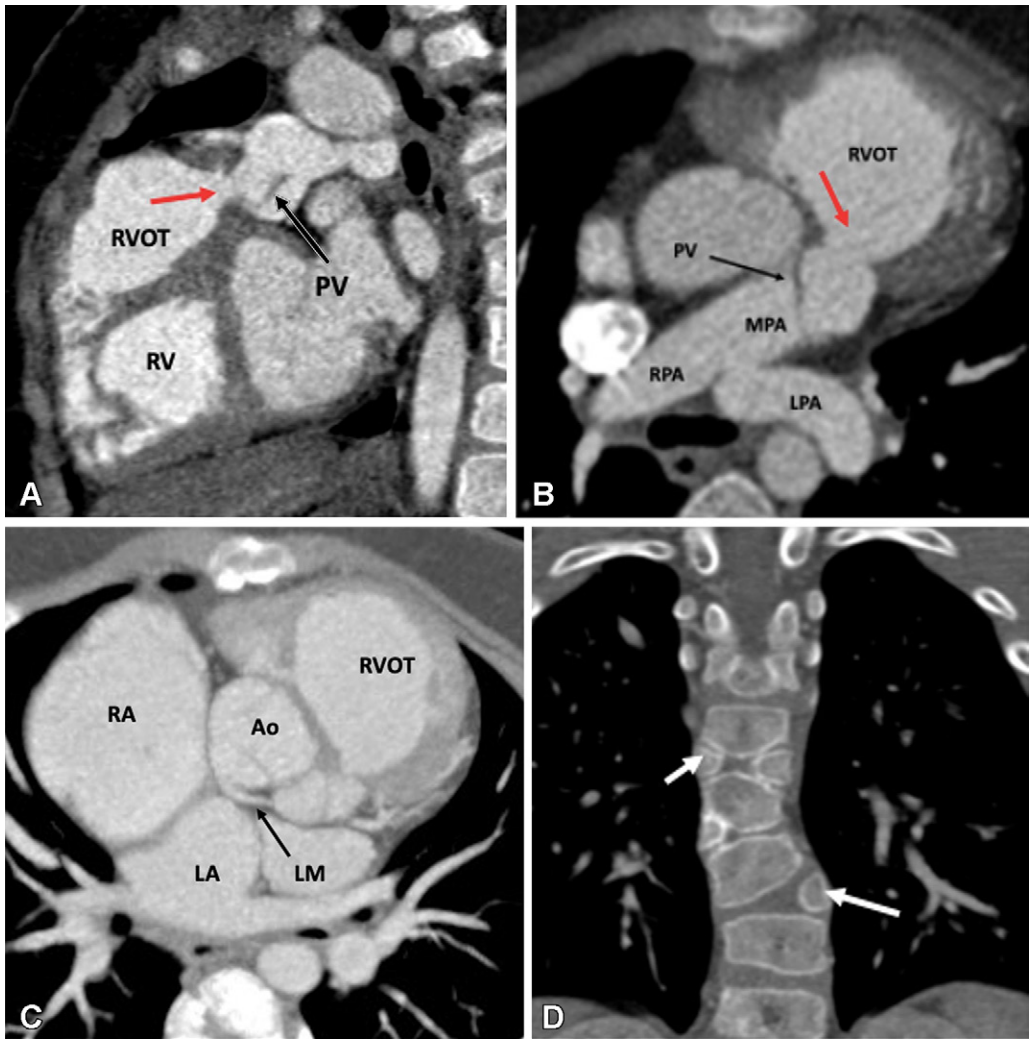

Figure 17: Postoperative appearance of TOF-type DORV after VSD closure with LV routing, infundibular resection, and patch augmentation of the RVOT up to the main pulmonary artery in a 4-month-old male infant. **(A)** Sagittal oblique and **(B)** axial multiplanar reconstruction CT images show dilated RV and RVOT. There is residual subvalvular narrowing (red arrow). The residual pulmonary valve tissue is shown with a black arrow. The MPA, RPA, and LPA appear normal. **(C)** Axial maximum intensity projection (MIP) CT image shows anomalous origin of the left main coronary artery (black arrow) from the noncoronary sinus with retroaortic course. **(D)** Coronal reformatted MIP CT image shows multiple hemivertebrae (white arrows). Ao = aorta, DORV = double-outlet right ventricle, LA = left atrium, LM = left main, LPA = left pulmonary artery, LV = left ventricle, MPA = main pulmonary artery, PV = pulmonary valve, RA = right atrium, RPA = right pulmonary artery, RV = right ventricle, RVOT = right ventricular outflow tract, TOF = tetralogy of Fallot, VSD = ventricular septal defect.

can be dextroposed (anterior and to the right of the PA) or levoposed (anterior and to the left of the PA) (Fig 14). The conus refers to the thick muscular structure that interposes between the leaflets of arterial and atrioventricular valves. During fetal development, the subaortic conus involutes and is represented by aortomitral continuity. In DORV, the subaortic conus persists, leading to loss of aortomitral continuity. The presence of bilateral conuses was initially used to differentiate TOF from DORV, but studies have shown that bilateral conuses may be absent in some patients with DORV and could be present in healthy individuals (82,83). Despite this, presence and length of the conuses should be reported, as these features impact surgical technique. The collective assessment of various modifiers helps in characterizing the different DORV variants (Figs 15, 16). Besides this, CT imaging is also helpful in simultaneous assessment of various anomalies associated with DORV (ie, atrioventricular valve stenosis and atresia, straddling, and complete AV canal defect) (84–86).

CT can be used for the assessment of both the palliative and corrective surgeries performed in DORV. CT images enable reliable diagnosis of various postoperative complications related to the VSD (residual), conduit (calcification, stenosis, thrombosis), intraventricular tunnel (stenosis, leak, aneurysm), outflow tracts (RVOT obstruction, LVOT obstruction), PAs (stenosis, aneurysm), and aorta (coarctation and recoarctation) (Table 4, Fig 17). The retrospective ECG-gated scan is useful for ventricular function analysis, aiding early prediction of imminent ventricular failure (87). It is important to tailor the contrast agent injection protocol according to the type of surgical repair, such as the BT shunt, bidirectional Glenn shunt

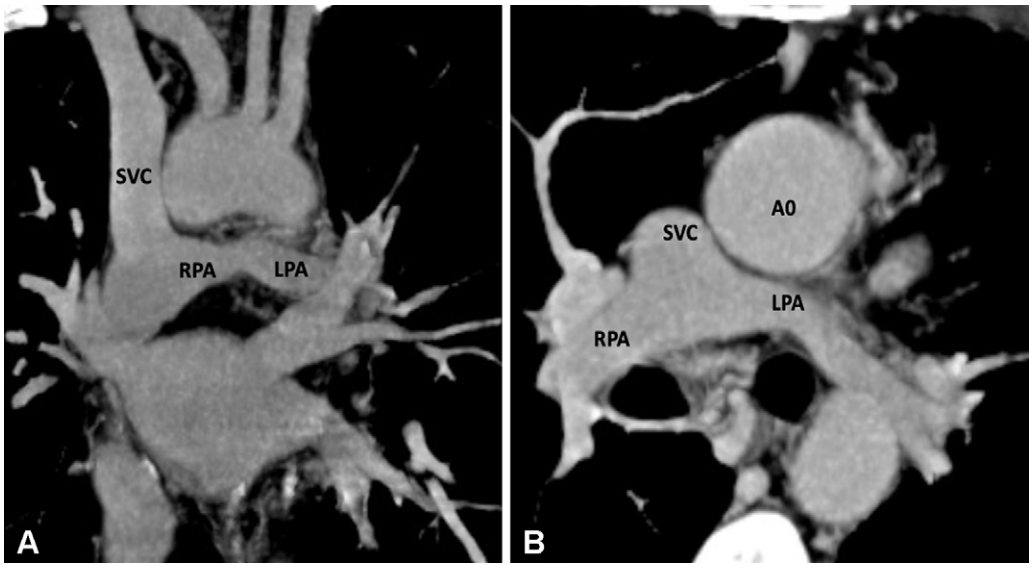

Figure 18: Postoperative appearance of DORV with functional single ventricle after bidirectional cavopulmonary shunt in a 31-month-old boy. **(A)** Coronal oblique and **(B)** axial maximum intensity projection CT images show end-to-side anastomosis of the superior vena cava to the right pulmonary artery after division of the superior cavoatrial junction. In this patient, bidirectional cavopulmonary shunt was performed as an intermediate procedure to staged Fontan operation. Ao = aorta, DORV = double-outlet right ventricle, LPA = left pulmonary artery, RPA = right pulmonary artery, SVC = superior vena cava.

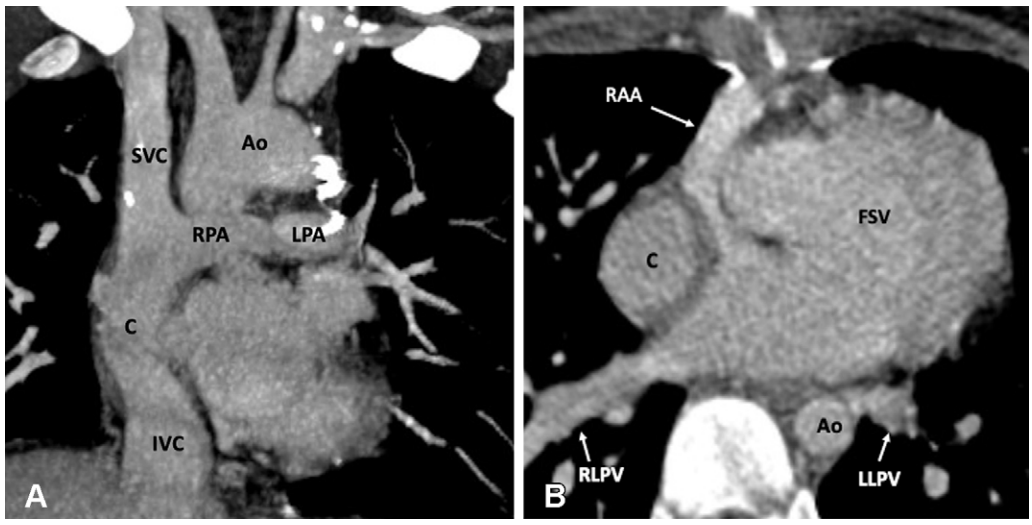

Figure 19: Postoperative appearance of DORV with functional single ventricle after extracardiac Fontan procedure in an 8-year-old girl. **(A)** Coronal oblique maximum intensity projection (MIP) CT image shows the superior and inferior connection of the conduit to the RPA and IVC, respectively. The SVC is connected to the RPA. No evidence of any conduit stenosis, calcification, or thrombosis is seen. **(B)** Axial MIP CT image shows an extra-atrial conduit placed entirely outside the right atrium. Ao = aorta, C = conduit, DORV = double-outlet right ventricle, FSV = functional single ventricle, IVC = inferior vena cava, LLPV = left lower pulmonary vein, LPA = left pulmonary artery, RAA = right atrial appendage, RLPV = right lower pulmonary vein, RPA = right pulmonary artery, SVC = superior vena cava.

(Fig 18), total cavopulmonary connection, and Fontan circulation (Fig 19). While evaluating patients with Fontan repair, the uniform opacification of the Fontan circuit and PAs are the main diagnostic challenges. The differential timing of superior vena cava and inferior vena cava opacification results in incomplete contrast agent mixing in the Fontan conduit, producing streaming artifacts that can mimic thrombosis. The dual-injection protocol is useful in these patients. This protocol involves simultaneous contrast agent injection in the upper and lower extremity veins, allowing dense uniform opacification of the Fontan circuit and PAs. As it is not possible to enhance both the aorta and Fontan conduit in the same phase settings, an early aortic phase scan is followed by a delayed phase scan for the complete evaluation of aortic pathologic conditions, the PAs, and the cavopulmonary circuit (Fig 20) (88,89). Single-injection single-phase CT is an alternative technique. A total of 3 mL of contrast agent per kilogram of body weight is injected with a constant rate of 2 mL/sec, followed by a saline chaser.

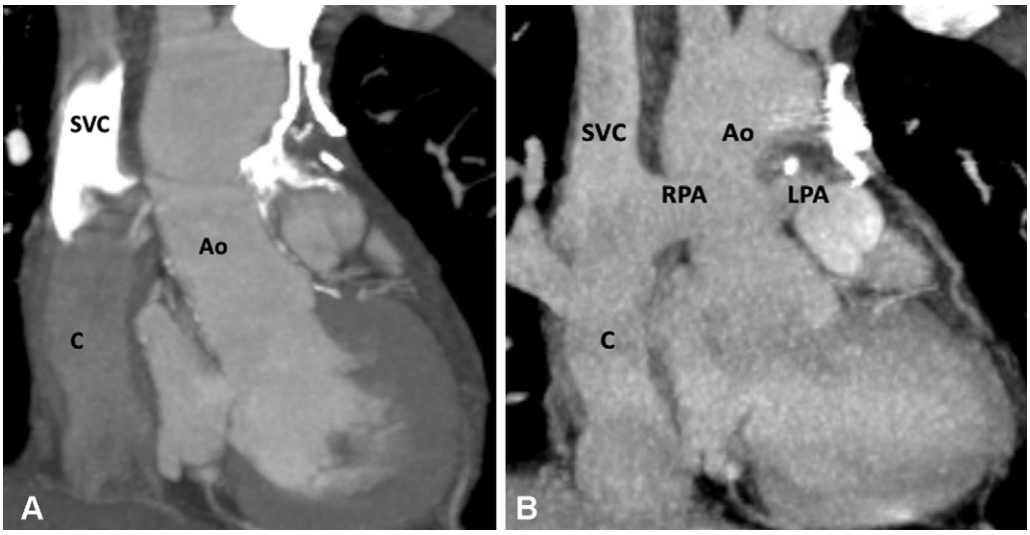

Figure 20: Extracardiac Fontan procedure biphasic acquisition protocol. **(A)** Coronal reformatted maximum intensity projection (MIP) CT image in the early arterial phase shows well-opacified aortic root. The Fontan circuit is not opacified, giving false impression of thrombosis. **(B)** Coronal reformatted MIP CT image in the late venous phase shows uniform opacification of the Fontan conduit. Ao = aorta, C = conduit, LPA = left pulmonary artery, RPA = right pulmonary artery, SVC = superior vena cava.

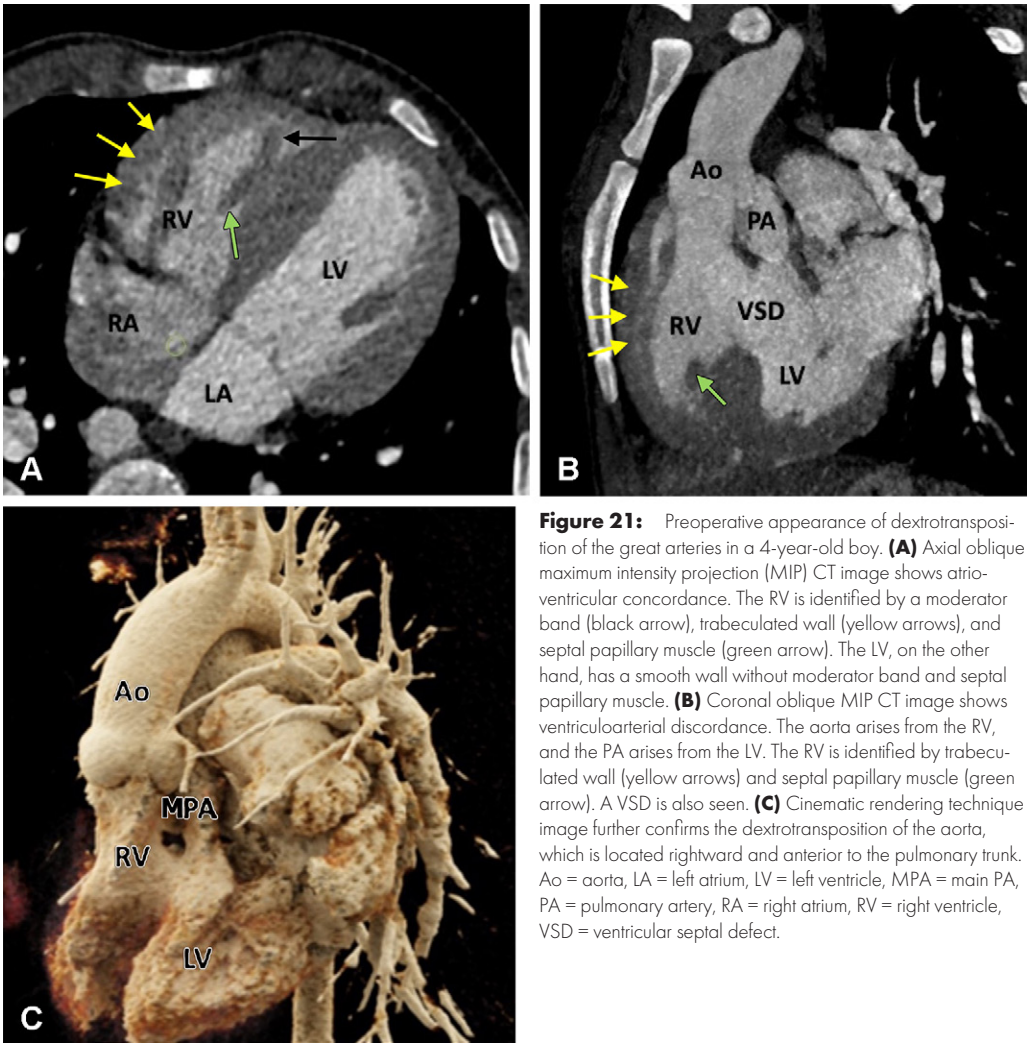

Figure 21: Preoperative appearance of dextrotransposition of the great arteries in a 4-year-old boy. **(A)** Axial oblique maximum intensity projection (MIP) CT image shows atrioventricular concordance. The RV is identified by a moderator band (black arrow), trabeculated wall (yellow arrows), and septal papillary muscle (green arrow). The LV, on the other hand, has a smooth wall without moderator band and septal papillary muscle. **(B)** Coronal oblique MIP CT image shows ventriculoarterial discordance. The aorta arises from the RV, and the PA arises from the LV. The RV is identified by trabeculated wall (yellow arrows) and septal papillary muscle (green arrow). A VSD is also seen. **(C)** Cinematic rendering technique image further confirms the dextrotransposition of the aorta, which is located rightward and anterior to the pulmonary trunk. Ao = aorta, LA = left atrium, LV = left ventricle, MPA = main PA, PA = pulmonary artery, RA = right atrium, RV = right ventricle, VSD = ventricular septal defect.

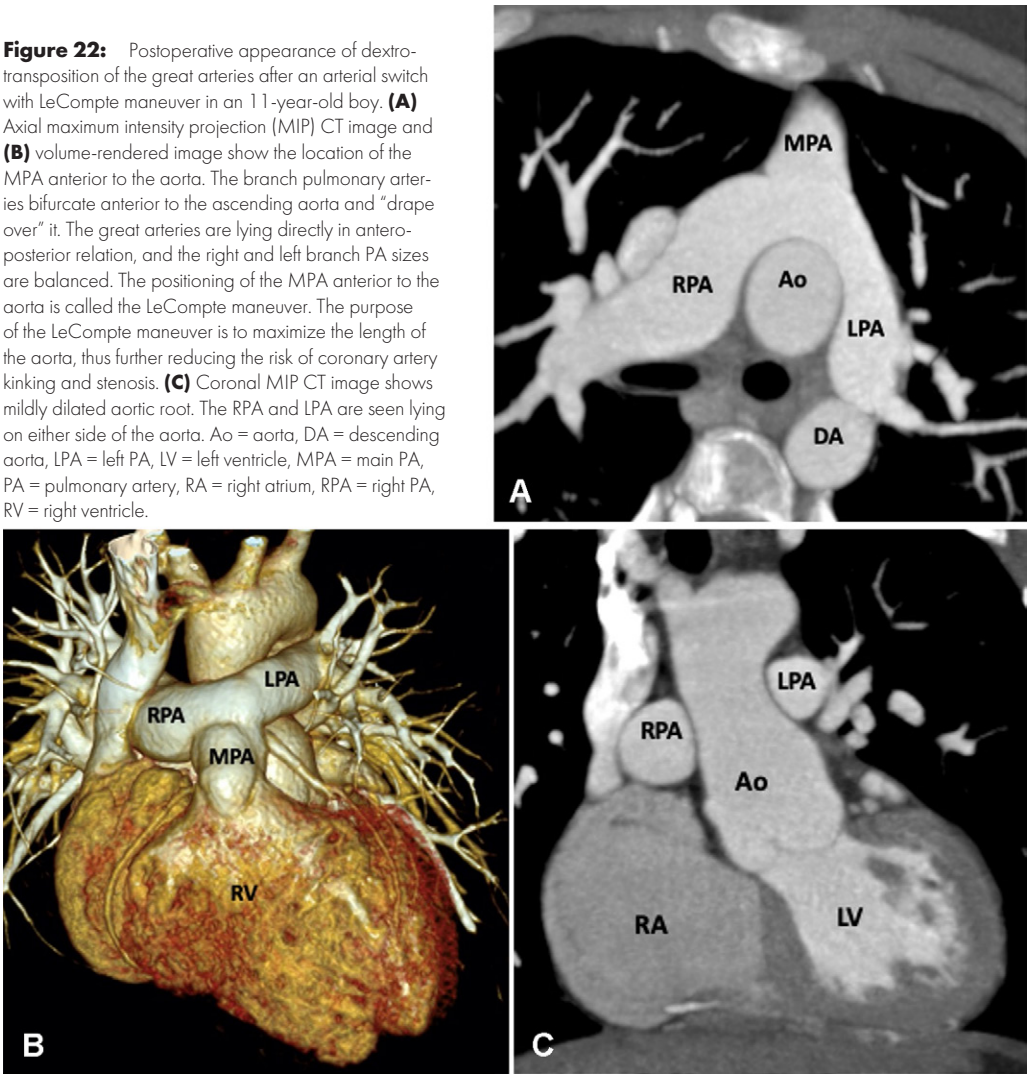

Figure 22: Postoperative appearance of dextrotransposition of the great arteries after an arterial switch with LeCompte maneuver in an 11-year-old boy. **(A)** Axial maximum intensity projection (MIP) CT image and **(B)** volume-rendered image show the location of the MPA anterior to the aorta. The branch pulmonary arteries bifurcate anterior to the ascending aorta and "drape over" it. The great arteries are lying directly in anteroposterior relation, and the right and left branch PA sizes are balanced. The positioning of the MPA anterior to the aorta is called the LeCompte maneuver. The purpose of the LeCompte maneuver is to maximize the length of the aorta, thus further reducing the risk of coronary artery kinking and stenosis. **(C)** Coronal MIP CT image shows mildly dilated aortic root. The RPA and LPA are seen lying on either side of the aorta. Ao = aorta, DA = descending aorta, LPA = left PA, LV = left ventricle, MPA = main PA, PA = pulmonary artery, RA = right atrium, RPA = right PA, RV = right ventricle.

The scan is initiated 70 seconds after contrast agent administration. If optimum aortic opacification is also needed, the injection rate is increased to 3–5 mL/sec a few seconds before scan initiation. The timing of the increase in contrast agent injection rate is determined by calculating the time to peak enhancement in the aorta from the test bolus injection. The time to peak enhancement is subtracted from the total duration of the injection. For example, if the total duration of the injection is 70 seconds, and the time to peak enhancement is 15 seconds, then the injection rate should be increased at 55 seconds (70 seconds − 15 seconds = 55 seconds). Contrast agent administration should be stopped at least 10 seconds before scan initiation to avoid streak artifacts in the PAs and superior vena cava (89).

Characteristics of D-TGA

D-loop transposition of the great arteries (D-TGA) is the second most common cyanotic congenital heart disease. It is characterized by ventriculoarterial discordance, in which the aorta arises from the RV and the PA arises from the LV (Fig 21). The letter *D* stands for dextrotransposition, which refers to the bulboventricular loop (ie, the position of the RV is on the right side). The aorta also tends to be on the right and anterior to the PA, and the main PA and ascending aorta are in a parallel pattern rather than the crossing pattern that is observed in healthy individuals. Because of the ventriculoarterial discordance, systemic venous blood from the right side of the heart passes to the aorta, and pulmonary venous blood passes through the left side of the heart to the lungs (90). Patient survival is dependent on intracardiac shunts, including atrial septal defect, PDA, and VSD.

D-TGA is usually associated with other cardiac anomalies. VSD is seen in approximately 60% of patients with D-TGA (91). VSDs can be simple (perimembranous type or muscular type) or more complex (inlet type, doubly committed subarterial type, malalignment type with associated outflow tract obstruction). A patent foramen ovale and PDA are usually seen at birth and allow a variable amount of mixing of oxygenated and deoxygenated blood. If the foramen is very small or closed, early intervention is necessary.

Surgical Approach

The Jatene arterial switch operation (ASO) is currently the surgical procedure of choice. Other surgical methods include

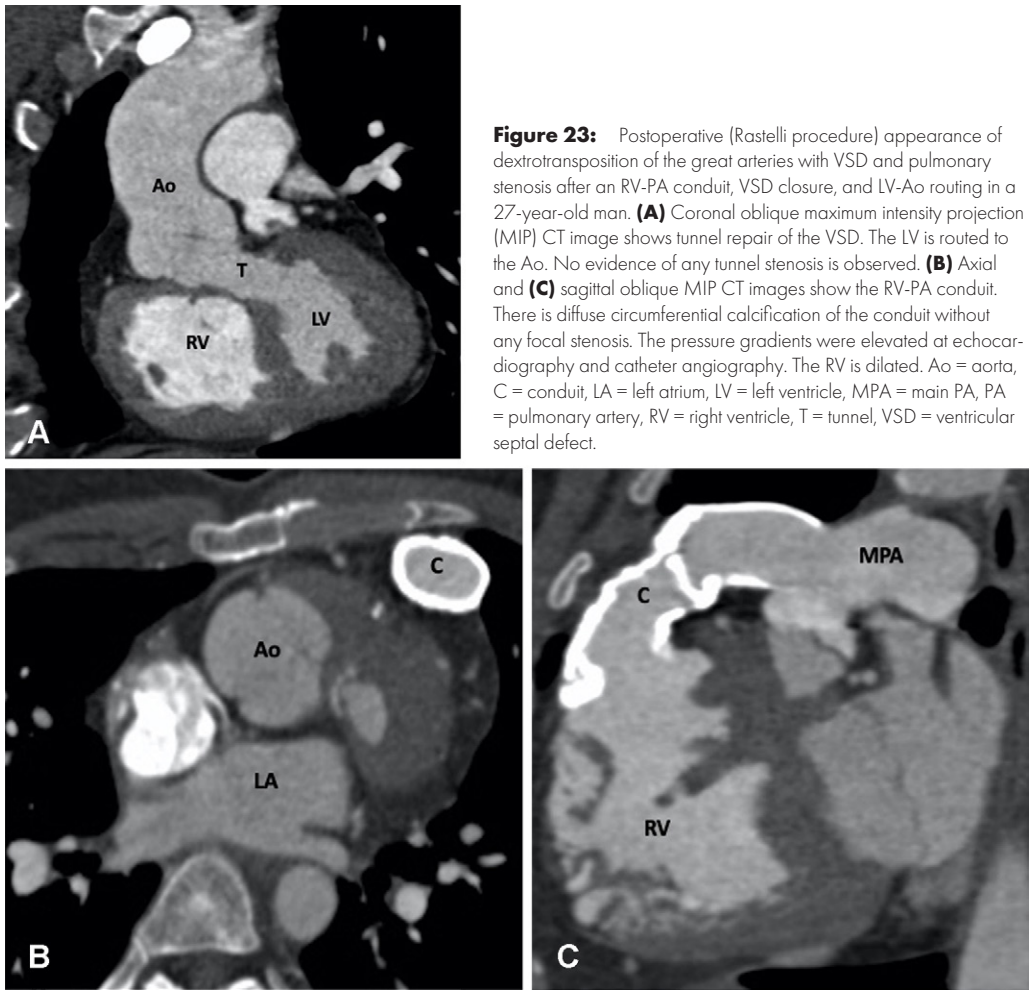

Figure 23: Postoperative (Rastelli procedure) appearance of dextrotransposition of the great arteries with VSD and pulmonary stenosis after an RV-PA conduit, VSD closure, and LV-Ao routing in a 27-year-old man. **(A)** Coronal oblique maximum intensity projection (MIP) CT image shows tunnel repair of the VSD. The LV is routed to the Ao. No evidence of any tunnel stenosis is observed. **(B)** Axial and **(C)** sagittal oblique MIP CT images show the RV-PA conduit. There is diffuse circumferential calcification of the conduit without any focal stenosis. The pressure gradients were elevated at echocardiography and catheter angiography. The RV is dilated. Ao = aorta, C = conduit, LA = left atrium, LV = left ventricle, MPA = main PA, PA = pulmonary artery, RV = right ventricle, T = tunnel, VSD = ventricular septal defect.

the atrial switch and Rastelli procedures. There are multiple variations of atrial switch, pioneered and reported by William Mustard and Ake Senning in separate reports. During an atrial switch procedure, a baffle or conduit is made that reroutes the systemic venous blood of the superior vena cava and inferior vena cava to the mitral valve and, consequently, to the LV, PA, and pulmonary circulation. A similar conduit is made by rerouting the pulmonary venous blood to the tricuspid valve, RV, aorta, and systemic circulation. Ventriculoarterial mismatch is left unrepaired. The anatomic LV continues to pump into the pulmonary circulation, and the anatomic RV pumps into the systemic circulation. The only difference between the Mustard and Senning procedures is the type of material used for creating baffles; pericardium is used for the Mustard procedure, while native atrial tissue is used in the Senning procedure (92–95).

Atrial switch was the procedure of choice for D-TGA from 1959 to the mid-1980s. However, because the RV functions as the systemic ventricle, it is predisposed to dysfunction and ultimately failure, which eventually leads to LV failure as well. Mid- and late-term follow-up evaluations demonstrated progressive late RV dysfunction and severe tricuspid regurgitation as the major complications of this procedure. Other complications include dysrhythmias, baffle obstruction, pulmonary hypertension, and even sudden death (96,97).

The high incidence of late-term complications of this procedure led to the continued search for an anatomic correction of D-TGA to return the great arteries to their normal ventricular connections. Several attempts were made for an anatomic correction until 1975, when Adib Dominos Jatene and colleagues first successfully performed the ASO. During the ASO, the pulmonary trunk and aorta are transected, and their positions are switched with each other so that the pulmonary root becomes the neoaortic root and the aortic root becomes the neopulmonary root. The coronary arteries are excised from the aorta with a small cuff of aortic wall and implanted into the neoaorta (98). In 1981, the LeCompte maneuver was described, which involves relocation of the PA anterior to the ascending aorta. This maneuver maximizes aortic length and reduces the likelihood of coronary artery kinking or compression (99). The ASO restores normal anatomic and physiologic circulation (Fig 22). Additionally, there is no postoperative ventriculoarterial mismatch as seen after atrial switch surgery. If the D-TGA is associated with VSD and PS, the Rastelli procedure is the procedure of choice. It includes VSD patch repair to the aortic valve, which allows the LV to eject blood through the aortic valve, and placement of a conduit between the RV and PAs (Fig 23). Réparation à l'etage ventriculaire (REV) is another procedure aimed at overcoming the drawbacks and limitations of the classic Rastelli operation, such as subaortic stenosis, late

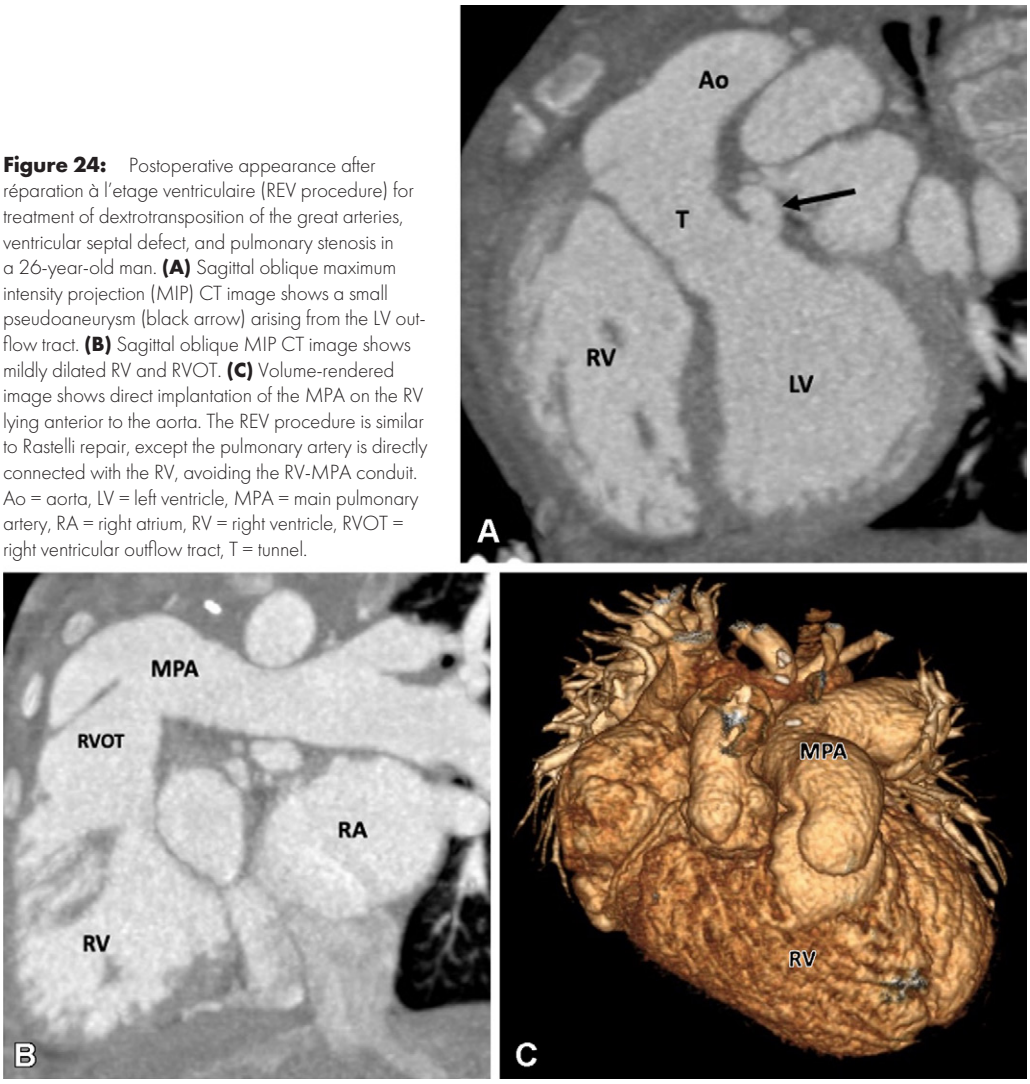

Figure 24: Postoperative appearance after réparation à l'etage ventriculaire (REV procedure) for treatment of dextrotransposition of the great arteries, ventricular septal defect, and pulmonary stenosis in a 26-year-old man. **(A)** Sagittal oblique maximum intensity projection (MIP) CT image shows a small pseudoaneurysm (black arrow) arising from the LV outflow tract. **(B)** Sagittal oblique MIP CT image shows mildly dilated RV and RVOT. **(C)** Volume-rendered image shows direct implantation of the MPA on the RV lying anterior to the aorta. The REV procedure is similar to Rastelli repair, except the pulmonary artery is directly connected with the RV, avoiding the RV-MPA conduit. Ao = aorta, LV = left ventricle, MPA = main pulmonary artery, RA = right atrium, RV = right ventricle, RVOT = right ventricular outflow tract, T = tunnel.

ventricular deterioration, and arrhythmias. Resection of the infundibular septum in the REV procedure allows for the placement of a straighter, smaller ventricular patch that bulges much less into the RV cavity. The extensive mobilization of the main pulmonary branches permits a direct connection with the RV, avoiding the need for an extracardiac conduit (Fig 24).

Common complications following an atrial switch procedure are atrial baffle leak (a physiologic atrial septal defect), baffle stenosis (systemic venous or pulmonary venous baffle obstruction), stenosis of the systemic and/or pulmonary outflow tracts, RV failure with tricuspid regurgitation, pulmonary hypertension, residual VSD, and conduction or rhythm disturbances. Many patients require pacemakers due to sinus node dysfunction and atrial arrhythmias. Complications associated with ASO include PA stenosis, coronary artery obstruction, pulmonary hypertension, arrhythmia, and aortic arch obstruction. Because the native pulmonary valve works as a neoaortic valve after ASO, patients who undergo this procedure are at risk for neoaortic valve regurgitation and neoaortic root dilatation in the late postoperative period (100,101). Complications specific to the Rastelli procedure include conduit obstruction and LVOT obstruction (102). The complications specific to the REV procedure include recurrent RVOT obstruction and, very rarely, LVOT obstruction (103).

Role of CT Imaging in D-TGA

Cardiac CT is rarely needed before surgical intervention for patients with D-TGA, except to delineate coronary anatomy and examine complex vascular anatomy in patients with heterotaxy syndrome. The checklist for preoperative evaluation includes origin and relationship of the great vessels, interatrial and interventricular communication, outflow tract (RVOT or LVOT) obstruction, semilunar (aortic or pulmonary) valve stenosis, status of ductal arteriosus (patent or closed), coronary artery anomalies, and aortic arch (interruption or coarctation) (Table 5). The commonly used classification system for coronary nomenclature is Leiden Convention coronary coding system, which unifies the annotation of coronary anatomy for thoracic surgeons and radiologists.

The coding system considers the coronary anatomy from a cranial view for a thoracic surgeon, as encountered during cardiac surgery, and caudal view for an imaging physician, as encountered during image interpretation. The first step of the

Table 5: Checklist for Preoperative Assessment of D-TGA

Ventricle loop
D-loop (RV on right side of LV)
Arterial loop
D-transposition (aortic valve lying anterior and to the right of the pulmonary valve)
Cardiac chambers
Enlargement or wall thickening
Systemic and pulmonary venous connections
VSD
No., size, and site
Aorta
Aortic root
Arch (right or left sided)
Configuration of branch vessels
Coronary artery anatomy
Normal or anomalous origin
Any vessel coursing anterior to RVOT
Concomitant anomalies
Cardiac (ASD)
Aortic pathologic feature (vascular rings)
Airway anatomy

Note.—ASD = atrial septal defect, D-TGA = D-loop transposition of the great arteries, LV = left ventricle, RV = right ventricle, RVOT = right ventricular outflow tract, VSD = ventricular septal defect.

Table 6: Checklist for Postoperative Assessment of D-TGA

After atrial switch
Status of baffle; systemic and pulmonary venous baffles (stenosis, leakage, and obstruction)
Pulmonary artery (central or branch pulmonary artery stenosis)
Outflow tracts (LVOT, RVOT obstruction)
Semilunar valve (aortic or pulmonary stenosis, aortic root dilatation)
Cardiac chambers (enlargement or wall thickening)
After arterial switch
Great vessel relationship
Pulmonary artery (central or branch pulmonary artery stenosis)
Outflow tracts (LVOT, RVOT obstruction)
Semilunar valve (aortic or pulmonary stenosis, aortic root dilatation)
Coronary arteries (anomalous course, ostial compressions, and atherosclerotic disease)
Cardiac chambers (enlargement or wall thickening)

Note.—D-TGA = D-loop transposition of the great arteries, LVOT = left ventricular outflow tract, RVOT = right ventricular outflow tract.

Leiden Convention system is that the surgeon takes position in the nonfacing sinus of the aorta looking toward the pulmonary orifice; the right- and left-hand–facing sinuses are then referred to as sinus 1 and 2, respectively. Next, a counterclockwise rotation is adopted starting at sinus 1, and the encountered coronary branches are described. Annotation of the normal anatomic pattern is 1R-2LCx, corresponding to the surgical coding system. The imaging physician also takes position in the nonfacing sinus of the aortic valve, but with the back toward the pulmonary valve, looking outward from the sinus. From this position, the right-hand sinus is sinus 1, and the left-hand sinus is sinus 2. Next, a clockwise rotation is adopted starting at sinus 1, and the encountered coronary branches are described. The normal anatomic pattern is annotated as described above (104).

The imaging targets after atrial switch include status of the systemic or pulmonary venous baffle (stenosis, leak, thrombosis), VSD (residual), PAs (main or branch PA stenosis), outflow tracts (RVOT or LVOT obstruction), and systemic RV functional assessment (Table 6). The venous pathways have a complex three-dimensional structure and are difficult to evaluate with echocardiography. The most common site of systemic venous pathway narrowing is at the entrance of the distal superior limb into the right atrium. CT is well suited for visualization of both the systemic and pulmonary venous pathways. These anatomic stenoses are usually treated by stent placements. CT is the imaging method of choice if any stent restenosis is suspected (105). After an atrial switch procedure, most patients need pacing and defibrillator leads, which are best observed at CT. Additionally, if the patient needs repeat electrophysiologic intervention, such as placement of biventricular pacing leads, CT is the modality of choice for evaluation of coronary venous anatomy. CT can also be used to calculate ventricular volumes, mass, and ejection fraction in patients when echocardiography is insufficient and cardiac MRI is not possible (106).

The objectives of postoperative imaging in ASO are evaluation of the relationships of the great vessels, integrity of reimplanted coronaries, neoaortic root dilatation, PA stenosis, and aortopulmonary collaterals. CT is typically reserved for patients with contraindications for cardiac MRI, particularly those with implanted devices (Fig 25). CT allows for complete two-dimensional and three-dimensional anatomic assessment of the neopulmonary root, neoaortic root, branch PAs, and reimplanted coronary arteries. Coronary artery lesions (ostial stenosis, kinking, anomalous course, and atherosclerotic disease) are commonly seen in patients after ASO and may cause myocardial ischemia leading to ventricular dysfunction, arrhythmias, and sudden death (107). CTA allows detailed evaluation of origin, course, and branching pattern of the coronary arteries (Fig 26). The branching angle of the coronary arteries can be evaluated in short- and long-axis planes. Studies have shown that stenosis greater than 50%, acute branching angle (<30°), and interarterial course are associated with adverse cardiac events after ASO (108). CT can provide thin-section images of the coronary arteries and can help define their relationship to adjacent cardiac structures or to the sternum. For patients undergoing angioplasty for PA stenosis, CT is the ideal method for evaluation of PA stents, as cardiac MRI is generally nondiagnostic.

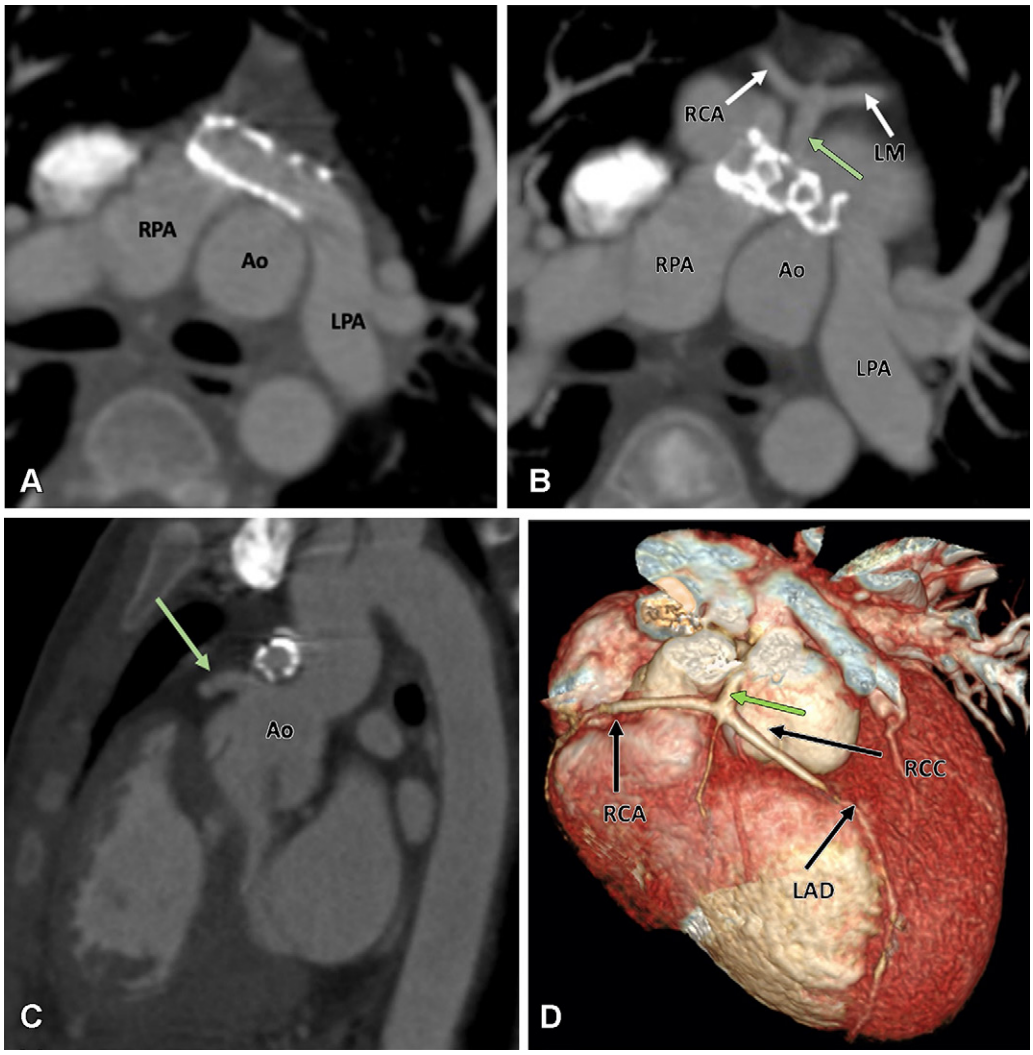

Figure 25: Postoperative appearance after an arterial switch procedure and LPA stent placement for treatment of dextrotransposition of the great arteries in a 14-year-old boy. **(A)** Axial maximum intensity projection (MIP) CT image shows the location of the main pulmonary artery anterior to the aorta. The patent stent is seen in the proximal LPA. The origin of the RPA is jailed. Stent placement was done to relieve recurrent LPA stenosis. **(B)** Axial and **(C)** sagittal MIP CT images show a single coronary artery (green arrow). A single common trunk arises from the aorta, which divides into the RCA and LM (white arrows in **B**). The LPA with stent is abutting the single coronary artery at its origin, but no evidence of ostial stenosis is seen. The aortic root appears dilated. **(D)** Volume-rendered image confirms the single coronary artery arising from right coronary sinus. Ao = aorta, LAD = left anterior descending artery, LM = left main trunk, LPA = left pulmonary artery, RCA = right coronary artery, RCC = right coronary sinus, RPA = right pulmonary artery.

Figure 26: Postoperative appearance after an arterial switch procedure for treatment of dextrotransposition of the great arteries in a 21-year-old woman. **(A)** Axial maximum intensity projection (MIP) CT image shows anomalous origin of the LM from the right coronary sinus with retroaortic course before dividing into the LAD and LCx. **(B)** Axial MIP CT image shows high origin of the RCA from the sinotubular junction with prepulmonic course before entering into the right atrioventricular groove. Ao = aorta, LA = left atrium, LAD = left anterior descending artery, LCx = left circumflex artery, LM = left main trunk, MPA = main pulmonary artery, RCA = right coronary artery.

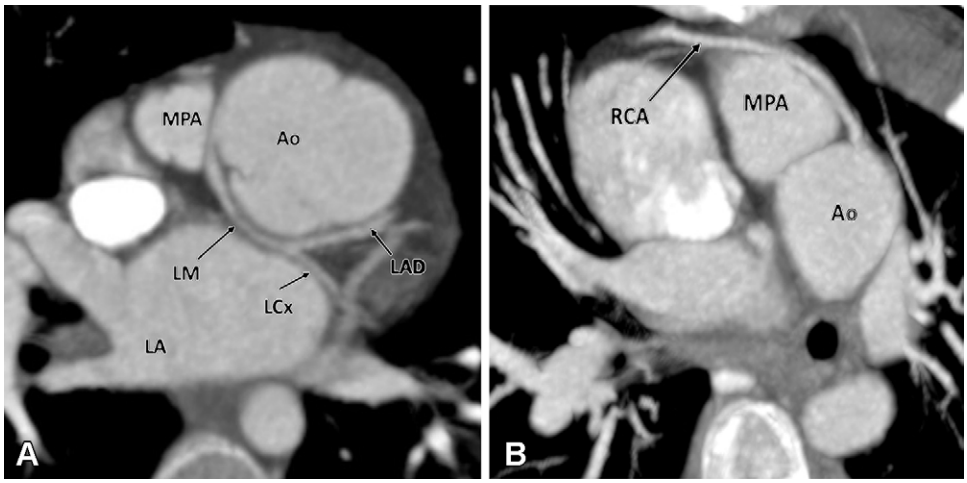

Table 7: Checklist for Preoperative Assessment of L-TGA

Ventricle loop
L-loop (RV on left side of LV)
Arterial loop
L-transposition (aortic valve lying anterior and to the left of the pulmonary valve)
Cardiac chambers
Enlargement or wall thickening
Systemic and pulmonary venous connections
VSD
No., size, and site
Aorta
Aortic root
Arch (right or left sided)
Configuration of branch vessels
Coronary artery anatomy
Normal or anomalous origin
Any vessel coursing anterior to RVOT
Concomitant anomalies
Cardiac (ASD)
Aortic pathologic feature (vascular rings)
Airway anatomy

Note.—ASD = atrial septal defect, L-GTA = L-loop transposition of the great arteries, LV = left ventricle, RV = right ventricle, RVOT = right ventricular outflow tract, VSD = ventricular septal defect.

Characteristics of L-TGA

L-loop transposition of the great arteries (L-TGA), also called congenitally corrected TGA (ie, cc-TGA), is characterized by atrioventricular and ventriculoarterial discordance. The letter *L* stands for levotransposition, meaning that there is levoposition of the morphologic RV. Systemic blood from the superior vena cava and inferior vena cava reaches the pulmonary circulation through the right-sided LV, and pulmonary venous blood reaches the aorta through the left-sided RV. Although blood is flowing in the right direction, it passes through the wrong ventricular chamber. Since the RV is not built to sustain the role of the left systemic ventricle in the long term, patients present with ventricular dysfunction. Therefore, the term *congenitally corrected TGA* is a misnomer. The aorta is also usually, but not universally, anterior and to the left, and the great arteries may be side by side. These patients are usually noncyanotic and diagnosed during routine cardiac evaluation at chest radiography or ECG.

On chest radiographs, the malposed ascending aorta produces a long convexity on the left upper mediastinal contour. The right PA appears to have a high takeoff because of an absent aortic shadow and is also quite prominent, indicating ventricular inversion. Besides this, cardiomegaly with increased pulmonary vascular markings secondary to a VSD can also be observed (109).

L-TGA is commonly associated with other cardiac anomalies, including VSD, LVOT obstruction, PS, Ebstein anomaly, situs inversus, dextrocardia, complete heart block, and reentrant tachycardias. A conotruncal type of VSD with some malalignment and occasional inlet extension is seen in approximately 70%–80% of patients. If the VSD is large, the PA may override the VSD and arise largely from the RV, resulting in DORV. Approximately 25%–50% of these patients have LVOT obstruction, which can occur at or below the level of the pulmonary valve. The great vessels show L-malposition configuration with the aorta lying anterior and to the left of the main PA. The interventricular septum lies in a straight anteroposterior plane with side-by-side ventricles. Levocardia usually exists with situs solitus, while dextrocardia is observed in approximately 25% of the cases (110).

Surgical Approach

Indications for surgical intervention include onset of symptoms or absence of symptoms with evidence of declining RV function. If there are no associated anomalies, medical follow-up is advised to identify the development of any tricuspid regurgitation or RV dysfunction. Anticipatory waiting is encouraged to achieve some weight gain prior to surgical intervention. If L-TGA is associated with large VSD, treatment depends upon patient age, as follows: *(a)* For patients younger than 3 months old, PA banding followed later by a double-switch operation is performed; *(b)* for patients who are 3–6 months of age, PA banding followed by a double-switch operation or direct double-switch operation, depending on institutional policy, is performed; *(c)* for patients older than 6 months, the double-switch operation is performed, provided that the patients have not developed irreversible pulmonary vascular disease. Furthermore, if L-TGA is associated with large VSD and LVOT obstruction (resulting in PS), treatment depends upon VSD routability, as follows: *(a)* For VSD-routable cases, the double-switch operation is performed; and *(b)* when the VSD is not routable, patients undergo a univentricular repair pathway (111).

The classic or traditional approach involves correction of the VSD and LVOT obstruction without correcting atrioventricular and ventriculoarterial discordance. This approach eliminates shunting and obstruction to blood flow, but the RV continues to function as a systemic ventricle. Over time, RV failure occurs due to its inability to cope with the systemic pressure load.

Anatomic operation for L-TGA involves correction of atrioventricular and ventriculoarterial discordance in the form of a double-switch operation (112). The term *double-switch operation* refers to the combination of the atrial switch (either Senning or Mustard operation) and Jatene ASO, with or without LeCompte procedure and reimplantation of the coronary arteries. Atrial switch corrects the atrioventricular discordance, and correction of ventriculoarterial discordance depends upon the presence of LVOT obstruction (pulmonary valve stenosis) and VSD location. In the absence of LVOT obstruction, ASO is performed to correct ventriculoarterial discordance. If LVOT obstruction is present and the VSD is routable, the Rastelli procedure is performed. Rerouting is done by creating a tunnel between the LV and aorta, using either pericardium (native or treated) or a synthetic patch. If LVOT obstruction is present and the VSD is not routable, patients undergo the Nikaidoh procedure and Fontan procedure (113,114). The LV

Figure 27: Preoperative appearance of congenitally corrected transposition of the great arteries in a 25-year-old woman. **(A)** Axial oblique maximum intensity projection (MIP) CT image shows atrioventricular discordance. The RV is identified by the moderator band (black arrow). **(B)** Coronal oblique MIP CT image shows ventriculoarterial discordance. The aorta arises from the left-sided RV, and the pulmonary artery arises from the right-sided LV. The RV is identified by the trabeculated wall (yellow arrow). A thick conal tissue (black arrow) is seen in the subpulmonic region. In the primitive ventricle, it is present in both the subpulmonic and subaortic regions. During transfer of the aorta to the LV, the subaortic component gets resorbed and is represented by fibrous continuity between the aortic and mitral valve leaflets. The subpulmonary component, however, persists and separates the pulmonary and tricuspid valve. A VSD is also seen (double arrow). **(C)** Volume-rendered image further confirms the levotransposition of the aorta, which is located leftward and anterior to the pulmonary trunk. Ao = aorta, CT = conal tissue, LA = left atrium, LV = left ventricle, MPA = main pulmonary artery, RA = right atrium, RV = right ventricle, VSD = ventricular septal defect.

can be rerouted to either pericardium (native or treated) or a synthetic patch can be used to baffle the VSD to the aorta using a continuous or interrupted suture line.

The Nikaidoh procedure is an alternative in patients whose anatomy precludes the Rastelli procedure (VSD located away from the LVOT, LVOT obstruction, or small RV). The original technique consists of aortic translocation and biventricular outflow tract reconstruction. The aortic root is harvested from the RV, relieving the LVOT by dividing the outlet septum and pulmonary valve annulus. The LVOT is then restored by translocating the aortic root posteriorly, followed by VSD closure. The RVOT is reconstructed with a pericardial patch. Repositioning of the native aortic root over the LV avoids the creation of a long intraventricular tunnel. This strategy, therefore, appears to prevent the development of LVOT obstruction, which is a frequent complication of Rastelli repair. Pulmonary stenosis is relieved by direct RV to main PA anastomosis, avoiding the use of a conduit, which decreases the incidence of RVOT reinterventions (115). Addition of the LeCompte maneuver prevents branch PA stenosis (116).

Role of CT Imaging in L-TGA

L-TGA is characterized by double discordance. Preoperative CT allows direct visualization of abnormal atrioventricular and ventriculoarterial relationships along with other associated anomalies (Table 7, Fig 27). RV dysfunction is the main concern in the preoperative period. Patients without significant associated intracardiac lesions usually do not experience symptoms of heart failure in childhood and do well until adult life. However, RV dysfunction progresses over time, as does tricuspid regurgitation. RV dysfunction usually remains subclinical for decades and typically manifests during the 4th and 5th decades of life. By 45 years of age, more than 30% of patients with isolated L-TGA and more than two-thirds of patients with associated lesions develop clinical congestive heart failure (117).

The imaging targets after double-switch repair include evaluation of the systemic or pulmonary venous baffle (stenosis, leak, thrombosis), VSD (residual), PAs (main or branch PA stenosis), neoaortic roots (dilatation), and ventricular functional assessment (Table 8, Fig 28) (90,92,93). Cardiac MRI is considered the method of choice for comprehensive evaluation of both

Table 8: Checklist for Postoperative Assessment of L-TGA

After double switch
Related to atrial switch
Status of baffle; systemic and pulmonary venous baffles (stenosis, leakage, and obstruction)
Pulmonary artery (central or branch pulmonary artery stenosis)
Outflow tracts (LVOT, RVOT obstruction)
Semilunar valve (aortic or pulmonary stenosis, aortic root dilatation)
Cardiac chambers (enlargement or wall thickening)
Related to arterial switch
Great vessel relationship
Pulmonary artery (central or branch pulmonary artery stenosis)
Outflow tracts (LVOT, RVOT obstruction)
Semilunar valve (aortic or pulmonary stenosis, aortic root dilatation)
Coronary arteries (anomalous course, ostial compressions, and atherosclerotic disease)
Cardiac chambers (enlargement or wall thickening)

Note.—L-TGA = L-loop transposition of the great arteries, LVOT = left ventricular outflow tract, RVOT = right ventricular outflow tract.

asymptomatic patients and patients who underwent surgery. CT is reserved for patients who cannot undergo postoperative MRI due to contraindications or indwelling devices expected to generate artifacts, such as pacemakers in patients who undergo ASO. CT provides information on the structure of the cardiovascular structures, including baffles, conduits, and coronary arteries (118).

Characteristics of TA

TA is a cyanotic heart disease in which a single common trunk arises from the heart instead of the aorta and pulmonary trunk. TA accounts for 0.7%–1.4% of all congenital heart diseases in live-born infants (incidence of 0.03–0.056 cases per 1000 live births) (119).

During normal embryologic development, a truncoconal septal wall develops that divides the single truncal root into separate aortic and pulmonary outflow tracts. TA develops if there is a failure in the development of the truncoconal septal wall. This also inhibits the proper creation of separate aortic and pulmonary valves, resulting in a single truncal valve. Usually, the single trunk overrides the ventricular septum and supplies systemic, pulmonary, and coronary circulation, but rarely, it may originate completely from the right or left ventricle. The truncal valve is typically tricuspid but can be bicuspid in certain cases. The leaflets are often thickened and deformed, resulting in a varying degree of stenosis and incompetency. TA is classified into different types on the basis of the pattern of origin of the PAs from the common trunk. According to the Collett and Edwards system, type 1 TA is characterized by the origin of both PAs from the short pulmonary trunk, which originates from the left lateral aspect of the common trunk. In type 2, the pulmonary trunk is absent, and the right and left PAs arise from the posterolateral aspect of the common arterial trunk. In type 3, the right and left PAs arise from the right and left lateral aspects of the trunk. Type 4 is characterized by pulmonary atresia, in which pulmonary flow is maintained by the MAPCAs (120). In another classification proposed by Van Praagh, types A1 and A2 are the same as types 1 and 2 of the Collett and Edwards classification. However, type A3 is characterized by atresia of the right or left PA with collateral flow to the ipsilateral lung, and type A4 is characterized by TA associated with an IAA (Fig 29) (121). TA is often accompanied by several structural anomalies, the most common of which include right-sided arch, double aortic arch, left superior vena cava, secundum atrial septal defect, and aberrant subclavian artery.

Surgical Approach

TA is usually diagnosed in the early neonatal period, and surgical correction is performed within the first few weeks after birth. Surgery involves patch closure of the VSD, detachment and connection of the PAs to the RV via a homograft, and alignment of the truncal valve with the LV; the truncal valve becomes the neoaortic valve.

The most challenging task in surgical repair is RVOT reconstruction. It can be established with a conduit, which is most commonly used by surgeons, or direct anastomosis of the PA to the RV. In type 1 TA, the pulmonary trunk is transected from the aorta, and a conduit is placed between the RV and remaining pulmonary trunk. In types 2 and 3, both branch PAs are nonconfluent. They are mobilized to create a confluence that is then connected to the RV through conduit placement. The conduits can be bioprosthetic (bovine jugular vein), homograft (pulmonary and aortic homograft), or made of polytetrafluoroethylene. The choice of conduit depends on several factors, including availability, patient size and hemodynamics, and surgeon preference. The bovine jugular vein conduit lacks immunogenic properties and is the most commonly used worldwide. However, there are a few disadvantages associated with the use of conduits. For instance, conduits cannot grow with age and have limited durability; therefore, patients typically require reoperation. Furthermore, conduits are prone to infection and thrombosis. During RVOT reconstruction, any present arch abnormalities, such as interruption and coarctation, are repaired in the same sitting (122).

Primary surgical complications include neoaortic valve stenosis or insufficiency, VSD patch leak, RV–to–pulmonary trunk conduit stenosis, and aortic arch obstruction (Figs 30, 31). Patients with neoaortic valve dysfunction require valvuloplasty, and those with pulmonary trunk conduit stenosis require homograft replacement later in life (123).

Role of CT Imaging in TA

Prior to surgical treatment, CTA is helpful for the identification of truncus type, delineation of the branch PAs and MAPCAs (specially in type A3), and evaluation of aortic arch status (interruption and coarctation) (Table 9). The primary role of CTA during the postoperative period is to evaluate the status

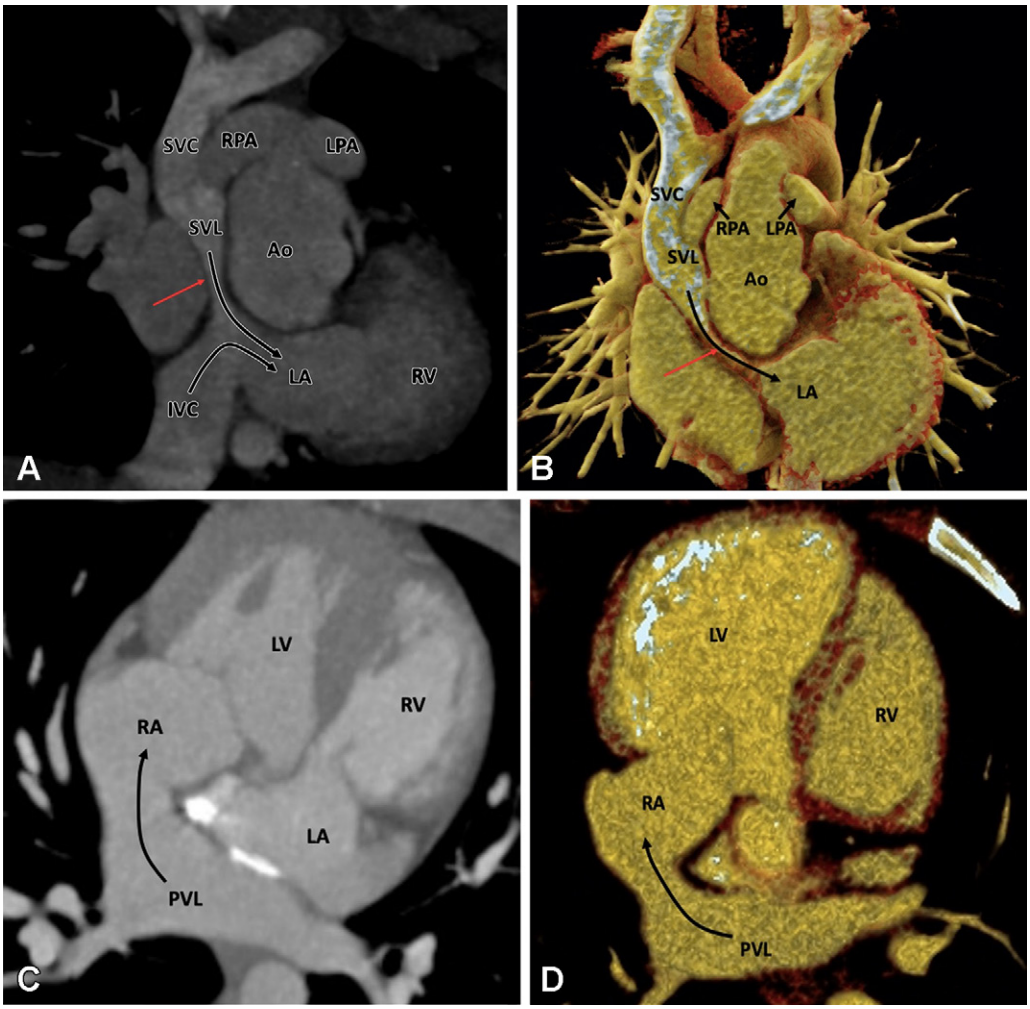

Figure 28: Postoperative appearance of levotransposition of the great arteries after double-switch operation (Senning procedure and arterial switch) in an 8-year-old boy. **(A)** Coronal oblique maximum intensity projection (MIP) CT image and **(B)** coronal oblique cut volume-rendered image show the systemic venous limb of the baffle emptying systemic venous blood into the left atrium and morphologic right ventricle (long curved black arrows). There is evidence of severe stenosis in the systemic venous limb (red arrow). Also, note the right and left pulmonary arteries (short straight black arrows in **B**) lying on either side of the aorta as the normal postoperative appearance of LeCompte maneuver. **(C)** Axial MIP CT image and **(D)** axial cut volume-rendered images show the pulmonary venous limb of the baffle emptying pulmonary venous blood into the right atrium and morphologic left ventricle (long curved black arrow). Ao = aorta, IVC = inferior vena cava, LA = left atrium, LPA = left pulmonary artery, LV = left ventricle, PVL = pulmonary venous limb, RPA = right pulmonary artery, RA = right atrium, RV = right ventricle, SVC = superior vena cava, SVL = systemic venous limb.

of the pulmonary homograft and neoaortic valve. Additionally, the aortic arch and branch PAs should be assessed for any residual or recurrent stenosis (Table 10). Early detection of neoaortic valve stenosis is important to prevent permanent damage to the LV.

Characteristics of IAA

IAA is characterized by anatomic discontinuity between the ascending and descending thoracic aorta. An understanding of arch development is essential to be able to identify aortic arch anomalies. The aortic sac is the first portion of the aorta to form, appearing as a dilated structure superior to the truncus arteriosus. The aortic sac then develops two horns, which inevitably give rise to the dorsal and ventral aorta. There are six pairs of arches connecting the dorsal and ventral aorta. During normal fetal development, the first, second, and fifth arches involute, and the principle arches forming aortic branches are third, fourth, and sixth. The third arch forms the common carotid and part of the internal carotid arteries. The fourth arch forms the definitive aortic arch and proximal part of the subclavian arteries. The distal part of the subclavian arteries is formed by the intersegmental branches. The dorsal part of the sixth arch forms the ducti arteriosus, and the ventral part forms the distal segments of the PA. The ventral aorta, forming the truncus arteriosus, divides into the ascending aorta and main pulmonary trunk. The paired dorsal aortae fuse to form a single trunk. IAA is a developmental abnormality of the truncus that leads to the anatomic and luminal disruption between the ascending and descending aorta. This discontinuity can be complete or partial, with a fibrous connecting band. Flow to the descending

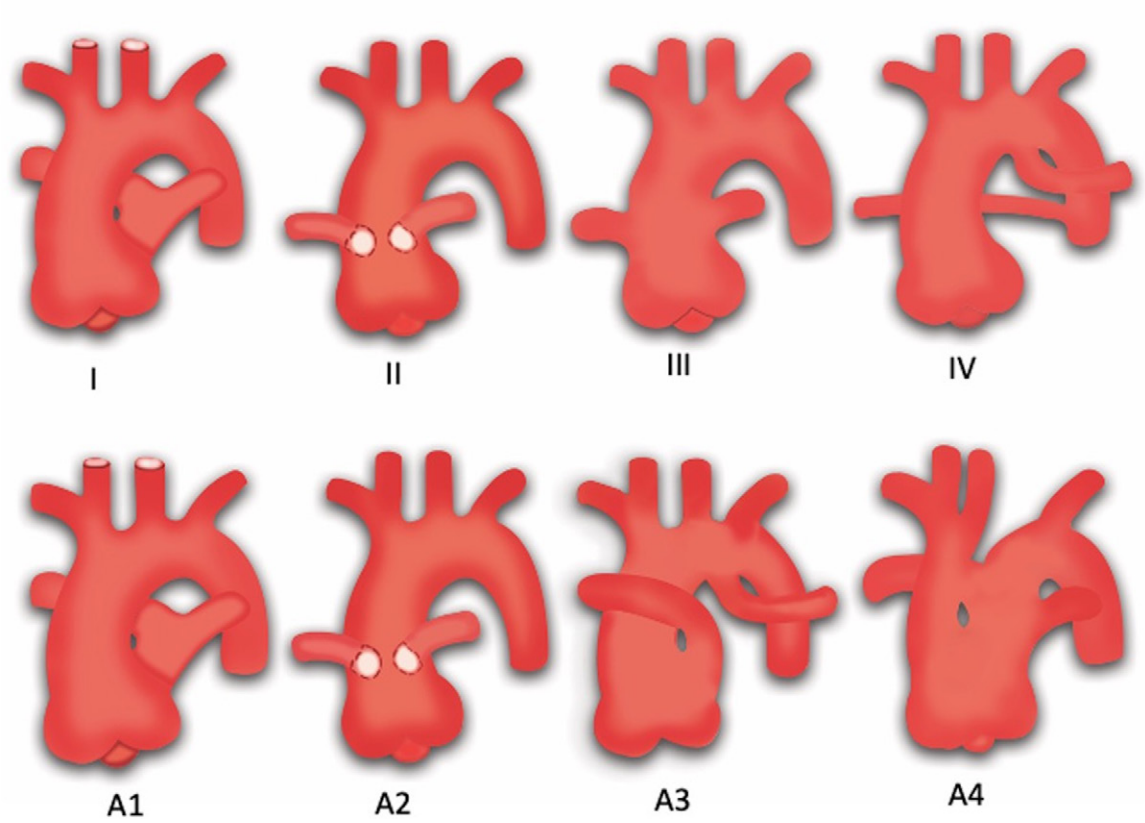

Figure 29: Diagram shows two commonly used classification systems for truncus arteriosus. Top row represents the Collett and Edwards system. Type I truncus arteriosus is characterized by origin of the main pulmonary trunk from the truncus, which further divides into the right and left pulmonary arteries; type II is characterized by the separate origin of the right and left pulmonary arteries from the posterior aspect of the truncus; type III is characterized by the separate origin of the right and left pulmonary arteries from the lateral aspect of the truncus; and type IV represents pseudotruncus (pulmonary atresia with a ventricular septal defect). Bottom row represents the Van Praagh system. Types A1 and A2 are equivalent to the Collett and Edwards types I and II, respectively; type A3 is characterized by atresia of the left or right pulmonary artery, with collateral flow to the ipsilateral lung; and type A4 is characterized by the presence of an associated interrupted aortic arch. (Adapted, with permission, from references 131 and 132.)

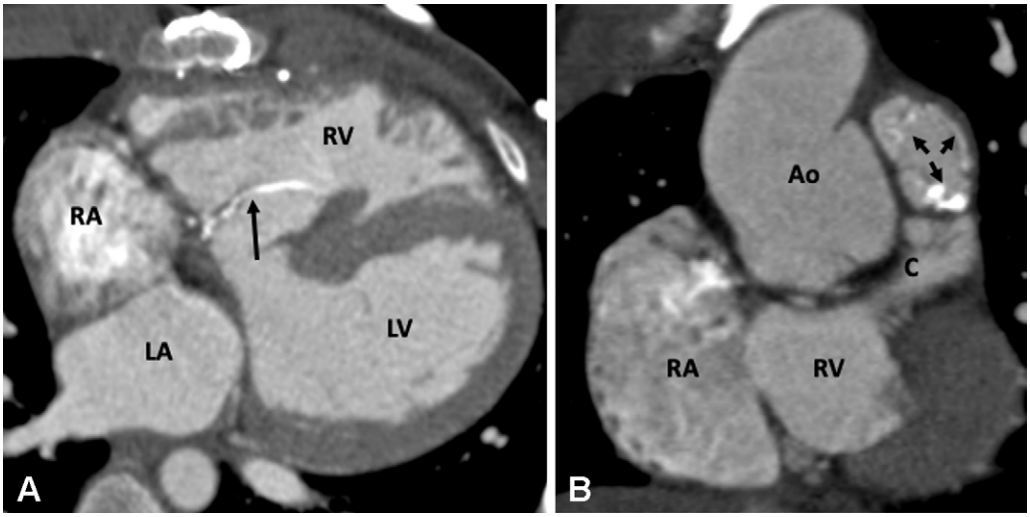

Figure 30: Postoperative appearance of truncus arteriosus after RV-PA conduit formation and VSD closure in an 11-year-old boy. **(A)** Axial contrast-enhanced CT image shows a calcified VSD patch bulging into the RV (black arrow). **(B)** Coronal oblique contrast-enhanced CT image shows the RV-PA conduit. The pulmonary valve leaflets show degenerative changes evident as leaflet calcifications (black arrows). Ao = aorta, C = conduit, LA = left atrium, LV = left ventricle, PA = pulmonary artery, RA = right atrium, RV = right ventricle, VSD = ventricular septal defect.

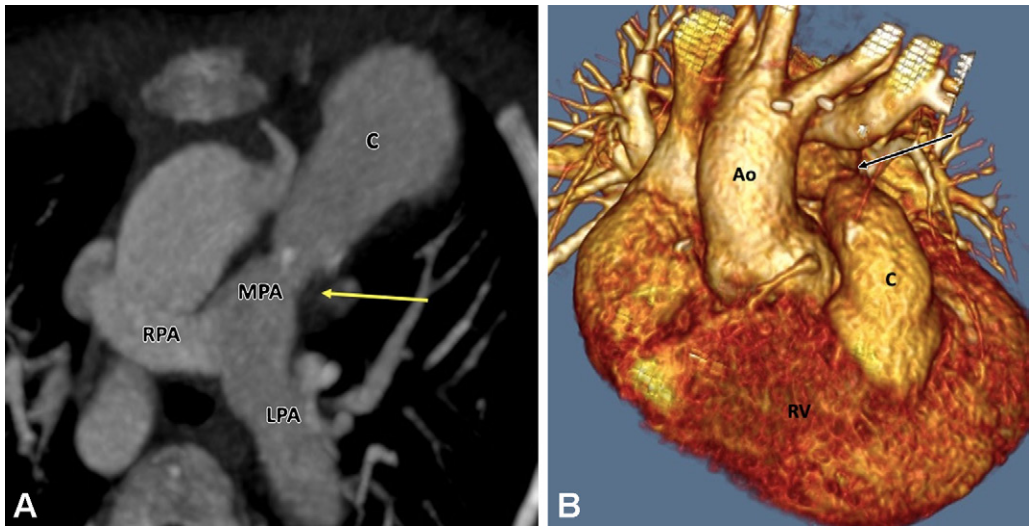

Figure 31: Postoperative appearance of truncus arteriosus after RV-PA conduit formation and VSD closure in a 13-year-old boy. **(A)** Axial maximum intensity projection CT image shows mild stenosis in the MPA at the anastomotic site of the conduit (yellow arrow). **(B)** Volume-rendered image confirms these findings. Ao = aorta, C = conduit, LPA = left PA, MPA = main PA, PA = pulmonary artery, RPA = right PA, RV = right ventricle, VSD = ventricular septal defect.

Table 9: Checklist for Preoperative Assessment of Truncus Arteriosus

Truncus
Type of truncus (Collet and Edwards type I, II, III, or IV or Van Praagh Type A-1, A-2, A-3, or A-4)
Pulmonary arteries
Present or absent
Origin (left lateral or posterior truncal wall)
Sizes: proximal and distal
VSD
No., size, and site
MAPCAs (Collet and Edwards type IV)
Origin, no., size, stenosis, course, and proximity to structures like veins and airways
Cardiac chambers
Enlargement or wall thickening
Systemic and pulmonary venous connections
Truncal valve
Bicuspid or tricuspid
Normal or thickened leaflets
Concomitant anomalies
Right-sided arch, double aortic arch, left superior vena cava, secundum ASD, and aberrant subclavian artery

Note.—ASD = atrial septal defect, MAPCAs = major aortopulmonary collateral arteries, VSD = ventricular septal defect.

Table 10: Checklist for Postoperative Assessment of Truncus Arteriosus

Pulmonary homograft
Normal or abnormal (degeneration, calcification, stenosis, or aneurysm)
Neoaortic valve
Normal or abnormal (stenosis, leaflets thickening, or aortic root dilatation)
Subaortic stenosis
VSD
Residual VSD
Cardiac chambers
Enlargement or wall thickening

Note.—VSD = ventricular septal defect.

aorta is dependent upon the PDA (124). IAA is classified into three types (type A, B, and C) depending on the site of aortic interruption. The interruption is located distal to the origin of the left subclavian artery in type A, between the left common carotid and left subclavian arteries in type B, and between the left common carotid and brachiocephalic arteries in type C (Fig 32). Type B IAA is the most common (78%), followed by type A (20%) and type C (2%) (125).

Many patients with IAA have extracardiac anomalies, the predominant being DiGeorge syndrome. The aortic valve is usually bicuspid (80%–90%), with varying degrees of commissural fusion and annular hypoplasia. In addition, posterior malalignment of the conal septum relative to the ventricular septum may lead to hemodynamically significant LVOT obstruction. Other factors contributing to LVOT obstruction include the bicuspid valve, hypoplastic aortic annulus, and prominent muscle bundle between LV free wall and LVOT, as recognized by Moulaert (126).

Patients with IAA present with shock or heart failure within the first 2 weeks of life because of physiologic closure of the PDA. Physical examination reveals tachycardia, tachypnea, and decreased femoral pulses. Due to the large VSD, a murmur may not appear until later, with increasing pulmonary blood flow.

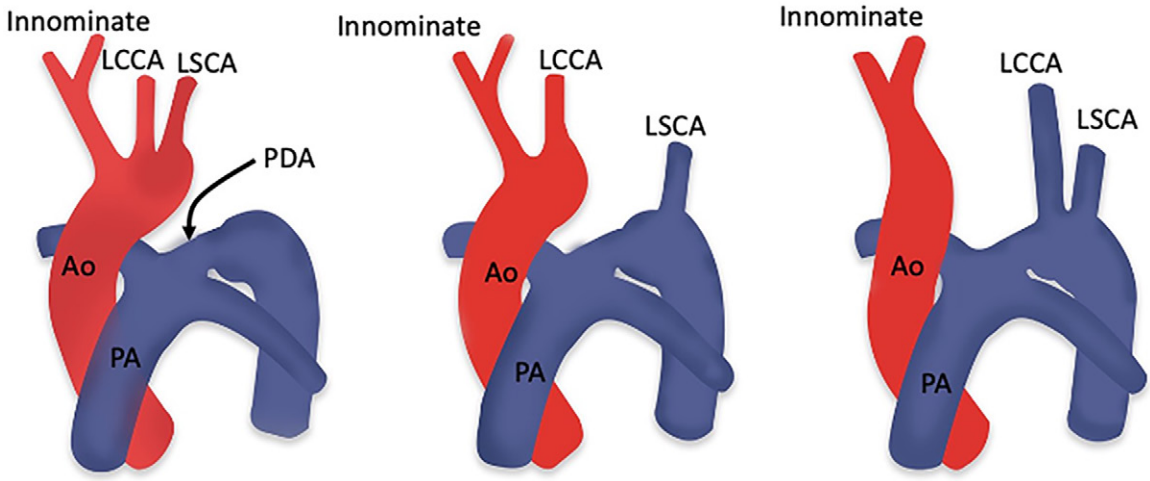

Figure 32: Diagrams showing the three types of interrupted aortic arch. Type A (left) is characterized by aortic arch interruption distal to the left subclavian artery origin; type B (middle) is characterized by aortic arch interruption between the origins of the left common carotid artery and left subclavian artery; and type C (right) is characterized by aortic arch interruption between the origins of the innominate and left common carotid arteries. Ao = aorta, LCCA = left common carotid artery, LSCA = left subclavian artery, PA = pulmonary artery, PDA = patent ductus arteriosus. (Reprinted, with permission, from reference 124.)

Similarly, the differential cyanosis between the upper and lower body is usually difficult to appreciate because of left-to-right shunting at the level of the VSD, allowing some oxygenated blood to travel to the descending thoracic aorta via the PDA. However, pulse oximetry may show higher oxygen saturation levels in the preductal arm (usually the right arm) compared with the lower body if the great vessels are normally related. If the great vessels are transposed, oxygen saturation may be higher in the lower body (reversed differential cyanosis) (127).

Surgical Approach

As soon as IAA is diagnosed, intravenous administration of prostaglandin is initiated to ensure patency of the ductus arteriosus. Surgical repair is performed after the initial workup. The main prerequisites in initial workup are screening for DiGeorge syndrome and LVOT assessment. Patients with DiGeorge syndrome have thymic and parathyroid aplasia or hypoplasia leading to the possibility of T-cell deficiency and hypocalcemia. Patients with T-cell deficiency are predisposed to graft-versus-host disease after transfusion with nonirradiated blood, and hypocalcemia requires calcium replacement because patients are already at increased risk for symptomatic hypocalcemia during hyperventilation and transfusion of citrated blood products. Early identification of these abnormalities may decrease the chances of early postoperative complications. Another important prerequisite is the diagnosis of LVOT obstruction, which may be underrecognized preoperatively. Several echocardiographic indexes may identify LVOT obstruction, including the indexed cross-sectional area of the LVOT, the subaortic diameter index, and the aortic valve diameter z score. Salem and colleagues demonstrated that patients with an aortic valve diameter less than 4.5 mm (z score < -5) subsequently develop LVOT obstruction, whereas those with aortic valve diameter greater than 4.5 mm (z score > -5) do not. Failure to diagnose and surgically correct significant LVOT obstruction is likely to result in persistent heart failure in the postoperative period (128).

The primary surgical treatments for IAA include mobilization of the aortic arch, followed by primary anastomosis. If mobilization cannot be performed due to a longer length of the interrupted segment, an artificial or homograft conduit is made to bridge the defect. Associated congenital anomalies, such as coarctation of the aorta and hypoplastic arch, are repaired in the same sitting. Postoperative complications include residual or recurrent arch obstruction, aneurysm formation at the surgical site, VSD patch leak, residual LVOT obstruction, and LV hypertrophy (129).

Role of CT Imaging in IAA

CTA can clearly delineate the aortic arch interruption, its type, length of interrupted segment, status of the arch branches, and diameters of the aorta proximal and distal to the interrupted segment (Fig 33). Other associated congenital anomalies, including VSD, the bicuspid valve, LVOT obstruction, and aortic stenosis, can also be assessed at CTA. In addition, CT is helpful in the assessment of tracheal or esophageal compression, if present (Table 11). The main objective of postoperative imaging is assessment of the anastomotic site. Various postoperative complications include anastomotic site narrowing and aneurysmal dilatation (Fig 34), as well as residual VSD, aortic valve stenosis, and LVOT obstruction (Table 12) (130).

Conclusion

Conotruncal anomalies are often associated with complex and unique geometry. CT has emerged as a robust diagnostic tool in preoperative and postoperative assessment of conotruncal anomalies. It can provide rapid, thin-section images to aid in preoperative planning and postoperative surveillance of conotruncal anomalies. The greatest clinical use of CT imaging is in patients who are critically ill or those with implanted

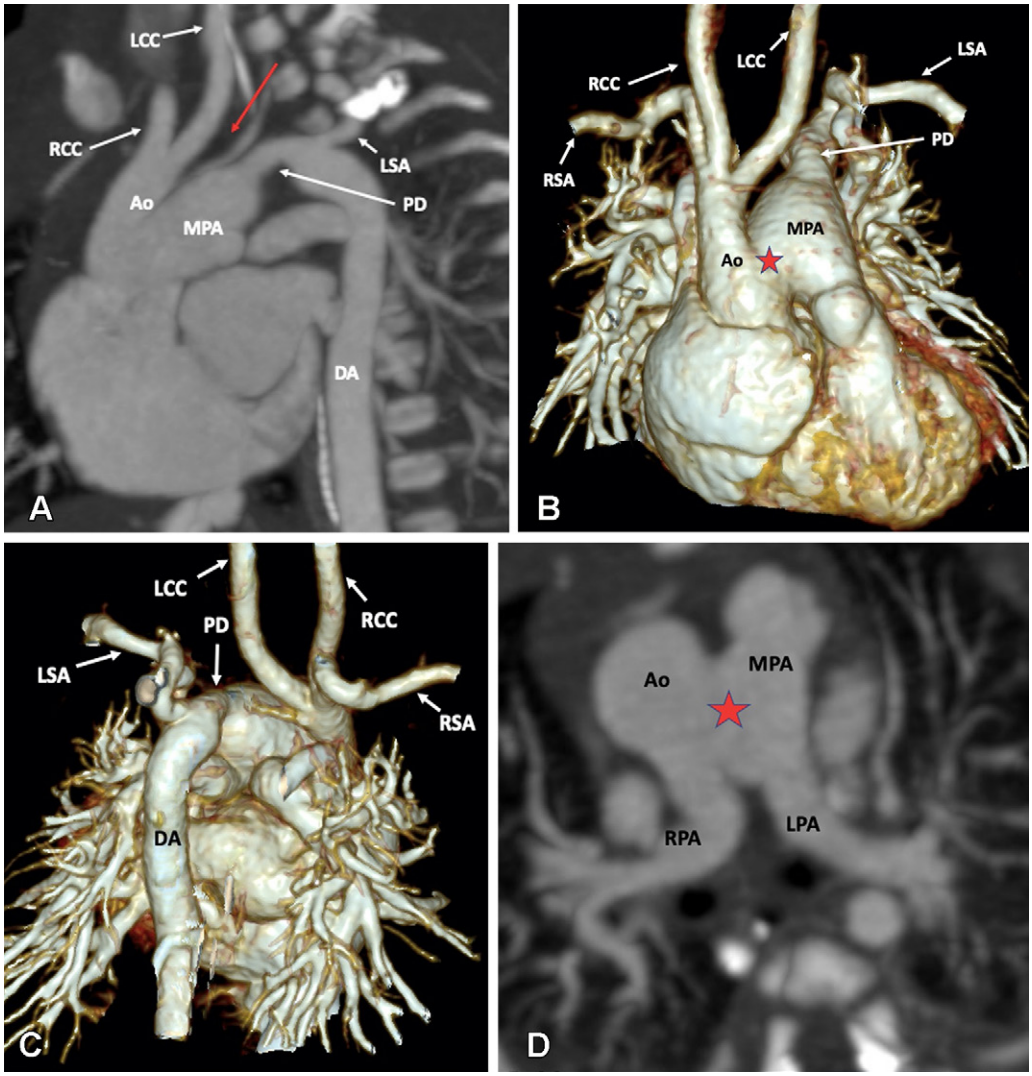

Figure 33: Preoperative appearance of type B interrupted aortic arch with aortopulmonary window in a neonate. **(A)** Sagittal oblique maximum intensity projection (MIP) CT image shows interrupted aortic arch (red arrow). Both the right and left common carotid arteries arise from the arch proximal to the site of interruption. The descending thoracic aorta is filled by a large left patent duct connecting the left pulmonary artery and descending thoracic aorta. **(B)** Anterior and **(C)** posterior three-dimensional volume-rendered images confirm the aortic arch interruption. The proximal ascending aorta and pulmonary trunk are connected, suggesting aortopulmonary window (red star in **B**). **(D)** Axial MIP CT image shows aortopulmonary window (red star). Ao = aorta, DA = descending aorta, LCC = left common carotid artery, LPA = left pulmonary artery, LSA = left subclavian artery, MPA = main pulmonary artery, PD = patent duct, RCC = right common carotid artery, RPA = right pulmonary artery, RSA = right subclavian artery.

devices. With continued advances in CT technology including ever more rapid acquisitions, continually declining radiation and contrast agent requirements, and more robust postprocessing options, the role of CT is likely to increase in the near future.

Disclosures of conflicts of interest: P.K. No relevant relationships. **M.B.** No relevant relationships.

References

1. Restivo A, Piacentini G, Placidi S, Saffirio C, Marino B. Cardiac outflow tract: a review of some embryogenetic aspects of the conotruncal region of the heart. Anat Rec A Discov Mol Cell Evol Biol 2006;288(9):936–943.
2. Mcleod G, Shum K, Gupta T, et al. Echocardiography in congenital heart disease. Prog Cardiovasc Dis 2018;61(5-6):468–475.
3. Frank L, Dillman JR, Parish V, et al. Cardiovascular MR imaging of conotruncal anomalies. RadioGraphics 2010;30(4):1069–1094.
4. Kang SL, Benson L. Recent advances in cardiac catheterization for congenital heart disease. F1000 Res 2018;7:370.
5. Goo HW, Park IS, Ko JK, Kim YH, Seo DM, Park JJ. Computed tomography for the diagnosis of congenital heart disease in pediatric and adult patients. Int J Cardiovasc Imaging 2005;21(2-3):347–365; discussion 367.
6. Leschka S, Oechslin E, Husmann L, et al. Pre- and postoperative evaluation of congenital heart disease in children and adults with 64-section CT. RadioGraphics 2007;27(3):829–846.
7. Yang D, Goo H. Pediatric 16-slice CT protocols: radiation dose and image quality. J Korean Radiol Soc 2008;59(5):333.
8. Einstein AJ, Moser KW, Thompson RC, Cerqueira MD, Henzlova MJ. Radiation dose to patients from cardiac diagnostic imaging. Circulation 2007;116(11):1290–1305.
9. Yamasaki Y, Kamitani T, Sagiyama K, Matsuura Y, Hida T, Nagata H. Model-based iterative reconstruction for 320-detector row CT angiography reduces radiation exposure in infants with complex congenital heart disease. Diagn Interv Radiol 2021;27(1):42–49.
10. Katzberg RW, Lamba R. Contrast-induced nephropathy after intravenous administration: fact or fiction? Radiol Clin North Am 2009;47(5):789–800, v.
11. Stacul F, van der Molen AJ, Reimer P, et al. Contrast induced nephropathy: updated ESUR Contrast Media Safety Committee guidelines. Eur Radiol 2011;21(12):2527–2541.

Table 11: Checklist for Preoperative Assessment of IAA

Aortic arch
Sidedness (right or left)
Type of arch interruption (type A, B, or C)
Length of arch interruption
Arch diameters (proximal and distal to interruption)
Source of descending aortic flow
PDA (unilateral or bilateral, size at both ends, insertional stenosis)
Rarely MAPCAs (origin, no., size, stenosis, course, and proximity to structures like veins and airways)
VSD
No., size, and site
LVOT
Normal or obstruction (check for the potential causes of LVOT obstruction, including malaligned VSD, bicuspid valve, AS, and prominent muscle of Moulaert)
Cardiac chambers
Enlargement or wall thickening
Systemic and pulmonary venous connections
Concomitant anomalies
Cardiac (ASD)
Tracheal or esophageal compression

Note.—AS = aortic stenosis, ASD = atrial septal defect, IAA = interrupted aortic arch, LVOT = left ventricular outflow tract, MAPCAs = major aortopulmonary collateral arteries, PDA = patent ductus arteriosus, RVOT = right ventricular outflow tract, VSD = ventricular septal defect.

12. Valverde I, Gomez-Ciriza G, Hussain T, et al. Three-dimensional printed models for surgical planning of complex congenital heart defects: an international multicentre study. Eur J Cardiothorac Surg 2017;52(6):1139–1148.
13. Krishnamurthy R. Neonatal cardiac imaging. Pediatr Radiol 2010;40(4):518–527.
14. Stefanovic S, Etchevers HC, Zaffran S. Outflow tract formation-embryonic origins of conotruncal congenital heart disease. J Cardiovasc Dev Dis 2021;8(4):42.
15. Han BK, Rigsby CK, Hlavacek A, et al. Computed tomography imaging in patients with congenital heart disease part i: rationale and utility. an expert consensus document of the Society of Cardiovascular Computed Tomography (SCCT): Endorsed by the Society of Pediatric Radiology (SPR) and the North American Society of Cardiac Imaging (NASCI). J Cardiovasc Comput Tomogr 2015;9(6):475–492.
16. Hellinger JC, Pena A, Poon M, Chan FP, Epelman M. Pediatric computed tomographic angiography: imaging the cardiovascular system gently. Radiol Clin North Am 2010;48(2):439–467, x.
17. Lee T, Tsai IC, Fu YC, et al. Using multidetector-row CT in neonates with complex congenital heart disease to replace diagnostic cardiac catheterization for anatomical investigation: initial experiences in technical and clinical feasibility. Pediatr Radiol 2006;36(12):1273–1282.
18. Han BK, Rigsby CK, Leipsic J, et al. computed tomography imaging in patients with congenital heart disease, part 2: technical recommendations. an expert consensus document of the Society of Cardiovascular Computed Tomography (SCCT): Endorsed by the Society of Pediatric Radiology (SPR) and the North American Society of Cardiac Imaging (NASCI). J Cardiovasc Comput Tomogr 2015;9(6):493–513.
19. Booij R, Dijkshoorn ML, van Straten M, et al. Cardiovascular imaging in pediatric patients using dual source CT. J Cardiovasc Comput Tomogr 2016;10(1):13–21.
20. Karlo C, Leschka S, Goetti RP, et al. High-pitch dual-source CT angiography of the aortic valve-aortic root complex without ECG-synchronization. Eur Radiol 2011;21(1):205–212.
21. Duan Y, Wang X, Cheng Z, Wu D, Wu L. Application of prospective ECG-triggered dual-source CT coronary angiography for infants and children with coronary artery aneurysms due to Kawasaki disease. Br J Radiol 2012;85(1020):e1190–e1197.
22. Paul JF, Rohnean A, Elfassy E, Sigal-Cinqualbre A. Radiation dose for thoracic and coronary step-and-shoot CT using a 128-slice dual-source machine in infants and small children with congenital heart disease. Pediatr Radiol 2011;41(2):244–249.
23. Motonaga KS, Khairy P, Dubin AM. Electrophysiologic therapeutics in heart failure in adult congenital heart disease. Heart Fail Clin 2014;10(1):69–89.
24. Tsai IC, Chen MC, Jan SL, et al. Neonatal cardiac multidetector row CT: why and how we do it. Pediatr Radiol 2008;38(4):438–451.
25. Habets J, Symersky P, van Herwerden LA, et al. Prosthetic heart valve assessment with multidetector-row CT: imaging characteristics of 91 valves in 83 patients. Eur Radiol 2011;21(7):1390–1396.
26. Rigsby CK, McKenney SE, Hill KD, et al. Radiation dose management for pediatric cardiac computed tomography: a report from the Image Gently 'Have-A-Heart' campaign. Pediatr Radiol 2018;48(1):5–20.
27. Ghoshhajra BB, Lee AM, Engel LC, et al. Radiation dose reduction in pediatric cardiac computed tomography: experience from a tertiary medical center. Pediatr Cardiol 2014;35(1):171–179.
28. Ketelsen D, Buchgeister M, Korn A, et al. High-pitch computed tomography coronary angiography-a new dose-saving algorithm: estimation of radiation exposure. Radiol Res Pract 2012;2012:724129.
29. Yang CC, Mok GS, Law WY, Hsu SM, Wu TH, Chen LK. Potential dose reduction of optimal ECG-controlled tube current modulation for 256-slice CT coronary angiography. Acad Radiol 2011;18(6):731–737.
30. Kang EJ. Clinical applications of wide-detector CT Scanners for cardiothoracic imaging: an update. Korean J Radiol 2019;20(12):1583–1596.
31. Stiller W. Basics of iterative reconstruction methods in computed tomography: A vendor-independent overview. Eur J Radiol 2018;109:147–154.
32. Hedgire SS, Baliyan V, Ghoshhajra BB, Kalra MK. Recent advances in cardiac computed tomography dose reduction strategies: a review of scientific evidence and technical developments. J Med Imaging (Bellingham) 2017;4(3):031211.
33. Gao W, Zhong YM, Sun AM, et al. Diagnostic accuracy of sub-mSv prospective ECG-triggering cardiac CT in young infant with complex congenital heart disease. Int J Cardiovasc Imaging 2016;32(6):991–998.
34. Jin KN, Park EA, Shin CI, Lee W, Chung JW, Park JH. Retrospective versus prospective ECG-gated dual-source CT in pediatric patients with congenital heart diseases: comparison of image quality and radiation dose. Int J Cardiovasc Imaging 2010;26(Suppl 1):63–73.
35. Young C, Taylor AM, Owens CM. Paediatric cardiac computed tomography: a review of imaging techniques and radiation dose consideration. Eur Radiol 2011;21(3):518–529.
36. Asferg C, Usinger L, Kristensen TS, Abdulla J. Accuracy of multi-slice computed tomography for measurement of left ventricular ejection fraction compared with cardiac magnetic resonance imaging and two-dimensional transthoracic echocardiography: a systematic review and meta-analysis. Eur J Radiol 2012;81(5):e757–e762.
37. Raman SV, Shah M, McCarthy B, Garcia A, Ferketich AK. Multi-detector row cardiac computed tomography accurately quantifies right and left ventricular size and function compared with cardiac magnetic resonance. Am Heart J 2006;151(3):736–744.
38. Bak SH, Ko SM, Jeon HJ, Yang HS, Hwang HK, Song MG. Assessment of global left ventricular function with dual-source computed tomography in patients with valvular heart disease. Acta Radiol 2012;53(3):270–277.
39. Arraiza M, Azcárate PM, De Cecco CN, et al. Assessment of left ventricular parameters in orthotopic heart transplant recipients using dual-source CT and contrast-enhanced echocardiography: comparison with MRI. Eur J Radiol 2012;81(11):3282–3288.
40. Bailliard F, Anderson RH. Tetralogy of Fallot. Orphanet J Rare Dis 2009;4:2.
41. Van Praagh R. The first Stella van Praagh memorial lecture: the history and anatomy of tetralogy of Fallot. Semin Thorac Cardiovasc Surg Pediatr Card Surg Annu 2009;12(1):19–38.
42. Maeda E, Akahane M, Kato N, et al. Assessment of major aortopulmonary collateral arteries with multidetector-row computed tomography. Radiat Med 2006;24(5):378–383.
43. Elshimy A, Khattab R, Hassan H. The role of MDCT in the assessment of cardiac and extra-cardiac vascular defects among Egyptian children with tetralogy of Fallot and its surgical implementation. Egypt J Radiol Nucl Med 2021;52(1):50.
44. Giannopoulos NM, Chatzis AK, Karros P, et al. Early results after transatrial/transpulmonary repair of tetralogy of Fallot. Eur J Cardiothorac Surg 2002;22(4):582–586.
45. Nollert G, Fischlein T, Bouterwek S, Böhmer C, Klinner W, Reichart B. Long-term survival in patients with repair of tetralogy of Fallot: 36-year follow-up of 490 survivors of the first year after surgical repair. J Am Coll Cardiol 1997;30(5):1374–1383.

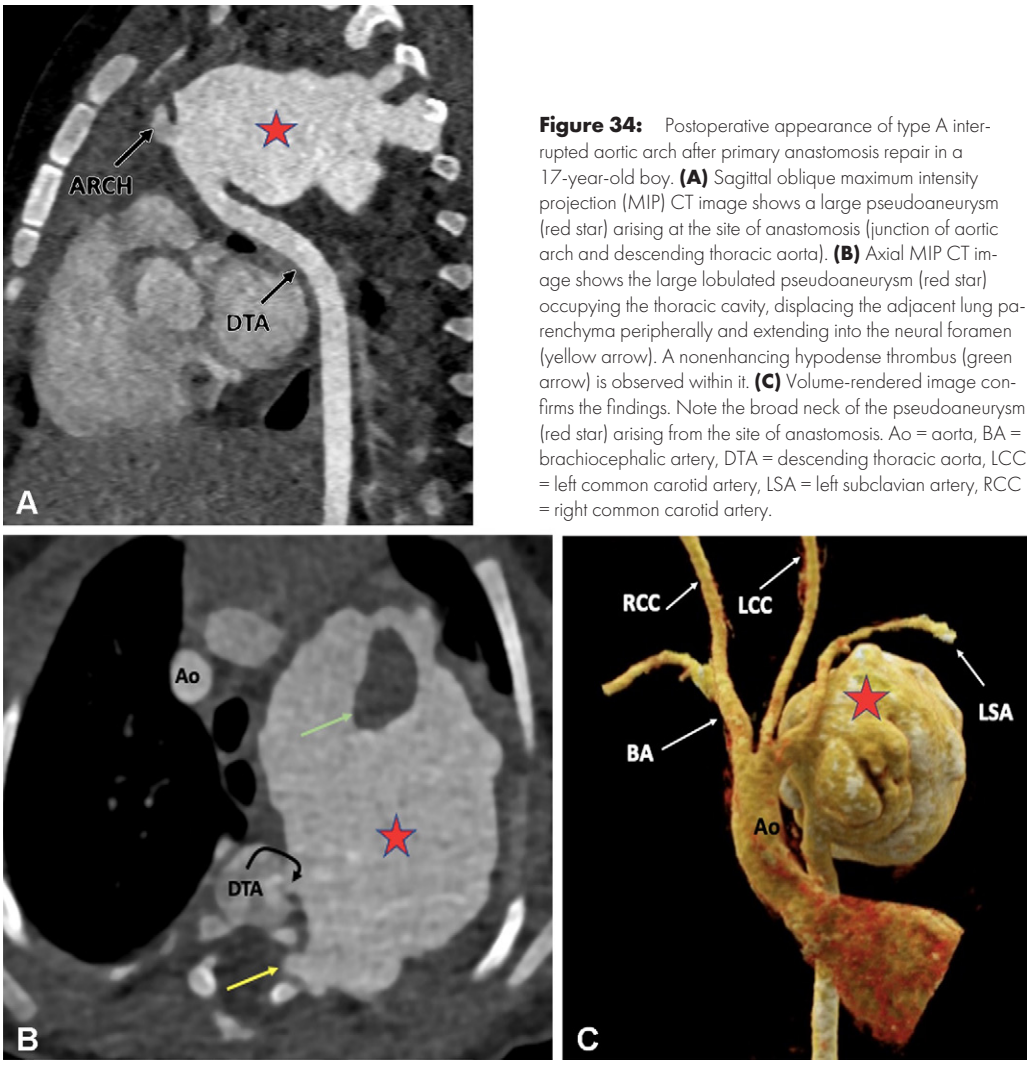

Figure 34: Postoperative appearance of type A interrupted aortic arch after primary anastomosis repair in a 17-year-old boy. **(A)** Sagittal oblique maximum intensity projection (MIP) CT image shows a large pseudoaneurysm (red star) arising at the site of anastomosis (junction of aortic arch and descending thoracic aorta). **(B)** Axial MIP CT image shows the large lobulated pseudoaneurysm (red star) occupying the thoracic cavity, displacing the adjacent lung parenchyma peripherally and extending into the neural foramen (yellow arrow). A nonenhancing hypodense thrombus (green arrow) is observed within it. **(C)** Volume-rendered image confirms the findings. Note the broad neck of the pseudoaneurysm (red star) arising from the site of anastomosis. Ao = aorta, BA = brachiocephalic artery, DTA = descending thoracic aorta, LCC = left common carotid artery, LSA = left subclavian artery, RCC = right common carotid artery.

Table 12: Checklist for Postoperative Assessment of IAA

Aortic arch
Anastomotic site narrowing or aneurysm
LVOT
Normal or residual obstruction
VSD
Residual VSD
Aortic root
Aortic or subaortic stenosis
Left ventricle
LVH

Note.—IAA = interrupted aortic arch, LVH = left ventricular hypertrophy, LVOT = left ventricular outflow tract, VSD = ventricular septal defect.

46. Piskin S, Unal G, Arnaz A, Sarioglu T, Pekkan K. Tetralogy of Fallot Surgical Repair: Shunt Configurations, Ductus Arteriosus and the Circle of Willis. Cardiovasc Eng Technol 2017;8(2):107–119.
47. Bauser-Heaton H, Ma M, Wise-Faberowski L, et al. Outcomes after initial unifocalization to a shunt in complex tetralogy of Fallot with MAPCAs. Ann Thorac Surg 2019;107(6):1807–1815.
48. Ikai A. Surgical strategies for pulmonary atresia with ventricular septal defect associated with major aortopulmonary collateral arteries. Gen Thorac Cardiovasc Surg 2018;66(7):390–397.
49. Oechslin EN, Harrison DA, Harris L, et al. Reoperation in adults with repair of tetralogy of fallot: indications and outcomes. J Thorac Cardiovasc Surg 1999;118(2):245–251.
50. Ong K, Boone R, Gao M, et al. Right ventricle to pulmonary artery conduit reoperations in patients with tetralogy of fallot or pulmonary atresia associated with ventricular septal defect. Am J Cardiol 2013;111(11):1638–1643.
51. Jonas RA, Freed MD, Mayer JE Jr, Castaneda AR. Long-term follow-up of patients with synthetic right heart conduits. Circulation 1985;72(3 Pt 2):II77–II83.
52. McGoon DC, Danielson GK, Puga FJ, Ritter DG, Mair DD, Ilstrup DM. Late results after extracardiac conduit repair for congenital cardiac defects. Am J Cardiol 1982;49(7):1741–1749.
53. Razzouk AJ, Williams WG, Cleveland DC, et al. Surgical connections from ventricle to pulmonary artery. Comparison of four types of valved implants. Circulation 1992;86(5 Suppl):II154–II158.
54. Warnes CA, Williams RG, Bashore TM, et al. ACC/AHA 2008 Guidelines for the Management of Adults with Congenital Heart Disease: Executive Summary: a report of the American College of Cardiology/American Heart Association Task Force on Practice Guidelines (writing committee to develop guidelines for the management of adults with congenital heart disease). Circulation 2008;118(23):2395–2451.
55. Hickey EJ, Veldtman G, Bradley TJ, et al. Late risk of outcomes for adults with repaired tetralogy of Fallot from an inception cohort spanning four decades. Eur J Cardiothorac Surg 2009;35(1):156–164; discussion 164.
56. Tatewaki H, Shiose A. Pulmonary valve replacement after repaired Tetralogy of Fallot. Gen Thorac Cardiovasc Surg 2018;66(9):509–515.

57. Geva T. Indications for pulmonary valve replacement in repaired tetralogy of fallot: the quest continues. Circulation 2013;128(17):1855–1857.
58. Flors L, Bueno J, Gish D, et al. Preprocedural imaging evaluation of pulmonary valve replacement after repair of tetralogy of Fallot: what the radiologist needs to know. J Thorac Imaging 2020;35(3):153–166.
59. Nakata S, Imai Y, Takanashi Y, et al. A new method for the quantitative standardization of cross-sectional areas of the pulmonary arteries in congenital heart diseases with decreased pulmonary blood flow. J Thorac Cardiovasc Surg 1984;88(4):610–619.
60. Koppel CJ, Jongbloed MRM, Kiès P, et al. Coronary anomalies in tetralogy of Fallot - A meta-analysis. Int J Cardiol 2020;306:78–85.
61. Nørgaard MA, Lauridsen P, Helvind M, Pettersson G. Twenty-to-thirty-seven-year follow-up after repair for Tetralogy of Fallot. Eur J Cardiothorac Surg 1999;16(2):125–130.
62. Ahmed S, Johnson PT, Fishman EK, Zimmerman SL. Role of multidetector CT in assessment of repaired tetralogy of Fallot. RadioGraphics 2013;33(4):1023–1036.
63. Rudski LG, Lai WW, Afilalo J, et al. Guidelines for the echocardiographic assessment of the right heart in adults: a report from the American Society of Echocardiography endorsed by the European Association of Echocardiography, a registered branch of the European Society of Cardiology, and the Canadian Society of Echocardiography. J Am Soc Echocardiogr 2010;23(7):685–713; quiz 786–788.
64. Davlouros PA, Karatza AA, Gatzoulis MA, Shore DF. Timing and type of surgery for severe pulmonary regurgitation after repair of tetralogy of Fallot. Int J Cardiol 2004;97(Suppl 1):91–101.
65. Gatzoulis MA, Balaji S, Webber SA, et al. Risk factors for arrhythmia and sudden cardiac death late after repair of tetralogy of Fallot: a multicentre study. Lancet 2000;356(9234):975–981.
66. Halliburton SS, Petersilka M, Schvartzman PR, Obuchowski N, White RD. Evaluation of left ventricular dysfunction using multiphasic reconstructions of coronary multi-slice computed tomography data in patients with chronic ischemic heart disease: validation against cine magnetic resonance imaging. Int J Cardiovasc Imaging 2003;19(1):73–83.
67. de Graaf FR, Schuijf JD, van Velzen JE, et al. Assessment of global left ventricular function and volumes with 320-row multidetector computed tomography: A comparison with 2D-echocardiography. J Nucl Cardiol 2010;17(2):225–231.
68. Raman SV, Cook SC, McCarthy B, Ferketich AK. Usefulness of multidetector row computed tomography to quantify right ventricular size and function in adults with either tetralogy of Fallot or transposition of the great arteries. Am J Cardiol 2005;95(5):683–686.
69. Xu J, Tian Y, Wang J, Xu W, Shi Z, Fu J. CT quantification of ventricular volumetric parameters based on semiautomatic 3D threshold-based segmentation in porcine heart and children with tetralogy of Fallot: accuracy and feasibility. World J Pediatr Surg 2019;2(3):e000073.
70. Harrison DA, Harris L, Siu SC, et al. Sustained ventricular tachycardia in adult patients late after repair of tetralogy of Fallot. J Am Coll Cardiol 1997;30(5):1368–1373.
71. Inoue Y, Igawa O, Iitsuka K. Aneurysm of the right ventricular outflow tract after surgical repair of Tetralogy of Fallot: three-dimensional computed tomography findings. Europace 2009;11(1):130.
72. Benson LN, Nykanen D, Freedom RM. Endovascular stents in congenital heart disease. Prog Cardiovasc Dis 1996;39(2):165–186.
73. Baikoussis NG, Apostolakis E, Papakonstantinou NA, Sarantitis I, Dougenis D. Safety of magnetic resonance imaging in patients with implanted cardiac prostheses and metallic cardiovascular electronic devices. Ann Thorac Surg 2011;91(6):2006–2011.
74. Nazarian S, Hansford R, Roguin A, et al. A prospective evaluation of a protocol for magnetic resonance imaging of patients with implanted cardiac devices. Ann Intern Med 2011;155(7):415–424.
75. Bacha EA, Scheule AM, Zurakowski D, et al. Long-term results after early primary repair of tetralogy of Fallot. J Thorac Cardiovasc Surg 2001;122(1):154–161.
76. Yim D, Dragulescu A, Ide H, et al. Essential modifiers of double outlet right ventricle: revisit with endocardial surface images and 3-dimensional print models. Circ Cardiovasc Imaging 2018;11(3):e006891.
77. Bharucha T, Hlavacek AM, Spicer DE, Theocharis P, Anderson RH. How should we diagnose and differentiate hearts with double-outlet right ventricle? Cardiol Young 2017;27(1):1–15.
78. Sridaromont S, Feldt RH, Ritter DG, Davis GD, Edwards JE. Double outlet right ventricle: hemodynamic and anatomic correlations. Am J Cardiol 1976;38(1):85–94.
79. Bashore TM. Adult congenital heart disease: right ventricular outflow tract lesions. Circulation 2007;115(14):1933–1947.
80. Walters HL 3rd, Mavroudis C, Tchervenkov CI, Jacobs JP, Lacour-Gayet F, Jacobs ML. Congenital Heart Surgery Nomenclature and Database Project: double outlet right ventricle. Ann Thorac Surg 2000;69(4 Suppl):S249–S263.
81. Fredenburg TB, Johnson TR, Cohen MD. The Fontan procedure: anatomy, complications, and manifestations of failure. RadioGraphics 2011;31(2):453–463.
82. Ebadi A, Spicer DE, Backer CL, Fricker FJ, Anderson RH. Double-outlet right ventricle revisited. J Thorac Cardiovasc Surg 2017;154(2):598–604.
83. Rosenquist GC, Clark EB, Sweeney LJ, McAllister HA. The normal spectrum of mitral and aortic valve discontinuity. Circulation 1976;54(2):298–301.
84. Bharati S, Kirklin JW, McAllister HA Jr, Lev M. The surgical anatomy of common atrioventricular orifice associated with tetralogy of Fallot, double outlet right ventricle and complete regular transposition. Circulation 1980;61(6):1142–1149.
85. Pacifico AD, Kirklin JW, Bargeron LM Jr. Repair of complete atrioventricular canal associated with tetralogy of Fallot or double-outlet right ventricle: report of 10 patients. Ann Thorac Surg 1980;29(4):351–356.
86. Sondheimer HM, Freedom RM, Olley PM. Double outlet right ventricle: clinical spectrum and prognosis. Am J Cardiol 1977;39(5):709–714.
87. Rizvi A, Deaño RC, Bachman DP, Xiong G, Min JK, Truong QA. Analysis of ventricular function by CT. J Cardiovasc Comput Tomogr 2015;9(1):1–12.
88. Sandler KL, Markham LW, Mah ML, Byrum EP, Williams JR. Optimizing CT angiography in patients with Fontan physiology: single-center experience of dual-site power injection. Clin Radiol 2014;69(12):e562–e567.
89. Ghadimi Mahani M, Agarwal PP, Rigsby CK, et al. CT for assessment of thrombosis and pulmonary embolism in multiple stages of single-ventricle palliation: challenges and suggested protocols. RadioGraphics 2016;36(5):1273–1284.
90. Fulton DR, Fyler DC. D-transposition of the great arteries. In: Keane JF, Lock JE, Fyler DC, eds. Nadas' Pediatric Cardiology. 2nd ed. Philadelphia, Pa: Saunders Elsevier, 2006; 645–661.
91. Mertens LL, Vogt MO, Marek J, Cohen MS. Transposition of the great arteries. In: Lai WW, Mertens LL, Cohen MS, Geva T, eds. Echocardiography in Pediatric and Congenital Heart Disease: From Fetus to Adult. Chichester, UK: Wiley-Blackwell; 2009; 398–416.
92. Mustard WT, Chute AL, Keith JD, Sirek A, Rowe RD, Vlad P. A surgical approach to transposition of the great vessels with extracorporeal circuit. Surgery 1954;36(1):31–51.
93. Senning A. Surgical correction of transposition of the great vessels. Surgery 1959;45(6):966–980.
94. Mustard WT. Successful two-stage correction of transposition of the great vessels. Surgery 1964;55:469–472.
95. Mustard WT, Keith JD, Trusler GA, Fowler R, Kidd L. The Surgical Management of Transposition of the Great Vessels. J Thorac Cardiovasc Surg 1964;48(6):953–958.
96. Marathe SP, Talwar S. Surgery for transposition of great arteries: A historical perspective. Ann Pediatr Cardiol 2015;8(2):122–128.
97. Moe TG, Bardo DME. Long-term outcomes of the arterial switch operation for d-transposition of the great arteries. Prog Cardiovasc Dis 2018;61(3-4):360–364.
98. Jatene AD, Fontes VF, Paulista PP, et al. Anatomic correction of transposition of the great vessels. J Thorac Cardiovasc Surg 1976;72(3):364–370.
99. Lecompte Y, Zannini L, Hazan E, et al. Anatomic correction of transposition of the great arteries. J Thorac Cardiovasc Surg 1981;82(4):629–631.
100. Legendre A, Losay J, Touchot-Koné A, et al. Coronary events after arterial switch operation for transposition of the great arteries. Circulation 2003;108(Suppl 1):II186–II190.
101. Schwartz ML, Gauvreau K, del Nido P, Mayer JE, Colan SD. Long-term predictors of aortic root dilation and aortic regurgitation after arterial switch operation. Circulation 2004;110(11 Suppl 1):II128–II132.
102. Kreutzer C, De Vive J, Oppido G, et al. Twenty-five-year experience with rastelli repair for transposition of the great arteries. J Thorac Cardiovasc Surg 2000;120(2):211–223.
103. Di Carlo D, Tomasco B, Cohen L, Vouhé P, Lecompte Y. Long-term results of the REV (réparation à l'ètage ventriculaire) operation. J Thorac Cardiovasc Surg 2011;142(2):336–343.
104. Koppel CJ, Vliegen HW, Bökenkamp R, et al. The Leiden Convention coronary coding system: translation from the surgical to the universal view. Eur Heart J Cardiovasc Imaging 2022;23(3):412–422.
105. Cook SC, McCarthy M, Daniels CJ, Cheatham JP, Raman SV. Usefulness of multislice computed tomography angiography to evaluate intravascular stents and transcatheter occlusion devices in patients with d-transposition of the great arteries after mustard repair. Am J Cardiol 2004;94(7):967–969.
106. Puranik R, Muthurangu V, Celermajer DS, Taylor AM. Congenital heart disease and multi-modality imaging. Heart Lung Circ 2010;19(3):133–144.
107. Mayer JE Jr, Sanders SP, Jonas RA, Castañeda AR, Wernovsky G. Coronary artery pattern and outcome of arterial switch operation for transposition of the great arteries. Circulation 1990;82(5 Suppl):IV139–IV145.

108. Michalak KW, Sobczak-Budlewska K, Moll JJ, et al. Can we predict potentially dangerous coronary patterns in patients with transposition of the great arteries after an arterial switch operation? Cardiol Young 2019;29(11):1350–1355.
109. Hegde M. Role of Radiography in Congenital Heart Diseases. In: Vijayalakshmi IB, Syamasundar Rao P, Chugh R, eds. A comprehensive approach to congenital heart diseases. New Delhi, India: Jaypee Brothers Medical Publishers, 2013; 190–202.
110. Kumar TKS. Congenitally corrected transposition of the great arteries. J Thorac Dis 2020;12(3):1213–1218.
111. Saxena A, Relan J, Agarwal R, et al. Indian guidelines for indications and timing of intervention for common congenital heart diseases: Revised and updated consensus statement of the Working group on management of congenital heart diseases. Ann Pediatr Cardiol 2019;12(3):254–286.
112. Ilbawi MN, DeLeon SY, Backer CL, et al. An alternative approach to the surgical management of physiologically corrected transposition with ventricular septal defect and pulmonary stenosis or atresia. J Thorac Cardiovasc Surg 1990;100(3):410–415.
113. Hoashi T, Kagisaki K, Miyazaki A, et al. Anatomic repair for corrected transposition with left ventricular outflow tract obstruction. Ann Thorac Surg 2013;96(2):611–620.
114. Davies B, Oppido G, Wilkinson JL, Brizard CP. Aortic translocation, Senning procedure and right ventricular outflow tract augmentation for congenitally corrected transposition, ventricular septal defect and pulmonary stenosis. Eur J Cardiothorac Surg 2008;33(5):934–936.
115. Raju V, Myers PO, Quinonez LG, et al. Aortic root translocation (Nikaidoh procedure): Intermediate follow-up and impact of conduit type. J Thorac Cardiovasc Surg 2015;149(5):1349–1355.
116. Talwar S, Muthukkumaran S, Choudhary SK, Airan B. The expanding indications for the Lecompte maneuver. World J Pediatr Congenit Heart Surg 2014;5(2):291–296.
117. Dobson R, Danton M, Nicola W, Hamish W. The natural and unnatural history of the systemic right ventricle in adult survivors. J Thorac Cardiovasc Surg 2013;145(6):1493–1501; discussion 1501–1503. [Published correction appears in J Thorac Cardiovasc Surg 2015;149(3):950.]
118. Ranganath P, Singh S, Abbara S, Agarwal PP, Rajiah P. Computed Tomography in Adult Congenital Heart Disease. Radiol Clin North Am 2019;57(1):85–111.
119. McElhinney DB, Driscoll DA, Emanuel BS, Goldmuntz E. Chromosome 22q11 deletion in patients with truncus arteriosus. Pediatr Cardiol 2003;24(6):569–573.
120. Collett RW, Edwards JE. Persistent truncus arteriosus; a classification according to anatomic types. Surg Clin North Am 1949;29(4):1245–1270.
121. Van Praagh R, Van Praagh S. The anatomy of common aorticopulmonary trunk (truncus arteriosus communis) and its embryologic implications. A study of 57 necropsy cases. Am J Cardiol 1965;16(3):406–425.
122. de Siena P, Ghorbel M, Chen Q, Yim D, Caputo M. Common arterial trunk: review of surgical strategies and future research. Expert Rev Cardiovasc Ther 2011;9(12):1527–1538.
123. Sinzobahamvya N, Boscheinen M, Blaschczok HC, et al. Survival and reintervention after neonatal repair of truncus arteriosus with valved conduit. Eur J Cardiothorac Surg 2008;34(4):732–737.
124. Bravo-Valenzuela NJ, Peixoto AB, Araujo Júnior E. Prenatal diagnosis of congenital heart disease: A review of current knowledge. Indian Heart J 2018;70(1):150–164.
125. Celoria GC, Patton RB. Congenital absence of the aortic arch. Am Heart J 1959;58(3):407–413.
126. LaPar DJ, Baird CW. Surgical Considerations in Interrupted Aortic Arch. Semin Cardiothorac Vasc Anesth 2018;22(3):278–284.
127. Fiore AC, Peterson RE, Huddleston CB. Repair of interrupted aortic arch with ventricular septal defect. In: Ross M, ed. Critical heart disease in infants and children. 3rd ed. Philadelphia, Pa: Elsevier, 2019; 565–571.e1.
128. Salem MM, Starnes VA, Wells WJ, et al. Predictors of left ventricular outflow obstruction following single-stage repair of interrupted aortic arch and ventricular septal defect. Am J Cardiol 2000;86(9):1044–1047, A11.
129. Schreiber C, Eicken A, Vogt M, et al. Repair of interrupted aortic arch: results after more than 20 years. Ann Thorac Surg 2000;70(6):1896–1899; discussion 1899–1900.
130. Sato S, Akagi N, Uka M, Kato K, Okumura Y, Kanazawa S. Interruption of the aortic arch: diagnosis with multidetector computed tomography. Jpn J Radiol 2011;29(1):46–50.
131. Valle C, Hadley M. (2018). Truncus Arteriosus. In: DeFaria Yeh D., Bhatt A. (eds) Adult Congenital Heart Disease in Clinical Practice. Cham, Switzerland: Springer, 2018.
132. Cabalka AK, Edwards WD, Dearani JA. Truncus Arteriosus. Thoracic Key: Fastest thoracic insight engine. https://thoracickey.com/truncus-arteriosus-5/. Published July 27, 2016. Accessed February 16, 2021.